

Damage Estimation of a Ship's Hull using ICCP system Measurements

thesis

Daniël Booms

Damage Estimation of a Ship's Hull using ICCP system Measurements

thesis

by

Daniël Booms

to obtain the degree of Master of Science
at the Delft University of Technology,
to be defended publicly on Wednesday April 17, 2019 at 13:00.

Student number: 4284216
Project duration: September 1, 2018 – April 17, 2019
Thesis committee: Prof. dr. R. Ross, TU Delft, chairman
Dr. A. Rodrigo Mor, TU Delft, supervisor
Dr. Ir. M. Popov, TU Delft

An electronic version of this thesis is available at <http://repository.tudelft.nl/>.

Abstract

Most ocean-going ships are fitted with an impressed current cathodic protection (ICCP) system. The currents impressed by this system onto the seawater find their way to corroding parts of the ship's hull, and prevent the hull from corroding. The electric field resulting from the currents around the ship is called the electric signature. This signature is a threat in seas with mines, as mines explode when they detect this signature. Therefore controlling the signature is important, especially to naval ships. In order to be able to control the signature the location and size of corrosion damage needs to be known. Today no method exists for corrosion damage estimation on a sailing ship. This study aims to develop a method for corrosion damage estimation using only measurements of an ICCP system. The research question is: To what accuracy and with what measurements can the damage distribution on a ship's hull be reconstructed? The quality of the damage reconstruction is evaluated by how well the signature is estimated.

First an analytical model is used to explore the theoretical limits of damage reconstruction. This shows damage reconstruction is limited by the number of measurement electrodes. Then damage reconstruction by numeric model inversion is attempted, but is shown to be unattainable. The proposed solution is damage reconstruction by repeatedly calculating for different damage configurations, comparing the calculated measurements to the true ones, and iterating until an optimum is found. This method works well on a ship geometry if 140 measurement sensors are used.

In order to verify the damage reconstruction algorithm a scale model facility is developed. The produced field sensors show shifting offsets that are not explained, but good linearity with the electric field. Simulations and measurements with a calibration source show good similarity, but a factor of 1.6 difference that is not explained. Test with sacrificial anodes show large variations over time and a large dependency on the sailing speed.

The results show that corrosion damage reconstruction using only on-ship measurements can be achieved. The resolution of damage reconstruction is limited by the number of measurement electrodes, at least one hundred are needed for the signature to be resolved. Current ships have between one and eight measurement electrodes; it is recommended future ships will have at least one hundred. These results furthermore indicate that time-dependent effects should be included in the physical model used for the simulations.

Preface

This thesis is for graduation, finishing the education, at the Delft University of Technology and for this the master Electrical Engineering passing all requirements and protocol, after 'most six years aboard. This research was done together, by TU Delft mentioned before and TNO in close rapport.

It was good to be at TNO, and my thanks all colleagues should know Supervisors Eugene, Taco, supervising like Odysseus' Menthoor, giving answer to my questions, helping with many suggestions. My friends of the hands-on sessions, the scale model testing corps. And of course my awesome room mates, stopping me from getting bored. you I want to thank therefore.

I want to thank my fiancée, Esther, helping me every day. I want to thank my Good Father, showing step-by-step my course. I rejoice for He is my Lord. I thank my parents for support, my zub quite often my resort, my friends who went this road before and those friends who now I precede, those at least and many more remain unnamed for evermore.

And the author unexiting, still is writing, still is writing, on this bland and dreary thesis, on the same text as before. But on some day by defending his research he makes an ending, and not one more second spending, turns around and leaves the floor. He will not look back but forward, giving nó bow, nó encore, as these days return no more.

Daniël Booms

Den Haag, ante diem octavum Kalendas Aprilis Anno Domini MMXIX

Contents

| | |
|---|-----------|
| Preface | v |
| List of Symbols | ix |
| List of Acronyms | xi |
| 1 Introduction | 1 |
| 2 Theoretical framework | 5 |
| 2.1 Electro-Chemical basis | 5 |
| 2.2 Historical research | 6 |
| 2.2.1 Conclusions from the literature | 8 |
| 2.3 Research questions | 9 |
| 3 Inverse Problems and Methods | 11 |
| 3.1 Introduction | 11 |
| 3.2 On ICCP systems | 11 |
| 3.3 Ill-posed problems | 13 |
| 3.4 Solutions | 13 |
| 3.4.1 Evaluation metric | 13 |
| 3.4.2 Structure of inverse methods | 15 |
| 4 Analytic and Numeric Methods | 17 |
| 4.1 Introduction | 17 |
| 4.2 Mathematical model | 17 |
| 4.2.1 General physical description | 17 |
| 4.2.2 Numerical method classification and selection | 20 |
| 4.2.3 Analytical method. | 21 |
| 4.3 Inverse problem assembler | 22 |
| 4.3.1 Defining the error | 22 |
| 4.3.2 The use of the gradient. | 22 |
| 4.3.3 Analytical model | 23 |
| 4.3.4 Finite element model | 23 |
| 4.4 Regularisation | 24 |
| 4.4.1 Regularisation of the analytical model. | 24 |
| 4.4.2 Regularisation of the FEM model | 25 |
| 4.5 Inverse solver. | 25 |
| 4.6 Software implementation. | 26 |
| 4.7 Simulation experiments | 28 |
| 4.7.1 Analytic model inversion | 28 |
| 4.7.2 Finite element model inversion simulation | 31 |
| 4.7.3 Interpretation of the simulation experiments | 31 |
| 5 Brute Force Method | 33 |
| 5.1 Introduction | 33 |
| 5.2 The Brute Force Method | 33 |
| 5.3 Brute Force Inversion Simulations. | 34 |
| 5.3.1 Robustness analysis | 34 |
| 5.3.2 Interpretation of the simulation experiments | 35 |

| | | |
|----------|--|-----------|
| 6 | Scale-Model Experiments | 37 |
| 6.1 | Objectives | 37 |
| 6.2 | Measurement Set-up and Materials | 37 |
| 6.3 | Sensors selection for electric potential and field measurements | 39 |
| 6.3.1 | Method | 39 |
| 6.3.2 | Results | 41 |
| 6.4 | Sacrificial Anode Cathodic Protection | 42 |
| 6.4.1 | Method | 42 |
| 6.4.2 | Results | 43 |
| 6.5 | Impressed current cathodic protection | 44 |
| 6.6 | Verification of the inverse method | 45 |
| 6.7 | Interpretation of the scale model experiments | 45 |
| 7 | Conclusions | 49 |
| 7.1 | Conclusions and discussion on inverse methods | 49 |
| 7.2 | Conclusions and discussion on scale model analysis | 50 |
| 7.3 | Answers to the research questions | 50 |
| 8 | Recommendations | 51 |
| | Bibliography | 53 |
| A | Finite element method | 57 |
| A.1 | Discrete formulation | 57 |
| A.2 | Meshing of the domain | 58 |
| A.3 | Basis functions | 58 |
| A.4 | Assembling system matrices and source vectors | 59 |
| A.4.1 | Assembling A from the system. | 59 |
| A.4.2 | Assembling f from the sources and implementing the boundary conditions | 59 |
| B | Results of the test with the slate | 61 |
| C | Additional scale model blueprints | 79 |

List of Symbols

| | |
|-----------|---|
| A | Capacitance matrix of the finite element problem, linking voltages to charges |
| a | x -gradient of basis function |
| b | y -gradient of basis function |
| c | z -gradient of basis function |
| \vec{D} | Electric displacement field in C m^{-2} |
| D | Time-area matrix of the finite element problem, linking charges to unknown current densities |
| d | Offset of basis function |
| \vec{E} | Electric field strength in V m^{-1} |
| F | Faraday's constant, electric charge per mole of electrons, $F = 96485 \text{C mol}^{-1}$ |
| f | Source vector of the finite element problem |
| G | Gibbs free energy in J |
| I | Electric current in A |
| I^a | Vector of known anode currents |
| I^c | Vector of unknown cathode currents |
| \vec{J} | Electric current density in A m^{-2} |
| J^n | Outward normal electric current density in A m^{-2} |
| j^u | Column vector of unknown current densities (A m^{-2}) for the finite element problem |
| K | Coulomb's constant $8.9876 * 10^9 \text{N m}^2 \text{C}^{-2}$ |
| k | Index variable, used for column indices |
| N | Number of elements in the finite element domain |
| n | Number of nodes in the finite element system |
| \hat{n} | Normal unit vector |
| n^e | Number of exchanged electrons |
| p | Polarisation curve function |
| p^0 | Constant term of the linearised polarisation curve |
| p^1 | Linear term of the linearised polarisation curve |
| Q | Charge in C |
| q | Volumetric charge density in C m^{-3} |
| q^A | Surface charge density in C m^{-2} |
| R | Resistance matrix in Ω |
| r | Index variable, used for row indices |
| R^{-1} | Conductance matrix in S |
| R^a | Resistance matrix for anode influences in Ω |
| R^c | Resistance matrix for cathode influences in Ω |
| U | Electric potential in J C^{-1} |
| u | Vector of discrete voltages, unknowns in the finite element problem |
| V | Voltage in V |
| v | Test function in the weak form of the Poisson equation |
| V^h | Finite element approximation of the voltage, continuous variable |
| V^m | Vector with measured voltages |
| \vec{x} | Position vector in m |
| x | Euclidean coordinate in m |

| | |
|---------------|--|
| y | Euclidean coordinate in m |
| z | Euclidean coordinate in m |
| Γ | Boundary of the finite element problem, boundary of Ω |
| Ω | Domain of the finite element problem |
| α | Area of a facial element in m^2 |
| γ | Boundary of a subdomain, boundary of ω |
| δ | Damage fraction of the ships hull, value between 0 (fully coated) and 1 (fully uncoated) |
| ε | Permittivity in $F m^{-1}$ |
| ζ | Error of the inverse problem |
| η | Element domain |
| κ | Global node index label |
| λ | Global node index label |
| λ^2 | Weight factor |
| μ | Global node index label |
| ν | Global node index label |
| π | Constant, half the circumference of a unit circle, 3.14159... |
| σ | Electric conductivity in $S m^{-1}$ |
| τ | Time constant in s |
| v | Volume in m^3 |
| φ | Basis function of the finite element problem |
| ω | Subdomain of the finite element problem, $\omega \in \Omega$ |

N.B. Superscripts are part of names, subscripts denote indices of matrices or vectors.

List of Acronyms

- ADC** analog-to-digital converter
- Ag/AgCl* silver-silverchloride
- BEM** boundary element method
- BFGS** Broydon-Fletcher-Goldfarb-Shanno
- DC** direct current
- FDM** finite difference method
- FEM** finite element method
- HDPE** high-density polyethylene
- ICCP** impressed current cathodic protection
- LM** Levenberg-Marquardt
- MFS** method of fundamental solutions
- PDE** partial differential equation
- RMS** root-mean-square
- RSS** residual sum of squares

1

Introduction

Ocean-going ships made of steel corrode rapidly below the waterline, therefore they are coated. Some parts of a ship, such as the propellers and the shafts, cannot be coated because they are moving. A coating would just not stick, and thereby make the corrosion worse. Also coatings degrade over time and they get damaged.

Exposed parts of the ship made of different metal alloys will form a galvanic cell in the seawater. For instance the bronze of a propeller might become the cathode, the steel of the hull the anode, the seawater the electrolyte, and an internal connection the return path. On a larger ship the bow and the stern might be at a different electrochemical potential, and either of them could become cathode or anode in this corrosion galvanic cell, without the need for other materials. When these corrosion reactions take place an electric current is present in the seawater.

An old and common way to protect steel structures against corrosion is the placement of sacrificial anodes. These consist of a metal alloy with a more negative reduction potential than the steel of the ship. This sacrificial anode is then corroded instead of the ship, hence it's name. These sacrificial anodes are usually made of zinc or aluminium. The disadvantage of sacrificial anodes is that they can only protect a limited surface area, a few times their own. For large ships sacrificial anodes are usually placed near unprotected parts, but they cannot protect the entire hull. An example of a sacrificial anode placed near a propeller can be seen in fig. 1.1

To enhance protection on large ships, impressed current cathodic protection (ICCP) systems are used, usually in combination with sacrificial anodes. This ICCP system forces a current into the water through one or more anodes. These currents find their way to unprotected parts of the hull and there reverse the corrosion reaction. Reference electrodes are used to measure potentials on the hull. The magnitude of the anode currents is controlled so the potentials on the hull are within a range of potentials for which it is known the hull does not corrode. An overview of an ICCP system can be seen in fig. 1.2. Figure 1.2 shows the components of the cathodic protection system that are placed on the hull of a ship. Both the impressed current anodes and the sacrificial anodes come in different shapes like bar, elliptical, and round, see fig. 1.3. When an ICCP anode is installed, a large shield is placed



Figure 1.1: Sacrificial anode near a propeller, obtained from [6].

around it as can be seen in fig. 1.4. This is to protect the hull near the anode from extreme potentials.

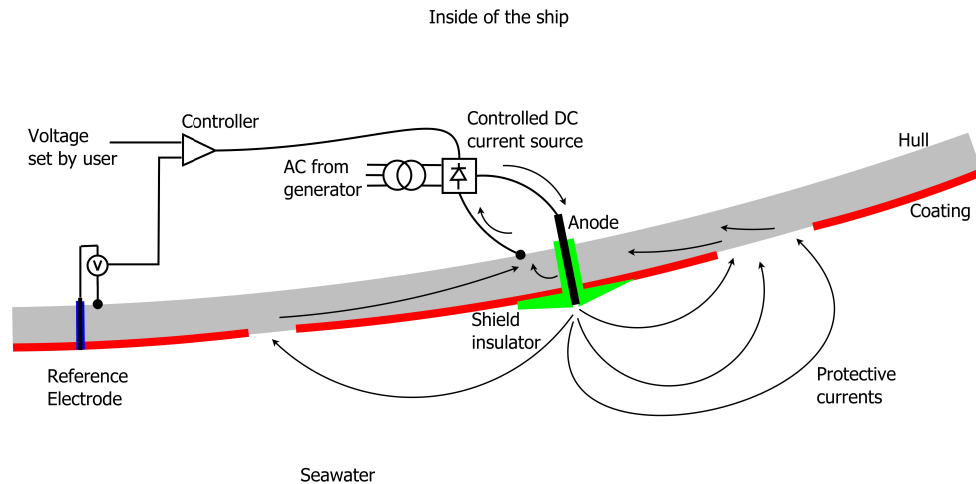


Figure 1.2: Schematic overview of an ICCP system.

Due to the corrosion process and the ICCP system currents, electric fields exist around the ship. These fields are called the electric signature. The signature is measured by naval mines in order to detect ships. For naval ships the signature should therefore be minimised, but preferably without compromising the corrosion protection. In order to do this optimisation it is important to know the damage distribution of the underwater part of the hull, as current finds its way to damaged parts. Preferably, this damage distribution is determined using an on-board system. Future naval ships will have a system that assesses and manages the fields around the ship and keeps the resulting threat within safe limits. Determination of the damage to the hull will be one of the subsystems of such a system. Also from an economic point of view it is interesting to be able to determine a damage distribution without docking or divers. The main question is: To what accuracy and with what measurements can the damage distribution on a ship's hull be reconstructed? These measurements could comprise measurements of fields at the ship's hull and data from the ICCP system. Up to this day a system using on-ship measurements for determining damage distribution on the underwater hull has not been developed.



Figure 1.3: A sacrificial anode, an ICCP anode, and a reference electrode, obtained from [6]. The width of the sacrificial anode is 1 m.



Figure 1.4: ICCP anode and shield around it, obtained from [6].

This thesis develops a method for determining the underwater damage distribution of a ship's hull using only on-ship measurements, and verifies this method both with simulations and using scale-model tests. In chapter 2 an introduction to the chemistry and the historical research is given. After this the research questions are posed. In chapter 3 explores the nature of the problem and gives a general outline for the solution. In chapter 4 analytic and numeric methods are developed for determining the damage distribution using ICCP system measurements, and simulation experiments with these methods are explained. In chapter 5 a brute force method for damage reconstruction is developed and simulations are conducted on actual ship geometries. In chapter 6 the development of a scale model testing facility and experiments with a scale model are explained, and the results shown. In chapter 7 the conclusions of the entire research are summarised. In chapter 8 recommendations are given for further research.

2

Theoretical framework

This chapter gives an introduction to the chemistry used in this thesis, mainly for the nomenclature. Also an overview of historical research is given.

2.1. Electro-Chemical basis

When an unprotected vessel is put in seawater, the most active parts of the hull will corrode. If noble parts, like bronze propellers, are present, these will become cathodes in a galvanic cell consisting of the hull, the noble metal and the sea as electrolyte. The corrosion reaction consists of an oxidation reaction



and a reduction reaction, either



or



depending on the pH of the water. For the full reaction a change in Gibbs free energy ΔG can be calculated, but this change in Gibbs free energy can also be measured as a potential difference ΔU between the half reactions (2.1) and (2.2), because

$$\Delta G = -n^e F \Delta U. \quad (2.4)$$

Here n^e is the number of electrons exchanged and F is the Faraday constant. The Gibbs free energy of reduction for the half reactions can be influenced by an electric potential, that is by injecting electrons. If the applied potential is low enough, the change in Gibbs free energy becomes positive and the corrosion will not happen spontaneously any longer. An ICCP system injects a current in the water that finds its way to corroding spots. This system tries to keep the oxidation half-reaction (2.1) at a certain safe potential compared to a reference. This reference is usually a Ag/AgCl reference cell, described by the reaction:



This reaction has a very well known reduction potential. Several reference cells are usually distributed on the vessel. One lead of a voltmeter is then welded to the hull and the other to the reference cell. This way it can be measured if the ship, at the location of the measurement, is safe from corrosion.

The actual rate of corrosion is not linearly dependent on the potential. Where the potential is governed by thermodynamics, the corrosion rate is governed by kinetics. The resulting relation is highly complex and dependent on the pH, the speed of the vessel, the oxygen

concentration in the water and the history of corrosion, to name the important ones. The rate of corrosion can be measured as a normal current density J^n . The potential difference with reference to the Ag/AgCl reference cell is a voltage and is denoted with V . The curve of the relation $J^n = p(V)$ is called the *polarisation curve*. This polarisation curve is usually experimentally obtained for bare materials. If a material is not fully exposed the *damage fraction* $0 \leq \delta \leq 1$ is defined to be linear with the current density: $J^n = \delta \cdot p(V)$. The distribution of the damage fraction over the entire hull is called the *damage distribution*[10, 15].

An ICCP system causes currents to flow and charge to appear around the vessel. These currents and charges are associated with an electric field distribution and an electric potential distribution, via the Poisson equation

$$\nabla^2 V(\vec{x}) = -\nabla \cdot \vec{E}(\vec{x}) = \frac{-q(\vec{x})}{\varepsilon(\vec{x})}, \quad (2.6)$$

and Ohm's law

$$\vec{J}(\vec{x}) = \sigma(\vec{x})\vec{E}(\vec{x}), \quad (2.7)$$

which in the geometry of the vessel are subject to several kinds of boundary conditions. The main question is whether from measurements of the currents, charges, potentials or fields around the ship, the sources of the corrosion currents, that is the damage distribution, can be reconstructed. For the description of this problem the system and the outcome are known, but the boundary conditions are not. Therefore these type of problems are referred to as *inverse problems*.

The Poisson equation (2.6) is a second order differential equation. For this equation three different types of boundary conditions can be applied: Dirichlet (fixing V), Neumann (fixing J^n) and Robin (fixing the relation between V and J^n , for example using a polarisation curve). A specific inverse problem might often be defined in more than one way using different combinations of boundary conditions.

2.2. Historical research

Tokyo Institute of Technology 1987-1993

The idea of using measurements of the ICCP system for estimating damage to the object protected by the ICCP system appears for the first time in literature in an article from 1989 [16]. In this article it is explained how a boundary element method (BEM) can be used for the inverse problem. This article was written by three researchers of the department of mechanical engineering of the Tokyo Institute of Technology: Kishimoto, Miyasaka, and Aoki. Some years before these three had already come up with the idea of using BEM for making models of corrosion. This research was published in Japanese and in English [4, 22].

In the proposed method measurements of the electrical potential are taken near every element in the water, for the anode a Dirichlet boundary condition is taken and then the current density at the hull can be reconstructed.

The results are then not quite good yet, but they can be improved by regularisation of the matrix by singular value decomposition and the estimation of the effective rank of the matrix. A slightly improved version of this model was presented in a book in 1993 [3].

Universidade Federal do Rio de Janeiro 1991-2016

About the same time as research was going on in Japan, in Brazil researchers of the faculty of civil engineering of the Federal university of Rio de Janeiro were also researching the application of BEM to the description of corrosion. They were civil engineers whose main concern was prediction if a structure would last, developing methods for an analysis over time[28, 29]. An important conclusion was that polarisation curves might change over time and that they are a complex result of the electrochemical history.

In more recent years this department again started to do research on this subject, now employing a method of fundamental solutions (MFS) in combination with a genetic algorithm for optimisation [30–32]. For this method the polarisation curve is assumed to be known

very precisely. This is used to construct a Robin boundary condition at the hull. The genetic algorithm makes the process rather slow. In [31], published in 2014, it is mentioned work is done on the inverse problem using MFS and that it will be published later, but they have as of yet not done so.

Brunel University Uxbridge 2000-2004

Between 2000 and 2004 research into inverse corrosion problems using BEM has been done at Brunel University in Uxbridge, UK. In [20] the authors give a method for determining the polarisation curves of a structure protected by a cathodic protection system. This method is a BEM-based genetic algorithm. The BEM problem is written down using Robin boundary conditions and some shape of the polarisation curve is assumed. Some sensors are placed on the cathode and anode, the genetic algorithm alters the parameters of the polarisation curve until the outcome fits these constraints. The polarisation curve can then be converted to a corrosion state. It has to be noted that here both the number of sensors (5) is low, and the number of unknowns is low (4). In [19] the very same method is explained in more detail, but this time applied to optimal anode positioning. In [21] this method is applied specifically to the detection of coating defects in cathodically protected underground pipelines. Here the sensors are located all on the same side of the pipe and some distance away from the pipe. This way, a lot of sensors are needed. 15 sensors in order to detect a mere 4 defects in their 2D model and 24 sensors to detect and localize damage in one of the 512 elements in their 3D model. But in this process anode information is not taken into account. Some important assumptions are however taken: The conductivity of the intact coating is taken to be 0, it is assumed the number of defective elements does not exceed a certain threshold and that an element is either fully defective or not. Still the results are rather sensitive to noise. In [43] they repeat a part of the previous paper, elaborate on their method and also show the application on a ship.

BEASY Ltd, Southampton 2001-2005

In the UK there is a company called BEASY Ltd. that develops modelling software for cathodic protection and signature problems. In [23] the authors from this company develop a method of optimising the performance of an ICCP system by optimising anode positions and currents. In [26] and [24] a method is developed for determining the damage to the coating of a ship. It also uses BEM and an iterative optimisation routine. An assumption of the coating damage is made, then the BEM equations are calculated. The outcome of the voltages at reference cell positions is calculated and fed into the objective function. This objective function is the error between the calculated potential at reference cells and the measured potential. That outcome goes to the optimisation routine, Sequential Linear Programming. This is a multivariable search method, and it uses Taylor series approximations of polarisation curves to construct Robin boundary conditions. This routine then changes the damage distribution and the process repeats. What is important to this method is that not all elements on the surface of the ship are altered by the optimisation routine. Instead, only in seven points the coating is altered, and in between the coating state is interpolated. This way the number of design variables is reduced by a large amount. The results however are still quite good, multiple defects of different sizes are still detected and localised. The quality of the solution increases with the number of reference cells and with the number of coating points, but optimal results are obtained when the ratio between them is about 1:2. The report [24] a somewhat more elaborate explanation of the method of article [26] is given, with more examples and figures. In their next papers they continue their work, showing how the signature is minimised given known damage [27], and how given known damage the anodes of the ICCP system are placed in an optimal way [25].

French Military

At the end of the last decade research has been done into damage estimation of a ship's hull in France by the military in collaboration with a university. In 2009 an article was published on corrosion diagnosis based on measurements of the electric field some distance away from the ship [12]. An inverse BEM model is constructed, but the number of points where the

field is measured (3-axes) is 1400. They use Tikhonov's regularisation method to regularise the system of equations. The results are overall very good and precise, except near the propellers because of the complex geometry.

In [13] this method is explained in more detail and the method for test on scale models is explained.

More details still as well as information on the research leading to this model can be found in the Ph.D. thesis of Guibert [11].

Korean Military

The Korean Military, in collaboration with some universities, have done extensive research into electric and magnetic signatures, and into ways to minimise them. Most of their publications are on the magnetic signature, but they have one remarkable publication on inverse electric modelling [9]. Remarkable because their method differs somewhat from the others. Instead of using a BEM they use what they call a *material sensitivity analysis* which is a cascade of the Augmented Lagrangian Method and the Adjoint Variable Method. The underwater surface of the hull is divided into elements and some measurement line under the ship is chosen. On this measurement line electric field vectors are measured. No sensors on the ship are used. The hull is modelled as a Neumann boundary. The number of observation points was 303 and the number of mesh elements on the hull was 1101. The results of this method are quite detailed and very good. For off-ship measurements this Korean method outperforms the French one. This Korean method was also applied to inverse magnetic problems [8, 14, 45].

German Military

The German military in recent years also took interest in electric and magnetic signature prediction and management. They outsourced research into this subject mainly to the University of Duisburg-Essen. The main focus of this work was on the prediction of signatures in a changing environment [33]. However, last year in a presentation [37] they showed an idea for an inverse model. It was not yet a full inverse method, but by adding current sensors to the ICCP anodes they could predict the direction and distance of damages on the hull. The fact that they used current sensors and not potential sensors was the main new idea in this presentation.

Other Sources

Beside the sources mentioned several others have written on the subject of damage prediction using measurement of the ICCP system and the inverse electric model of vessels. These include an Iranian oil company [1], the Chinese Military [44], the Chinese Offshore Oil Company [40], and some more Japanese and Brazilian researchers [2, 18]. They all have in common that they use BEM and that their papers do not present actual new information.

2.2.1. Conclusions from the literature

Conclusions can be drawn from the literature.

Concerning the problem of the reconstruction of damage to the hull from measurements on the ICCP system. This problem has been solved with different types of input data:

- With external sensors (French and Korean research);
- With sensors on the hull (Japanese, German, Brazilian, and Uxbridge Research);
- Without extra sensors (Southampton Research).

The problem has been solved in different fashions:

- Using a Boundary Element Method (Most common);
- Using a Method of Fundamental Solutions (Brazilian research);
- Using a Material Sensitivity Analysis (Korean research);

- Using a Finite Element Method (No one as of yet, but it could probably be done).

And using a very diverse range of optimisation algorithms. Of these solutions only the BEM based solution with external sensors has been prototyped.

More input data from measurements leads to better results. For this research however no external sensors can be used, as the problem has to be solved out at sea, without interfering with the mission of the ship. This has also been proven possible, but the amount of sensor data needed for a certain accuracy remains unknown.

Another conclusion is that all inverse problems can be solved in the same way, because they are in effect the same problem. All of the following problems have in common that the system is known and the boundary conditions are not:

- localisation of damage to the hull;
- reconstruction of polarisation curves;
- optimal positioning and setting of anodes.

It can also be concluded that some questions remain unanswered:

- What type of discrete model of the ship is best suited for inverse analysis?
- What sensors are needed for accurate damage reconstruction, how many of them, and where should they be located?
- How can a damage reconstruction method be verified?
- How can a damage reconstruction method be implemented in the ICCP system or signature management system?

2.3. Research questions

Given the conclusion from the literature the research question of this thesis is:

To what accuracy and with what measurements can the damage distribution on a ship's hull be reconstructed?

With subquestions:

- What type of mathematical model is best suited for inversion?
- Can a damage reconstruction method be implemented on a scale model?
- How could a damage reconstruction method be implemented on a ship?

The research focuses on two major topics: the development of a mathematical model and the development of a scale model facility. In the end these are connected so the scale model experiments verifies the mathematics developed.

3

Inverse Problems and Methods

3.1. Introduction

Forward problems are problems where the system and the boundary conditions are known and the outcome, the derived quantities, are not. Inverse problems are problems where some part of the outcome is known, but either the system or its boundary conditions are not. For the problem in this study the boundary conditions at the hull are unknown, and therefore it is an inverse problem. This chapter explores the nature of the problem and develops a general approach for solving it.

3.2. On ICCP systems

Several sources of data for construction of an inverse model are available. To see where they originate a brief look into the ICCP system is needed. In order to illustrate the functioning of an ICCP system a model of a one meter long ship is taken as illustrated in fig. 3.1. This ship

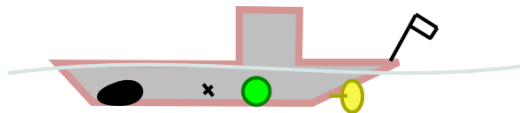


Figure 3.1: Illustration of ship model used in this section with along the hull from left to right: coating damage, reference electrode, ICCP anode, propeller.

has an ICCP system with one anode and one reference electrode. The system controls the anode current as to keep the voltage at the reference electrode in safe range (between -0.75 and -0.85 V to silver-silverchloride ($Ag/AgCl$)). In this safe range no corrosion on the hull will occur; at higher voltages the hull corrodes, and at lower voltages hydrogen is produced, which damages the coating. Initially all the current of the anode flows to the propeller of the ship, the voltage distribution along the keel of this situation can be seen in fig. 3.2a. Then a hole is made in the coating of the ship, and the voltage distribution changes (fig. 3.2b). The voltage measured by the reference electrode is now -0.4 V which is much too high. The ICCP system responds by increasing the current of the anode, so the voltage becomes safe again (fig. 3.2c). At each step the signature changes. In general a higher amount of damage results in a final situation with a higher signature.

When the damage distribution is unknown, some quantities are still known. These are:

- reference electrode voltages;
- anode currents;
- currents at reference electrodes, shields, and other non conductive parts. (0 A);
- uncoated metal polarisation curves.

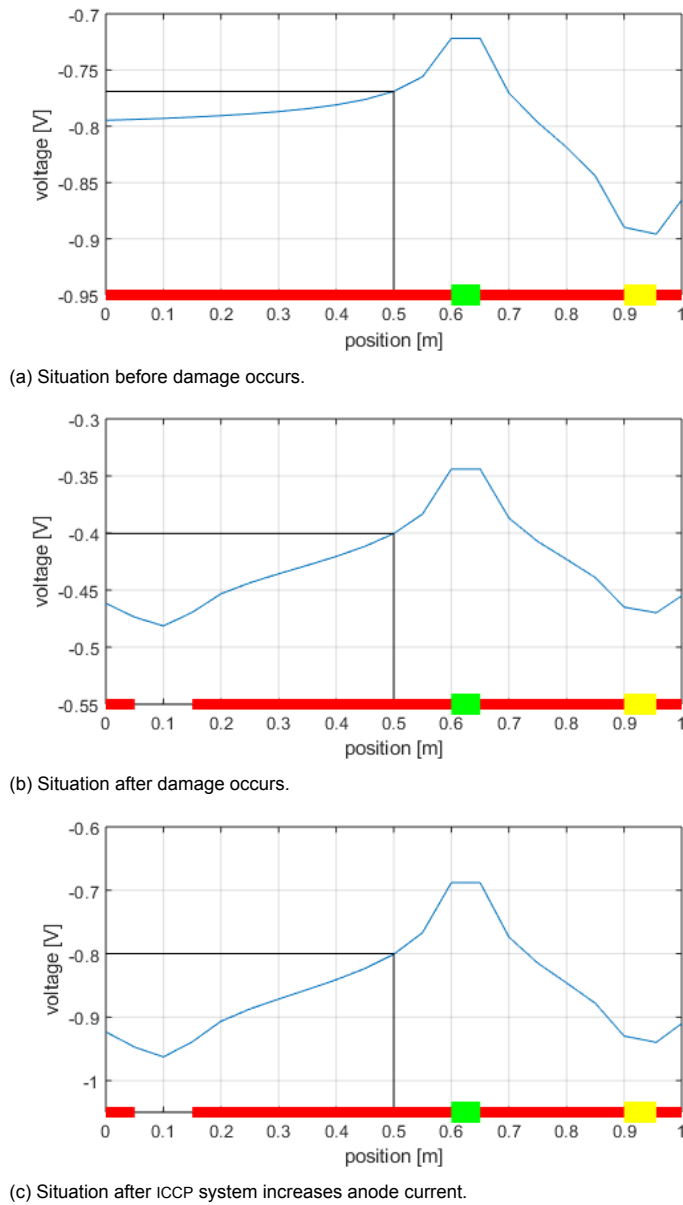


Figure 3.2: Illustration of how an ICCP system reacts to damage occurring Blue graph: voltage on the hull for positions between 0 and 1 m. Bars on x-axis: red = coated part, green = anode location, none = damage, yellow = propeller.

Especially the first two will have something to reveal about the damage distribution. More data is obtained as the anode currents are varied and the reference electrode response is measured.

3.3. Ill-posed problems

The solution to the problem of reconstructing a damage distribution from measurements of fields or potentials caused by the ICCP system is not a straightforward one. The forward problem, given a damage distribution, polarisation curves, and ICCP system settings solving the potentials and fields, as done for the ship in the previous section, has always a unique solution. Furthermore this solution is continuous with the inputs in the mathematical sense. If the damage distribution or the ICCP currents are changed a little, the fields and potentials will only change a limited amount. Because of these two facts, that always a unique solution exists and the continuousness of this solution, the problem is called *well-posed* in the sense of Hamadard[38].

The inverse problem does not meet these criteria. For a given set of measurements of potentials and fields, known polarisation curves, and ICCP currents, multiple solutions for the damage distribution exist. In fact, an infinite number of solutions exist, illustrated for a simple configuration in fig. 3.3. In this figure three different one-dimensional damage distributions are shown, all with an anode between $x = 0.6$ and $x = 0.65$ m supplying 10 mA and reference electrode measuring at $x = 0.5$ m.

Because the inverse problem does not meet the criteria for well-posedness it is called *ill-posed*. In order to solve this problem the solution space has to be narrowed down or altered in such a way that only one solution remains. This is called *regularisation*.

3.4. Solutions

In this chapter three solutions to the inverse problem will be developed.

First will be the *analytic* model. This will be a model using simplified physics and a simplified geometry. It will serve the purpose of exploring the limits of inversion, answering the research question for an ideal scenario.

Second is the *numeric* model. This model attempts to invert a numerical model of the full physics and geometry. After the model is obtained, all research questions can be answered. Third is the *brute force* model. This model is not truly an inverse method as it solves the inverse problem by repeatedly solving the forward one. The damage distribution is described using a number of parameters, and the optimum of these parameters is found by solving the forward problem repeatedly, until it reaches the optimum. It will have the disadvantage that it is slow, but it is known from literature that it can work, and therefore it can be used for answering several of the research subquestions.

3.4.1. Evaluation metric

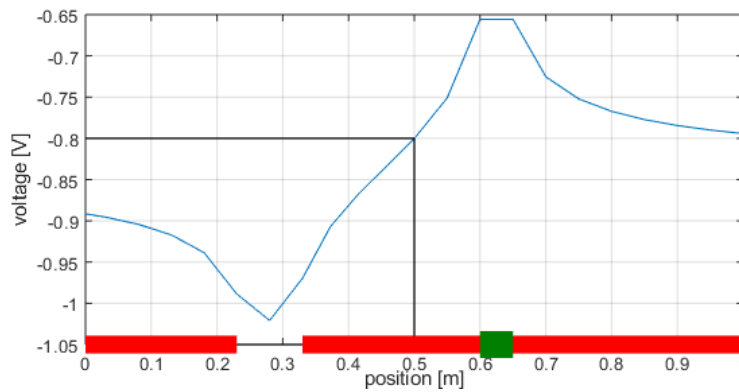
Before a method is developed its objectives have to be defined as well as a metric for quantification of the fulfilment of an implementation of the method. Because the damage reconstruction is to aid the purpose of signature estimation the objective is formulated in these terms. The objective of the method is:

To convert the quantities measured by the ICCP system of a vessel, possibly augmented with additional reference cells, using a description of the geometry of the vessel and a description of the physics involved, into a damage distribution on the hull, such that the electric signature at code depth is correctly predicted.

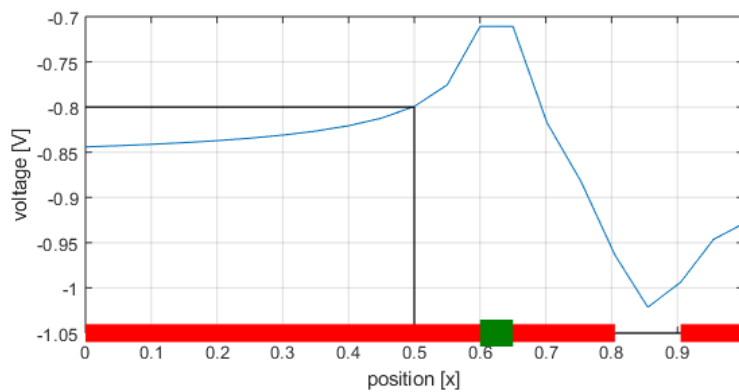
Here code depth is defined as the distance below the waterline that is equal to the width of the ship.

This is to be evaluated using this metric:

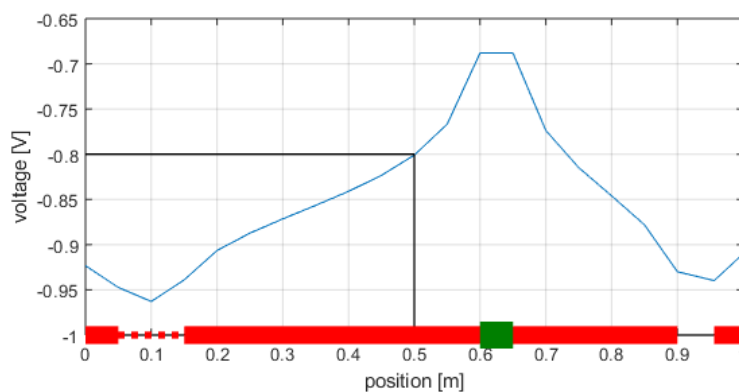
The normalised root-mean-square error of the predicted signature at code depth on a rectangle that is the projection of the vessel on



(a) 100% damage between $x = 0.23$ and $x = 0.33$ m.



(b) 100% damage between $x = 0.805$ and $x = 0.905$ m.



(c) 50% damage between $x = 0.05$ and $x = 0.15$ and 100% damage between $x = 0.9$ and $x = 0.965$ m.

Figure 3.3: Three damage distributions that give the same potential measurement *ceteris paribus*. Blue graph: voltage on the hull for positions between 0 and 1 m. Bars on x-axis: red = coated part, green = anode location, none = 100% damage, dotted red = 50% damage.

the code-depth plane plus twice the width of the ship on all four sides added, evaluated at evenly spaced points.

This RMS error will be named the signature error, denoted by the symbol E . Another metric for the evaluation of signature is more commonly used when evaluating the threat of detection. This second metric is:

The absolute error of the maximum of the norm of the predicted signature at code depth.

Because when assessing the threat of detection caused by the signature mainly the maximum value of the signature is important. The second metric will be calculated, but for the purposes of this thesis it will prove not to be very insightful because the maximum value of the signature is without exception dominated by the anodes and the propellers, which do not have to be reconstructed. If propellers in the future are coated, then this second metric will be relevant.

It has to be noted that it is unknown how ship detection by electric signature works in actual mines, and therefore simple general metrics are chosen for the scope of this research.

3.4.2. Structure of inverse methods

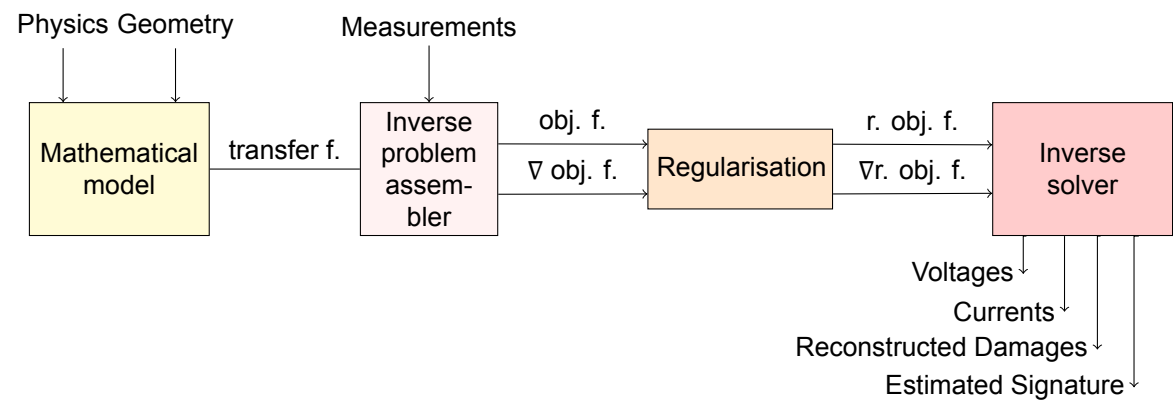


Figure 3.4: Block model of the method. transfer f. = transfer function, obj. f. = objective function, ∇ obj. f. = gradient of objective function, r. obj. f. = regularised objective function, ∇ r. obj. f. = gradient of regularised objective function.

The analytical and numeric methods will consist of four parts, these are pictured in fig. 3.4. Input to the method will be a physical description and a geometric model of the system and a set of measured quantities. The output of the model has to be a damage distribution on the surface of the geometry.

First, a mathematical model has to be made that incorporates both the geometry of the problem and the physics that have to be evaluated. This mathematical model has to produce a transfer function from damage fraction to measurements by reference electrodes at the hull.

The second part is the inverse model assembler. Using the transfer function and measurement data an error function can be defined. This error function is a measure of the difference between the voltages at the reference electrodes due to the input of the model and the true measured voltages at those electrodes.

The next part of the model adds a regularisation term. As the inverse problem is ill-posed extra equations or conditions may be enforced in order that certain solutions will be preferred over other ones.

The fourth part of the method is the solver of the inverse problem. This solver takes the regularised problem and tries to find an optimum for the error function. The output of this solver is a voltage, current and damage distribution.

The intention is to develop these parts or blocks of the method in an orthogonal way with well-defined interfaces between them. This way each part can be optimised separately without affecting the other parts [39]. Also different implementations of the same part can

easily be interchanged. Especially for the mathematical model block this is important; the mathematical model of a ship will be a big and slow numerical model and for the development of the other blocks and rapid testing a dummy mathematical model will be used that is representative but much simpler and faster.

In order to validate the entire method twin experiments will be conducted. This means the same model will be used to generate “measurement data” and to solve the inverse problem. A modified version of the block model of the method can be seen in fig. 3.5.

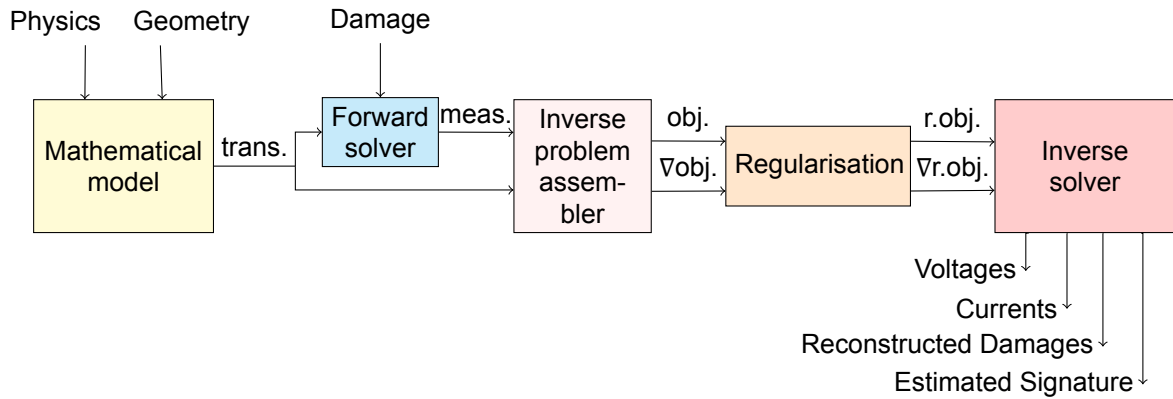


Figure 3.5: Decomposition of the method. trans. = transfer function, meas. = measurements, obj. = objective function, $\nabla \text{obj.}$ = gradient of objective function, r. obj. = regularised objective function, $\nabla \text{r. obj.}$ = gradient of regularised objective function.

The brute force method will be entirely different from the other methods as will not actually attempt inversion. A function will be constructed that describes the damage distribution on the entire geometry by a limited number of parameters. By iteratively running the forward (well posed) model with different parameters, these parameters can be optimised. The optimum of the parameters will then be the reconstructed damage distribution. The structure of the brute force method can be seen in fig. 3.6.

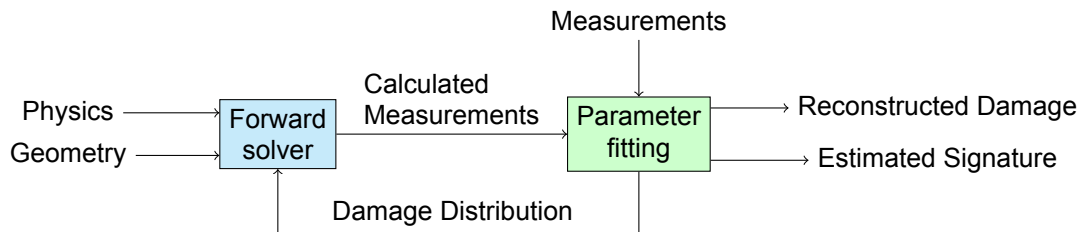


Figure 3.6: Structure of the brute force method.

4

Analytic and Numeric Methods

4.1. Introduction

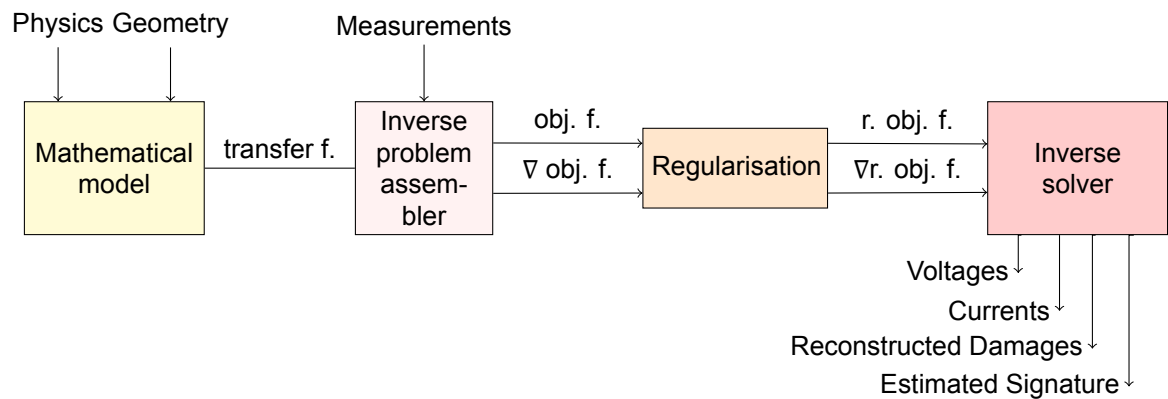


Figure 4.1: Block model of the method. transfer f. = transfer function, obj. f. = objective function, ∇ obj. f. = gradient of objective function, r. obj. f. = regularised objective function, ∇ r. obj. f. = gradient of regularised objective function.

In this chapter two inverse methods are developed. The first is the analytical method which is used for exploring the limits of these methods. Second is the the numerical method, a full inverse method. Both methods have the structure of fig. 4.1. In this order they are developed. After this both methods are used in simulations.

4.2. Mathematical model

The mathematical model integrates the physics involved in the problem with the geometrical description of the system under evaluation. The output of this model will be a transfer function. This transfer function takes a damage distribution as input and the corresponding measurement values as an output. The block view of the mathematical model can be seen in fig. 4.2. In this section the physics is explored and a numerical model derived, as well as an analytical dummy model developed.

4.2.1. General physical description

This subsection gives the physical description of the system, and derives the equations that have to be solved.

The system under review is an electrostatic one. It can be described by two of Maxwell's equations, Gauss's Law for Electricity:

$$\nabla \cdot \vec{D} = q, \quad (4.1)$$

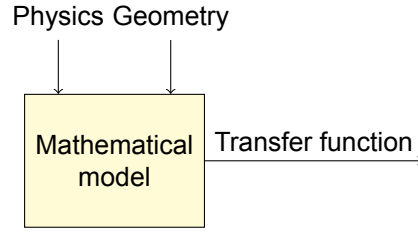


Figure 4.2: Block view of the mathematical model

and Faraday's law:

$$\nabla \times \vec{E} = \vec{0}. \quad (4.2)$$

Here q is the volumetric charge density in C m^{-3} , \vec{D} the electric flux density in C m^{-2} and \vec{E} the electric field strength in V m^{-1} .

In a linear medium the constitutive relation holds:

$$\vec{D} = \varepsilon \vec{E}, \quad (4.3)$$

where ε is the electric permittivity in F m^{-1} .

The electric (scalar) potential is defined as:

$$\nabla V = -\vec{E}. \quad (4.4)$$

This definition ensures that Faraday's law (eq. (4.2)) is met as $\nabla \times \nabla V = 0$ by the curl-gradient identity.

Equations (4.1), (4.3) and (4.4) result in Poisson's equation:

$$\nabla^2 V = -\nabla \cdot \vec{E} = \frac{-q}{\varepsilon}. \quad (4.5)$$

This is the partial differential equation that has to be solved numerically over the entire domain. Furthermore, considering conducting media in electrostatics Ohm's law holds:

$$\vec{J} = \sigma \vec{E}. \quad (4.6)$$

Where σ is the electric conductivity in S m^{-1} .

Using eq. (4.5) and eq. (4.6) current sources can be described:

$$\nabla \cdot \vec{J} = \sigma \cdot \frac{q}{\varepsilon}. \quad (4.7)$$

This now is a very misleading equation. The units are A m^{-3} , a current emerging from a volume. This means, if there is a domain Ω and a volume $\omega \in \Omega$ that is consubstantial with its surroundings, having parameters ε and σ , and if the boundary of ω is called γ , we can write eq. (4.7) as

$$\iiint_{\omega} \nabla \cdot \vec{J} d\omega = \iiint_{\omega} \sigma \cdot \frac{q}{\varepsilon} d\omega. \quad (4.8)$$

Then by Gauss's theorem

$$\oiint_{\gamma} \vec{J} \cdot \hat{n} d\gamma = \sigma \cdot \frac{Q}{\varepsilon}. \quad (4.9)$$

This source, giving rise to currents on the boundary γ of ω , can be described to have a charge Q as source inside ω . Here on both sides of the equation the unit is A, $\sigma \cdot \frac{Q}{\varepsilon} = I$

If the volume ω is made infinitesimally small, this means the current I originating in a material with parameters ε and σ can be represented by a point charge of magnitude $Q = \frac{\varepsilon \cdot I}{\sigma}$. This is actually how it is done in simulation software like comsol.

It is important to note that throughout this chapter a DC model is assumed. The charge

Q has to be a constant in order for the current distribution to be constant. However this means that the charge of which the current consists is created *ex nihilo*, which *violates the conservation of charge*. In these points

$$\nabla \cdot \vec{J} \neq 0. \quad (4.10)$$

In any physical system modelled currents can only appear out of nothing on the boundary of the modelled system. Boundary current sources can be modelled as charges.

If there exists an interface between a material 1 with permittivity ε_1 and conductivity σ_1 , and material 2 with permittivity ε_2 and conductivity σ_2 . And if there is a known normal electric field $\vec{E}_1 \cdot \hat{n}$ in material 1. What happens at the interface in normal direction can be described as

$$\varepsilon_1 \vec{E}_1 \cdot \hat{n} - \varepsilon_2 \vec{E}_2 \cdot \hat{n} = q^A, \quad (4.11)$$

and

$$\vec{J}_1 \cdot \hat{n} - \vec{J}_2 \cdot \hat{n} = \sigma_1 \vec{E}_1 \cdot \hat{n} - \sigma_2 \vec{E}_2 \cdot \hat{n} = 0. \quad (4.12)$$

For under static conditions, by definition, no charge is built up on the interface. For a known \vec{E}_1 , \vec{E}_2 and q^A can be calculated. If $\nabla \frac{\sigma}{\varepsilon} = 0$, $q^A = 0$, but otherwise under static conditions a field dependent charge will exist on the interface. This induced charge will have to be taken into account in the model.

The time constant of the process of the build-up of these charges can be approximated as

$$\tau \approx \frac{\varepsilon}{\sigma}. \quad (4.13)$$

With the σ and ε of the material with the highest conductivity. If this material is seawater $\tau \approx 10^{-9}$ s. Therefore the time-dependency of charge build-up on boundaries can be ignored.

Different types of boundary conditions can be implemented

- D0: $V = 0$
- D1: $V = V_1$
- N0: $\frac{\partial V}{\partial n} = 0$ ($\vec{J} \cdot \hat{n} = 0$)
- N1: $\frac{\partial V}{\partial n} = \frac{1}{\sigma} \vec{J}_1 \cdot \hat{n}$
- C1: $V = V_1$ and $\frac{\partial V}{\partial n} = \frac{1}{\sigma} \vec{J}_1 \cdot \hat{n}$
- R0: $V - p^{-1}(-\frac{\sigma}{\delta} \frac{\partial V}{\partial n}) = 0$

The first two being of the Dirichlet type, the next two of the Neumann type, C1 of the Cauchy type, and the last one of the Robin type. The ICCP anodes are current sources, so of type N1. The boundaries at the reference electrodes, the waterline, the infinite sea and infinite seabed would be of type N0, for no current escapes the modelled system in those places. The hull of the ship and the sacrificial anodes can be described by a Robin boundary condition because for the corrosion process:

$$\vec{J} \cdot \hat{n} = \delta p(V), \quad (4.14)$$

$$\sigma \vec{E} \cdot \hat{n} = \delta p(V), \quad (4.15)$$

$$-\sigma \frac{\partial V}{\partial n} = \delta p(V), \quad (4.16)$$

$$V - p^{-1}(-\frac{\sigma}{\delta} \frac{\partial V}{\partial n}) = 0. \quad (4.17)$$

Where the function p describes the (non-linear) polarisation curve of a fully uncoated surface, and δ is the damage fraction. $\delta = 0$ denotes a fully coated surface, and $\delta = 1$ denotes a fully uncoated surface.

4.2.2. Numerical method classification and selection

There are many numerical methods for solving partial differential equations, especially when they are of the Poisson kind. Wikipedia for instance lists 48 methods at the moment of this writing [41], though ordered somewhat idiosyncratically. The same method also might have very different names in different disciplines of engineering. Many of the methods are alike, some are very different, and not all of them can be used. In order to choose the best one they have to be categorised and criteria for selecting the best one have to be chosen.

The selection of the model will be done on the basis of these criteria:

1. Suitable for the problem's geometry and physics;
2. Usable for inverse problems;
3. Fast computation times;
4. High precision;
5. Straightforward and fast implementation;
6. Easy integration into other models.

Uniform or Nonuniform Node Distribution The easiest and fastest methods for solving partial differential equations (PDEs) are a number of finite difference methods (FDMs). These methods use a uniform discretisation of the domain. This however only works well if the domain has a simple shape, so no curved or complex boundaries. Although the material of the domain can be inhomogeneous or anisotropic when using FDM, uniform discretisation is usually inappropriate when material parameters change by orders of magnitude or when sources are located only in one place. Because the hull of the ship has a complex geometry, methods employing uniform node distribution are not suitable.

Element-by-Element or Node-by-Node computation Numerical methods for solving PDEs can either solve the physics on every node or on elements between the nodes. An element-by-element description is usually both more straightforward and computationally easier. When calculating the deformation of a domain, elements change shape, making an element-by-element description both hard to implement and inefficient to use. For this reason methods employing a node-by-node computation exist, these methods are usually called 'mesh-free'. In literature a meshfree method called method of fundamental solutions (MFS) is used for the problem [31]. Although there appears to be no very good reason for using meshfree methods, it is an option.

Domain or Boundary Mesh Some numerical methods for solving PDE, such as the finite element method (FEM) make a mesh on the entire domain of the problem. Others, such as the boundary element method (BEM) and the method of fundamental solutions (MFS) make a mesh only on the boundary of the domain and do not mesh the interior. This can only be done when the interior of the domain is homogeneous, isotropic and source-free. Only having to mesh the boundary is an obvious advantage, 'why mesh the domain if you don't have to?'. This advantage is however a superficial one. A method using only a boundary mesh will result in a system of equations in which all unknowns depend on all equations, giving a full matrix. For methods with a domain mesh, elements have only interaction with their direct neighbours and therefore the matrix will be very sparse. When using the same number of elements on the boundary using FEM and BEM, say N , BEM will require memory and runtime in $\mathcal{O}(N^2)$ whereas FEM will require only $\mathcal{O}(N\sqrt{N})$. Therefore in practical situations BEM and its meshfree version MFS only outperform FEM when the ratio boundary-to-volume is very small. If the mesh is refined, at some point FEM will always outperform BEM, but it might be hard to determine at what level of detail this would happen. The advantage of BEM over FEM for small meshes has led to a wide adoption of this method in literature, see chapter 2.

Choice Considering the requirements it has been chosen to use a finite element method, because it meets the criteria best. It can be used with complex geometries, it is computed element-by-element, and it has a domain mesh. Furthermore all models used within TNO are FEM-based and available in comsol's multiphysics software. Also the author is well-aquainted with FEM. The implementation is straightforward. The full implementation is explained in appendix A.

4.2.3. Analytical method

An analytical model is developed in order to gain understanding of inverse problems, and to have an extra tool for calculating field and potential distributions for simple geometries.

Given the plane $z = 0$, and the half-space below it $z > 0$. As the seawater is by convention in the positive z direction, that half is taken. The material of $z > 0$, is homogeneous, isotropic, and has permittivity ε and conductivity σ . The plane $z = 0$ is a perfect electrical insulator, therefore $\vec{j} \cdot \hat{z} = 0$ when considering a direct current (DC) situation. This is a natural Neumann boundary condition. In the plane is a lattice of nodes of some kind, and within a closed domain on the plane the nodes of the lattice are numbered 1 to n .

On all of these points small hemispherical current sources exist. They are not point sources as the current goes only into the seawater, in half of the directions. If the radii of the hemispheres are small they do not influence the fields. The potential in point k caused by such a source in point r is described by

$$U_{k,r} = 2 \cdot K \cdot \tau \cdot \frac{I_r}{\|\vec{x}_r - \vec{x}_k\|} = \frac{I_r}{2\pi\sigma\|\vec{x}_r - \vec{x}_k\|} \text{ for } \vec{x}_r \neq \vec{x}_k. \quad (4.18)$$

In this equation U is the electric potential in J C^{-1} , this is the energy needed when moving a charge to this point source. Furthermore K is coulomb's constant ($8.9876 \cdot 10^9 \text{ N m}^2 \text{ C}^{-2}$), τ the material time constant in s, I the current of the source in A and \vec{x} the position. The factor 2 arises from the fact that the current is injected in only half the sphere, 2π sr. The positive direction for the current is in positive z direction, and the voltage drops when going from \vec{x}_r to \vec{x}_k . Note that these sources satisfy the boundary condition because the normal derivative of the potential in the plane is zero for this flat surface.

The observation point \vec{x}_k must not coincide with a source point \vec{x}_r as then the potential will not be defined. Therefore a second lattice of points will be used for observation of the potentials. The potential at a node k is then:

$$U_k = \frac{-I_1}{2\pi\sigma\|\vec{x}_r - \vec{x}_1\|} + \frac{-I_2}{2\pi\sigma\|\vec{x}_r - \vec{x}_2\|} + \dots + \frac{-I_n}{2\pi\sigma\|\vec{x}_r - \vec{x}_n\|}. \quad (4.19)$$

This can also be put into a matrix form:

$$U = R \cdot I. \quad (4.20)$$

Calculating the solution to the forward problem now is very straightforward. Note however that in no way current conservation is imposed on this system. Also no reference is yet chosen, this has to be done before applying Robin type boundary conditions. When the $Ag/AgCl$ reduction potential is chosen as a reference, the potential difference with the reference is the voltage V in V. Equation (4.20) can then be rewritten as

$$V = R \cdot I - U_\infty, \quad (4.21)$$

where U_∞ is the potential with respect to the $Ag/AgCl$ potential very far away from system. The fact that this potential is unknown, and cannot be measured straightforwardly, makes applying Robin conditions difficult. For the purpose of this model $U_\infty = 0$ is chosen. For a linearised Robin-type boundary condition goes:

$$\frac{1}{\alpha_r} I_r = \delta_r \cdot p^1_r V_r + \delta_r \cdot p^0_r. \quad (4.22)$$

Here $0 \leq \delta \leq 1$ denotes the damage fraction, p^1 and p^0 are the coefficients of the linearised polarisation curve and alpha is the surface area of the hemisphere. However, when combining eqs. (4.18) and (4.22) it becomes impossible to describe the influence of a Robin node on another node. The system must be rewritten.

Using eq. (4.18) and reversing cause and effect. The entire system of equations could be written:

$$R^{-1} \cdot V = I \quad (4.23)$$

In this system of equations Robin boundary conditions can be added as an entry in R^{-1} . This however requires two matrix inversions. One to make R^{-1} , then add the boundary conditions and invert again to solve the system. R^{-1} cannot be compiled directly as the currents cannot be written in terms of the voltages as the voltages are continuous and the currents discrete. The entries in R after this process are not insightful as they bear no direct relation to the geometry any longer. Given the difficulties of the implementation of Robin type boundary conditions, and that doing so would not aid the purpose of the analytical model, making inversion insightful, it is not done. Instead damages are added as a distribution of current sources, like the anodes, which are Neumann boundaries.

In summary the analytical model is a tool for evaluating methods of inversion that can be applied on Neumann problems on a flat geometry, but not on Robin problems.

4.3. Inverse problem assembler

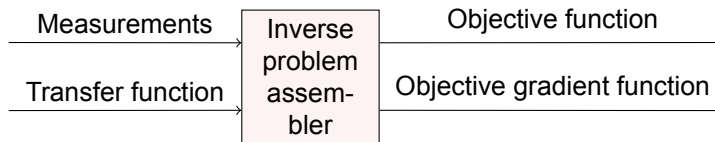


Figure 4.3: Block view of the Inverse problem assembler

The inverse problem assembler takes the transfer function and the measured data and generates an objective function, and if possible a gradient of that objective function as well. The structural diagram of this step can be seen in fig. 4.3.

4.3.1. Defining the error

The most common way to define the objective is the sum of the squares of all the individual errors made in the estimation of the measured voltages. This objective metric is known as the residual sum of squares (RSS). It is commonly used for optimisation problems. For a general problem

$$A \cdot u = f \quad (4.24)$$

The residual is defined:

$$\zeta(u) = A \cdot u - f. \quad (4.25)$$

And one tries to find the solution

$$u' = \arg \min_u \|\zeta(u)\|^2. \quad (4.26)$$

Here $\|\dots\|$ denotes the euclidean- or 2-norm. As this is the only norm used in this thesis the subscript 2 will be omitted and the subscript will be reserved for indices.

4.3.2. The use of the gradient

The gradient of ζ is important to know as for an optimum of a continuous function the gradient is zero:

$$\nabla(\|\zeta(u')\|^2) = 0. \quad (4.27)$$

Also if an evaluated point is not the solution, a new point for evaluation has to be chosen. To determine this point the gradient is required by some solver algorithms. Therefore the

gradient has to be evaluated by the solver of the inverse system. If the gradient is known analytically this evaluation is straightforward and very fast, for every evaluated point the gradient is evaluated once. If the gradient is not specified analytically it is usually evaluated using a finite difference approach, this requires two function evaluations per dimension of the gradient, and therefore it is very slow indeed.

4.3.3. Analytical model

For the analytical model the objective function can be defined in terms of the matrix R . The system is given as in eq. (4.21):

$$V = R \cdot I. \quad (4.28)$$

For the inverse method V has only to be calculated for locations of the measurement electrodes. So $V \in \mathbb{R}^m$ where m is the number of measurement points.

The vector I can be split in two parts. $I^a \in \mathbb{R}^{n_a}$ is the vector of known anode currents, usually these are only a few. $R^a \in \mathbb{R}^{m \times n_a}$ is the matrix that contains the entries from R corresponding to I^a . Likewise $I^c \in \mathbb{R}^{n_c}$ is the vector of unknown (cathode) currents, which is the larger part. $R^c \in \mathbb{R}^{m \times n_c}$ is the matrix that contains the entries from R corresponding to I^c . The system of eq. (4.28) can then be rewritten as

$$V = R^a \cdot I^a + R^c \cdot I^c. \quad (4.29)$$

V^m is the vector of measured voltages, then for a tested I^c the objective is

$$\|\zeta\|^2 = \|V^m - (R^a \cdot I^a + R^c \cdot I^c)\|^2 = \sum_{i=1}^m \zeta_i^2 = \sum_{i=1}^m (V^m - (R^a \cdot I^a + R^c \cdot I^c))_i^2. \quad (4.30)$$

Obtaining the derivative of this objective function is straightforward. Because the voltages V are proportional to the currents I^c by matrix R^c the Jacobian matrix of the residuals is simply R^c .

$$J(\zeta(I^c)) = \begin{pmatrix} \frac{\partial \zeta_1}{\partial I^c_1} & \dots & \frac{\partial \zeta_1}{\partial I^c_n} \\ \vdots & \ddots & \vdots \\ \frac{\partial \zeta_m}{\partial I^c_1} & \dots & \frac{\partial \zeta_m}{\partial I^c_n} \end{pmatrix} = -R^c \quad (4.31)$$

and the gradient of the objective becomes

$$\nabla(\|\zeta\|^2) = -2\zeta^T R^c. \quad (4.32)$$

4.3.4. Finite element model

In case of the FEM model the objective function can be written in a similar fashion as in the previous section. For the FEM model is given in the previous section

$$A \cdot u = f. \quad (4.33)$$

When inverting the problem the information of the polarisation curve equations is not present because the polarisation curve depends on the damage fraction, which is unknown. However, at some points the value of V , and thus the value of u is known. If these known values are added as Dirichlet conditions, the system becomes

$$A^i \cdot u = f^i, \quad (4.34)$$

Here it is defined that

$$f^i = f + D j^u, \quad (4.35)$$

where D is a time-area matrix that links current densities to charges. This matrix is only dependent on the geometry.

The residual can be defined as the current in these Dirichlet points. These currents should be zero.

$$\zeta(j^u) = -A \left(A^{i-1} f^i(j^u) \right) \quad (4.36)$$

The resulting Jacobian is

$$J(\zeta(j^u)) = \begin{pmatrix} \frac{\partial \zeta_1}{\partial j^u_1} & \cdots & \frac{\partial \zeta_1}{\partial j^u_n} \\ \vdots & \ddots & \vdots \\ \frac{\partial \zeta_m}{\partial j^u_1} & \cdots & \frac{\partial \zeta_m}{\partial j^u_n} \end{pmatrix} = -A \cdot A^{i-1} \cdot D, \quad (4.37)$$

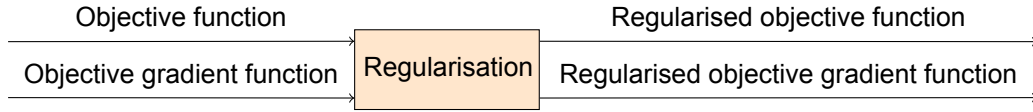
and consequently the objective function is

$$\nabla(\|\zeta\|^2) = -2\zeta^T A \cdot A^{-1} \cdot D. \quad (4.38)$$

The obvious disadvantage here is that the inverse A^{i-1} has to be calculated. This requires that this inverse is well-defined and stable. This can be evaluated by calculating the condition number of the matrix. For the FEM the condition number of A^i is however generally about $10^{10} - 10^{12}$ which is appalling. This means that using the numeric model might lead to very noisy results, or even very wrong results. This will be verified by simulation.

The condition number of this matrix can be improved in two ways. The first way is by adding more reference electrodes. If all FEM nodes are part of a reference electrode the condition number is one, as should be. The second way is by radically simplifying the geometry. On the simple geometry on test, if the number of reference electrodes is increased to the unrealistic number of a thousand, the condition number is still $10^8 - 10^9$, which is not good enough.

4.4. Regularisation



The system of equations describing the inverse problem has many more unknowns than equations. This means that the solution of this system will not be unique. Because of this the system is said to be ill-posed in the sense of Hadamard [38]. The challenge is to find within the many possible solutions the correct one. Equations can be added in order to give preference to solutions that satisfy some condition, this process is called regularisation.

One of the most used regularisation methods is the method of Tikhonov, named after the soviet mathematician who invented it [38]. What Tikhonov's method does is adding a term to the objective function eq. (4.26) so it becomes

$$u' = \arg \min_u (\|\zeta(u)\|^2 + \lambda^2 \|\Gamma \cdot u\|^2). \quad (4.39)$$

Γ is the set of equations that is added and λ^2 is a scalar weight factor. Usually Γ is a constant square matrix but it does not necessarily have to be.

In this method it is chosen to let the regularisation matrix approximate the Laplacian operator in order to favour solutions that have small Laplacians in all points and therefore are smooth. This is sensible because very abrupt details or smoothed details will result in very similar signature, especially when evaluating as far away from the ship as codedepth. Other smoothing or low-pass regularisation matrices could have been possible as well but this one is chosen because it can easily be constructed regardless of the underlying geometry [5, ch3.2].

4.4.1. Regularisation of the analytical model

For the analytical method the sources are located on a square lattice, much like the pixels of an image. Therefore the effect of regularisation is that of a Laplacian convolution filter, that is:

$$\Gamma \cdot I^c \quad (4.40)$$

and

$$h *_2 I^{cm} \quad (4.41)$$

give the same result. In eq. (4.40) $*_2$ denotes the two-dimensional convolution. I^c is a vector but I^{cm} is matrix. Both contain the same entries. h is the Laplacian (edge detection) filter kernel:

$$h = \begin{pmatrix} -\frac{1}{3} & -\frac{2}{3} & -\frac{1}{3} \\ -\frac{2}{3} & 4 & -\frac{2}{3} \\ -\frac{1}{3} & -\frac{2}{3} & -\frac{1}{3} \end{pmatrix}. \quad (4.42)$$

Various implementations of this kernel are however possible. The frequency domain behaviour of the filter kernel is shown in fig. 4.4. The x and y axes are in units of the Nyquist frequency. If the lattice of the sources is refined the relative frequency behaviour will stay the same, but the regularisation will give different results as the Nyquist frequency shifts.

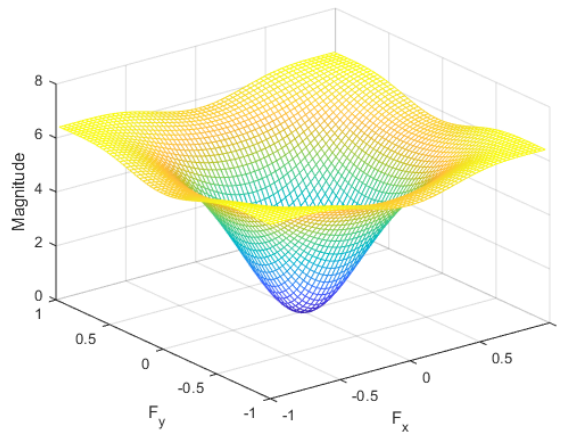


Figure 4.4: Spatial frequency domain response of the Laplacian filter.

4.4.2. Regularisation of the FEM model

The Laplacian regularisation condition can be translated into saying that on each element the current density should be the average of that of its neighbours [5, ch3.2]. For this to be implemented the element connectivity of the mesh has to be derived. The matrix Γ will then be a sparse square matrix of which all elements (i, j) will be -1 if element i and j are neighbours. The diagonal entries will be the sum of the number of neighbours. The effect of this regularisation matrix is dependent on the actual discretisation of the geometry. For an irregular mesh is not possible to define a frequency response, but the effect of mesh refinement is the same as with the analytical model.

The gradient of the added regularisation term is

$$2\lambda^2 \Gamma \cdot \Gamma \cdot u. \quad (4.43)$$

This term can then be added to the gradient.

4.5. Inverse solver

The inverse solver is the step of the method that finally reconstructs the damage. It takes the regularised objective function and finds its minimum using the gradient of the regularised objective function. The block view of the inverse solver can be seen in fig. 4.5.

Many solver algorithms exist for finding the minimum of an objective function. In literature all types varying between direct solvers [9] and genetic algorithms [43] have been used. If all solvers are ordered from simple to complex, based on the computational effort they require, these are on the opposite ends. Generally simple solvers have more strict requirements

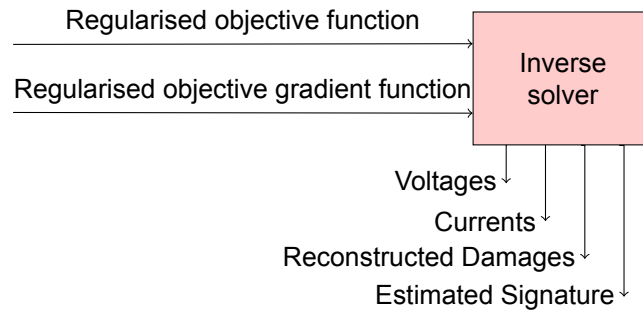


Figure 4.5: Block view of the inverse solver.

on the objective function and the more complex solvers have less. The normal strategy for choosing the solver algorithm is to pick the simplest one for which the objective function meets the requirements. For instance in matlab all common algorithms are built-in and they provide a selection table based on this strategy [36]. For this problem the objective function has the following properties:

1. It is ill-posed in the sense of Hadamard (but regularised);
2. It is continuous with the input;
3. It has an analytical jacobian and gradient;
4. It has a continuous jacobian and gradient;
5. It is unconstrained.

Direct solvers do not handle ill-posed problems very reliably. They give results but one never quite knows if it is the optimum, therefore they should not be used.

The next step in complexity are the gradient-based quasi-newton algorithms such as the Broydon-Fletcher-Goldfarb-Shanno (BFGS) or Levenberg-Marquardt (LM) algorithms. These are fast algorithms that use the gradient for determining the steps to make. These algorithms cannot handle constraints. These algorithms are very suitable.

The next step in complexity are the interior point methods. These can handle constraints and do not require gradients, but do use them if known analytically. As constraint handling is not necessary a gradient based algorithm is chosen.

4.6. Software implementation

In section 4.6 the flow of the implementation in software can be seen. A large part of the software relies on the proprietary software of comsol(blue steps) and matlab(red steps). The green steps are self-built matlab routines.

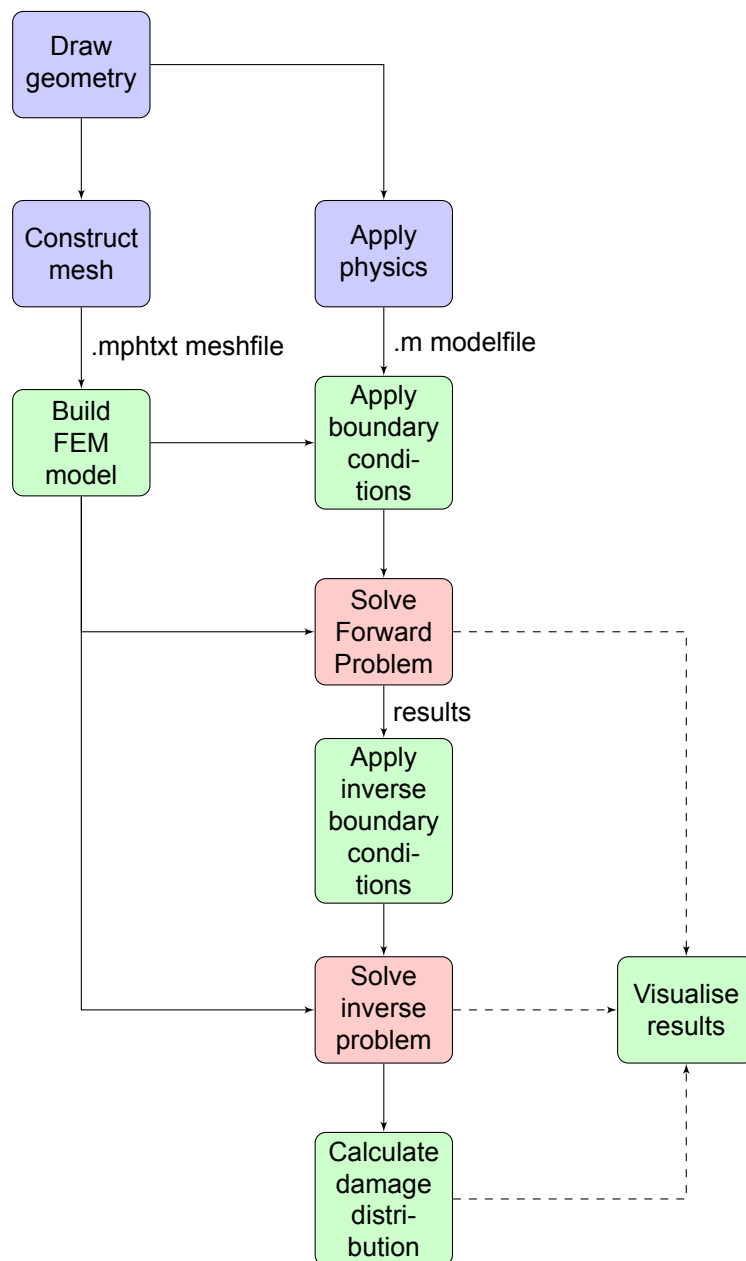


Figure 4.6: Flow of the software implementation. Blue steps are done in consol, green steps are built in matlab, red steps are built-in matlab routines.

4.7. Simulation experiments

4.7.1. Analytic model inversion

A first important question to ask on damage reconstruction models is: “What damages can be reconstructed and what cannot?”. This question can be subdivided with the characteristics of the damage: location, appearance, extent, number. In order to answer this question a series of tests using the analytical model have been conducted. For these first tests the most simple model of a ship has been used: a floating square slate of $60 \times 60\text{m}$. On this slate 9 points are homogeneously placed at locations $(x, y) = (\{10, 30, 50\}, \{10, 30, 50\})$ in all permutations. Of these 9 points the position of the one at $(10, 10)$ is an anode. At the other points measurement points will be placed. This geometry is shown in figs. 4.7 and 4.8. The \circ denotes the location of the anode, the $+$ denote the positions of the reference electrodes. These symbols will be used throughout further figures. In this figure the slate extends to the axis and the edges of the figure. Different configurations of the damage distribution have

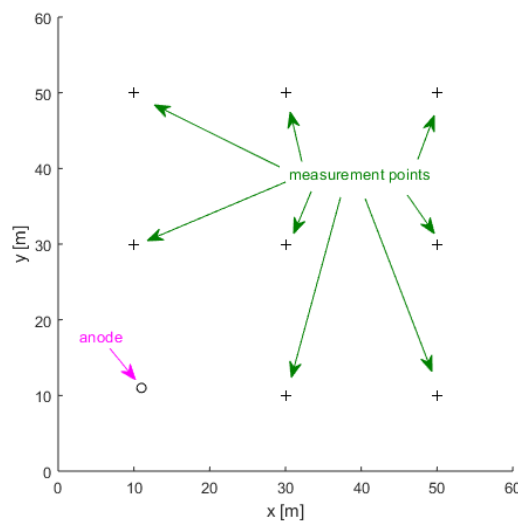


Figure 4.7: Location of anode and measurement electrodes on the slate.

been tested.

For each tested scenario 6 plots are made, ordered in 2 columns and 3 rows. An example is shown in fig. 4.9. The plots in the left column show the forwardly calculated scenario and the plots in the right column show the reconstruction by the inverse method.

The plots in the first row show a voltage distribution. Equipotential lines are displayed and the colour in between the equipotential lines denote the potential.

The plots in the second row show the current density distribution. Equal-current-density lines are plotted and their colour denotes the current density.

The plots in the third row show the norm of the signature at codedepth. Equal-signature lines are displayed and their colour denotes the norm of the electric field. The contour of the projection of the slate is also plotted. For a square slate the codedepth is not defined, but for this geometry the codedepth is chosen at $z = -10\text{m}$. The results and conclusions of these tests are listed in this section but the full set of images is added in appendix B.

Location of the damage and measurement points The location of the damage has a high influence on resolvability. The first conclusion that can be drawn is that damage reconstruction is hard when the damage is located beyond the measurement points, see figs. B.9 and B.10. This result is expected, as the damage gets outside the damaged area the sensors will not show very different measurement values.

Secondly the resolvability is dependent on the distance of the damage to the measurement points. If the damage is far away from all sensors the effect on the sensors is slight, and the

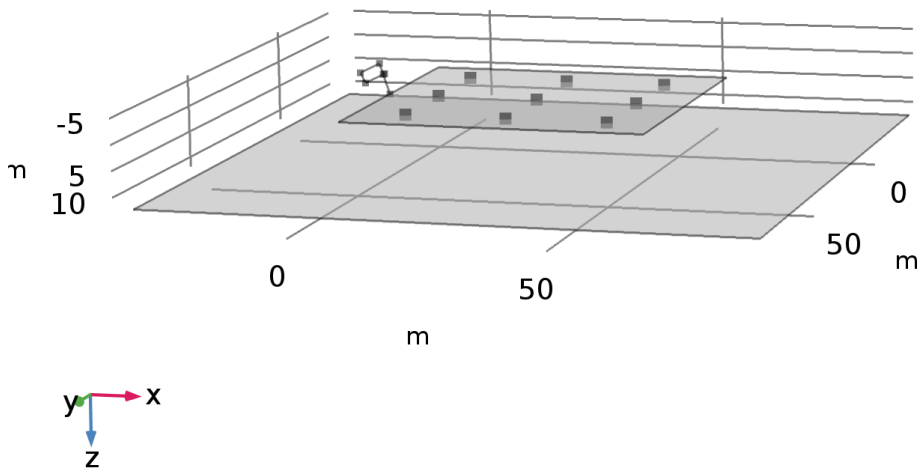


Figure 4.8: 3D-view of the geometry used for the analytic model inversion.

solution tends to a smoothed current distribution in a large area. Therefore the prediction of the signature of small damages far from the sensors is not that good, compare figs. B.3 and B.4.

Thirdly damages very close to anodes cannot easily be resolved as the effects of cathodes and anodes cancel at the measurement points, compare figs. B.5 and B.6.

Fourthly, resulting of the previous observations, the damage reconstruction is best when the measurement electrodes are distributed homogeneously, and not for instance just around the edge. This can be seen from figs. B.7 and B.8.

Appearance and extent of the damage Because of the regularisation all solutions resulting from the method are smooth. This means that very localised and abrupt damages are resolved to smooth damages as well. From figs. B.9 and B.10 it can be seen that an smooth and an abrupt damage located in the same point results in the exactly the same output from the inverse method. When evaluating the signature near the ship this will make a difference on the correctness of the prediction. Generally smooth damages are reconstructed better. Extensive damages fulfil the regularisation requirement better by themselves and are therefore reconstructed better, compare for instance figs. B.11 and B.12.

Number of damages Different damages can be reconstructed as separate damages when they are not too close. Generally if they are closer together than the measurement electrodes are they will not be seen as separate damages, see for instance figs. B.13 and B.14. For the prediction of the signature this will have not a significant effect however.

With the 8 measurement electrodes on the slate configurations up to three separate damages can be reconstructed, but with more damages the prediction of the signature will not be worse, see figs. B.15 and B.16.

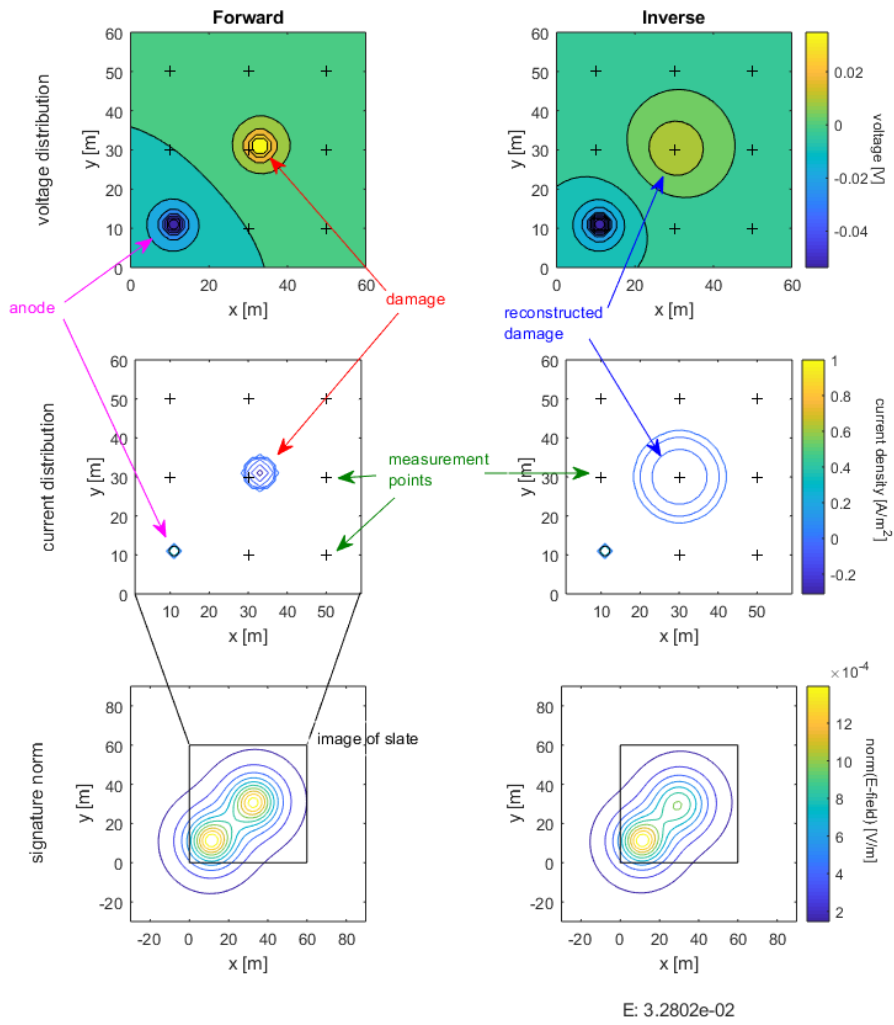


Figure 4.9: Example of the results of the resolving of damage on a slate.

4.7.2. Finite element model inversion simulation

The finite element model has been tested with the same kind of scenarios as the analytic model, but under enhanced conditions to make up for the ill-conditioned mathematical model. A dense grid of 52 reference electrodes has been placed on a flat rectangular boat, see fig. 4.10. One anode is present, a damaged patch can be placed and moved around.

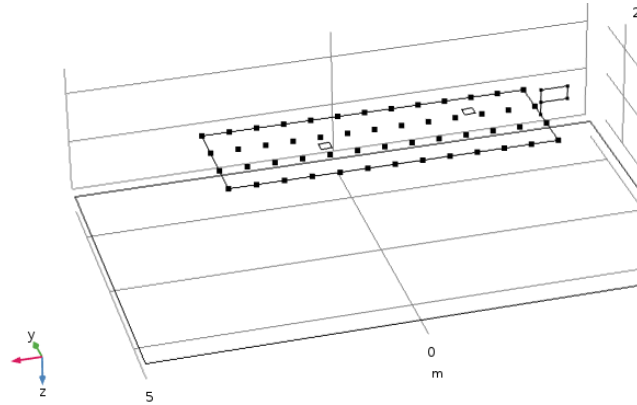


Figure 4.10: Configuration for the Finite Element Model Inversion.

The simulation results should mainly show the effects of the ill-conditioned model, and how this could be improved by adding measurement points or simplifying the geometry.

When testing the finite element model the results were as expected not very good. In fig. 4.11 it can be seen that inversion of a simple geometry using 52 reference electrodes does not give very accurate results. This also translates in an unresolved signature, and a bad performance against the second metric. More often the results are even worse, and no estimation of the damage can be made at all.

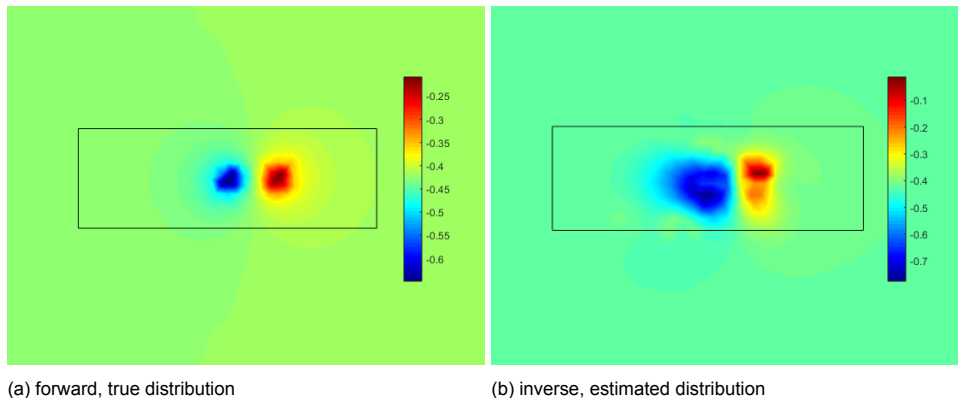


Figure 4.11: Comparison of forward and inverse hull voltage distributions calculated with the FEM model

4.7.3. Interpretation of the simulation experiments

The simulation using the analytic model gives a limiting case of how well inversion is possible. The finite element model does not perform up to this limit as it runs in to mathematical difficulties because of the bad condition number, which has to be solved for any numeric model attempting inversion. Signature prediction is not possible with the numeric inverse method.

With the current results the construction of an inverse method is abandoned.

5

Brute Force Method

5.1. Introduction

The brute force method is an alternative way of trying to reconstruct the damage distribution without making an inverse model. This chapter develops the brute force method and develops the simulations in which this method is used.

5.2. The Brute Force Method

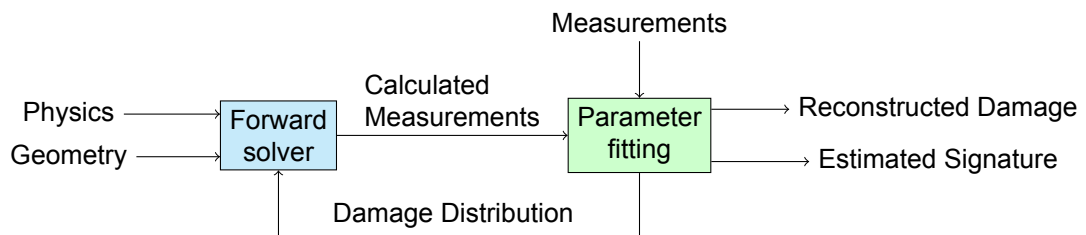


Figure 5.1: Structure of the brute force method.

The structure of the the brute force method can be seen in fig. 5.1. The damage distribution δ is described by a function of nine point locations and nine associated parameters.

$$\delta(x, y, z) = \frac{\sum_{i=1}^9 \frac{p_n}{r_n}}{\sum_{i=1}^9 \frac{1}{r_n}}. \quad (5.1)$$

Here p_n is the n -th parameter. And r_n is the distance to point n :

$$r_n = \sqrt{(x_n - x)^2 + (y_n - y)^2 + (z_n - z)^2}. \quad (5.2)$$

The points must be chosen around the hull so they give a good spatial coverage. For instance equidistantly on a plane or a hemicylinder under the ship. By putting the points closer to the hull the effects of the points become less overlapping.

The point locations are fixed, but the parameters associated with these points can be varied. The forward model, which is well posed, is calculated iteratively with different parameters. By fitting the resulting measurements to the real measurements by varying the parameters the damage distribution can eventually be found. Brute is however the correct description for this method, it is a time consuming method, and it does not give any insight in signature management measures, but it will work.

The results of this method are enhanced by running it for different anode current settings. More configurations of the anodes give more datapoints and make therefore the fit easier.

Also when the optimisation of the parameters is done, and the parameter for only one point is the highest, it might be possible to redistribute the points around that one point, in order to get a higher resolution.

5.3. Brute Force Inversion Simulations

The brute force inversion routine is constructed fully in comsol Multiphysics. A geometry is built and damage applied, the model is solved forwardly to generate measurement data. An external function is written which implements eq. (5.1). This function is passed parameters from comsol. Then an optimisation routine is used to fit the parameters to the measurements. The goal of this simulation is to see how well inversion is possible when using realistic physics.

In order to test the robustness of the brute force method, additional simulations are run where noise is added to the measurement data.

The brute force inversion works. When given a single damage the algorithm is able to locate this into one of nine sections using twelve reference electrodes. In order to arrive at the global optimum of the objective function is mandatory to start in multiple points because there are a lot of local optima. Convergence is enhanced by using different anode current combinations and large anode currents as to move far up the polarisation curve. The brute force algorithm takes five to six hours to calculate the damage distribution on the simple geometry used. Results of the brute force method are shown in fig. 5.2a and fig. 5.2b. It can be seen the signature estimation is not that great. Although the general damage

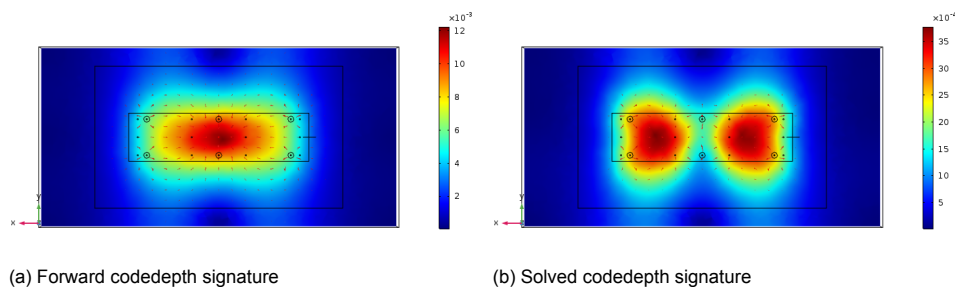


Figure 5.2: Comparison of forward and inverse hull voltage distributions calculated with the brute force model

location is determined correctly, it is spread out too much so at codedepth the signature is not well estimated. This is improved by increasing the number of sensors and interpolation points. How many interpolation points then are needed in order to resolve the signature? And how many sensors are needed to obtain this result?

The solution converges around a correct damage distribution if the number of sensors is two times the number of interpolation points. With less it does not always produce good results. This ratio (2:1) is much higher than it is for the analytical method (1:9). The difference is attributed to the difference in physical model and configuration, but more research into this is recommended.

The number of interpolation points needed depends on how well the signature should be predicted. In the simulation of fig. 5.3 a model of the ship Quest is fitted with 140 sensors, and the signature is predicted with an RMS error of 13.6%, and the maximum signature value is 13% off. As most ships today have between one and eight reference electrode sensors, 140 is a very large number.

5.3.1. Robustness analysis

The measurements of the reference electrodes are up to 200 mV apart when an anode or damage is close, but typically only 10 to 20 mV. The amount of noise or measurement error that can be sustained before the results deteriorate is also about this amount.

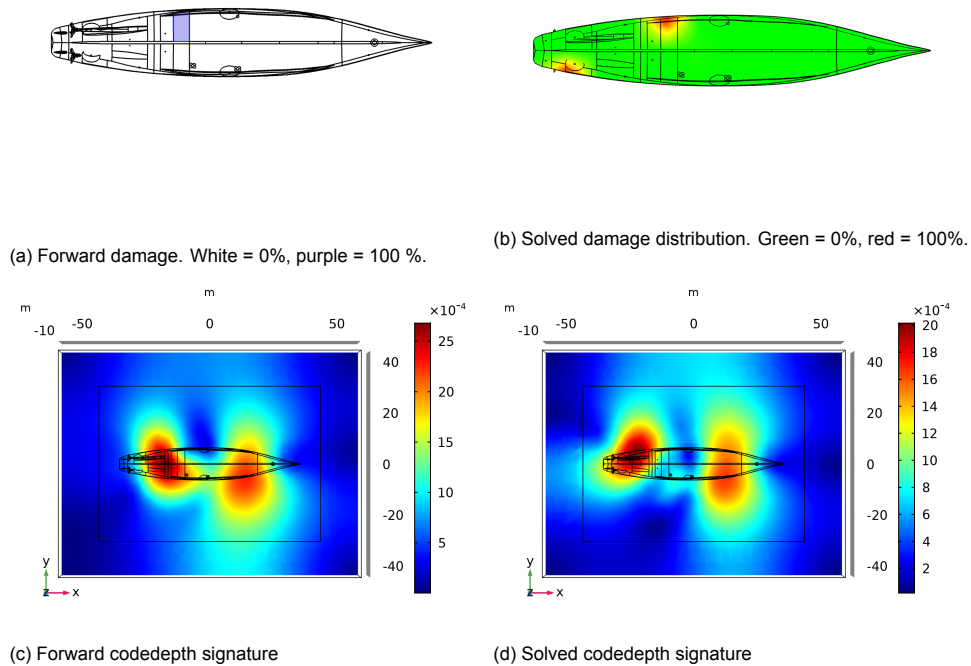


Figure 5.3: Comparison of forward and inverse damage distributions and signatures of the Quest with 140 reference electrodes. $E = 13.6\%$.

5.3.2. Interpretation of the simulation experiments

The brute force model is shown to work. The results of the brute force method can come close to the results of the analytical method but require both a lot of computation time and many more measurement electrodes.

The simulations show therefore what is possible using inversion, and how inversion can be attained. It also shows that implementing damage estimation in a signature management system will require improvements in the method, especially in calculation times. But as most ships of today have only a few reference electrodes, implementing damage estimation is not likely to be possible. If damage estimation is to be implemented on future ships they should have more reference electrodes. Preferably a hundred or more, but the number depends on how well the signature should be resolved. Is $E = 15\%$ good enough, and is E even the best metric?

6

Scale-Model Experiments

6.1. Objectives

At TNO a scale model testing facility is developed. The objectives of this facility are:

- Verification of the electro-chemical modeling approach;
- Validation of polarisation curves;
- Obtaining typical signature datasets;
- Prototyping ICCP systems and signature management measures;
- Verification of the inverse method.

The first and second of these objectives are the most important, because they have to be met before the others can. Therefore these two are important to this research as well. As the scale model facility is unique it has to be developed from scratch. Therefore many experiments focus on the validation of this test set-up.

6.2. Measurement Set-up and Materials

The test set-up developed at TNO consists of a number of parts. First is the open water tank in which the model will be placed and the signature measurements will be taken. This tank has inner length of 5.50 meters, inner width of 1.83 meters and a depth of 1.9 meters. It is made out of high-density polyethylene (HDPE), a suitable material because it does not conduct electricity and that will not take part in any electro-chemical reactions.

On the floor of the tank a measurement array is mounted. The array consists of 7 sensors mounted in line that measure the electric field in the water in three axes. The measurement array is adjustable in distance below the water level.

Above the water a motorised frame is constructed that can move in x and y direction. (For the purpose of the scale model: +x is towards the front of the ship, +y to starboard, and +z into the water.) To this frame either the scale model or the the calibration source can be mounted. These can then be moved around controlled by a script running on a connected computer. The tank with the measurement array and the calibration source can be seen in fig. 6.1. The alignment of the frame is done using a laser, see fig. 6.2. The calibration source is a device that is used to calibrate the measurement array. It consist of a variable DC current source, an ammeter and two electrodes. The electrodes are made of platinum, a very noble metal. They have a surface area of 1.00 cm² on either side, and they are placed in a rigid frame 300 mm apart, 200 mm below the waterline. The resulting electric field and current distribution can be calculated very precisely. By comparing measurements to the predicted values the sensors can be calibrated.

The scale model itself is a wedge shaped plastic ship. It has a length of 1140 mm and a draft of 230 mm. The side panels are 1100 × 330mm rectangles, with 3 × 10 mounting

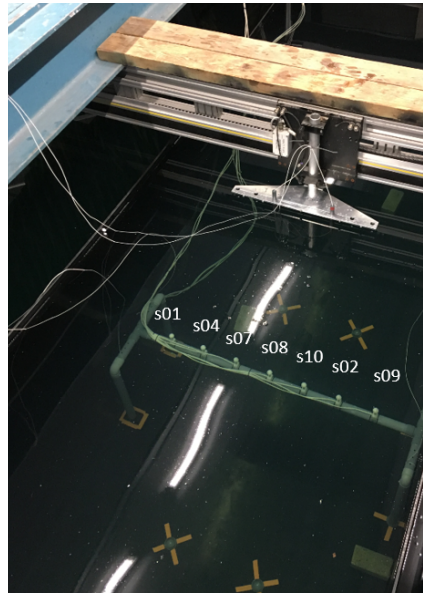


Figure 6.1: Measurement set-up with the calibration source above the measurement array.

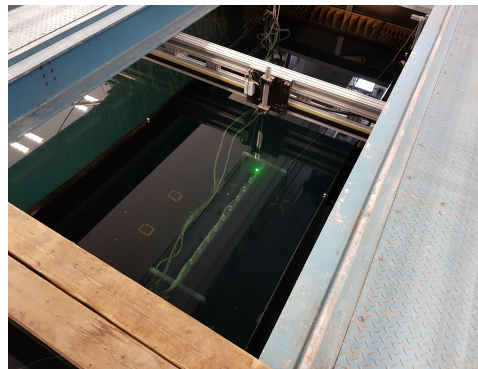


Figure 6.2: Laser alignment of the moving frame to the measurement array.

holes spaced equidistantly. On these mounting holes $100 \times 100\text{mm}$ patches of uncoated steel can be placed, but also sacrificial anodes of zinc, titanium ICCP anodes, or $Ag/AgCl$ reference electrodes. On the stern of the ship Nickel-Aluminium-Bronze circular plates, representing propellers, can be mounted. The materials have all been constructed in a way they can be quickly fitted in the mounting holes. If any mounting holes are not used they are closed with nylon bolts. This way different configurations can be quickly prototyped. The scale model, configured for sacrificial anode cathodic protection, can be seen in fig. 6.3. The same configuration can be seen in fig. 6.4 but then in the water. Further blueprints of the set-up can be seen in appendix C.

On the inside of the scale model electrical connections are made to a multi-cable block and from there the connection to the power sources and the measurement equipment on the shore is made. This measurement equipment comprises 3 16-channel analog-to-digital converters (ADCs), connecting to both the scale model and the measurement array. Up to 4 DC power sources, rated 50V/6A, are available. The ADC and the sources connect to a central computer using a serial connection. The computer runs labview software that controls both the measurements and the sources. This computer also communicates to the computer controlling the moving frame, giving move commands and receiving position measurements. A schematic of the test set-up can be seen in fig. 6.5.

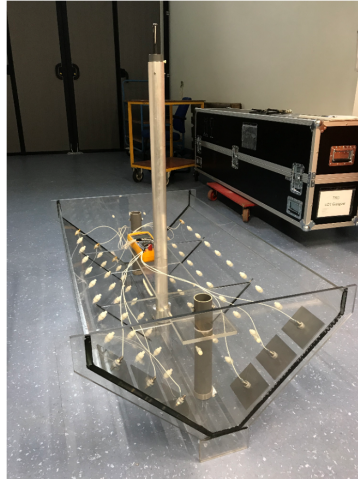


Figure 6.3: Scale model with sacrificial anode cathodic protection system test set up.

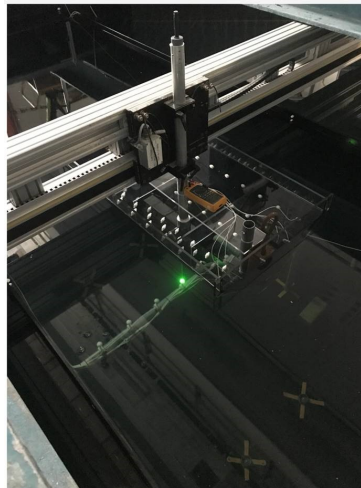


Figure 6.4: Sacrificial anode cathodic protection system test set up in the water.

6.3. Sensors selection for electric potential and field measurements

6.3.1. Method

In order to do electric field and potential measurements sensors are required, but these cannot be bought ready for use, therefore they had to be developed. Because the measurements are done in an electrolyte care has to be taken that the potentials and fields of interest are measured and not some electrochemical potential of the electrode material. For both field and potentials measurements reference electrodes are needed. These reference electrodes are chemically buffered so they will be very stable in different chemical environments. The application of the reference electrodes for potential measurement is shown in fig. 6.6. Note the exact similarity with the archetypical Daniell-Cell (fig. 6.7), two metals in a solution containing these metal's ions, these solutions make contact through something porous or a salt bridge, and the metals connect to a voltmeter. The potential of the redox reaction at the hull is measured against the strongly buffered silver-silverchloride ($Ag/AgCl$) redox reaction. It has to be noted that in many modern reference electrodes the silver chloride solutions is replaced by an organic matrix which contains the silver and chloride ions. For measuring the electric field inside the electrolyte the configuration of fig. 6.8 is used. By using two equally strong buffered electrodes it is certain their electro-chemistry is equal

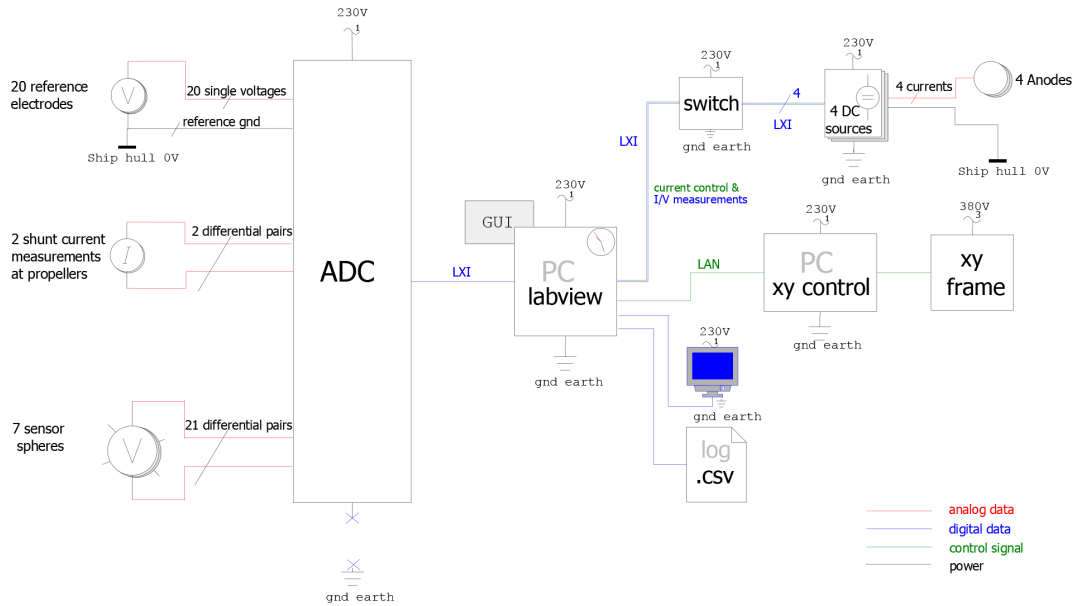


Figure 6.5: Schematic overview of the scale model set-up.

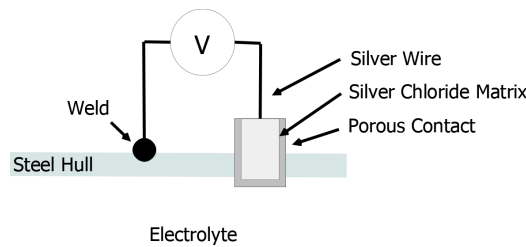


Figure 6.6: Potential measurement schematic.

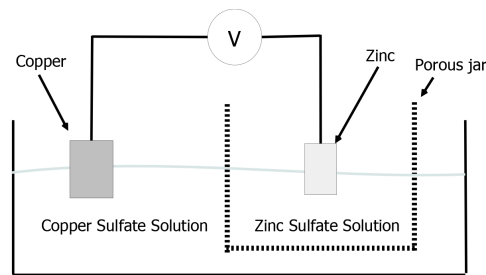


Figure 6.7: Daniell Cel.

and just the external field is measured. Because of the shape of the sphere the electric field measurement has to be divided by 1.5 [17]. The first main experiment conducted was the testing of two different types of reference electrodes fitted in 3 axes in a sphere. The first has a liquid silver chloride solution in a glass tube, the second a silver chloride matrix. The goal of this experiment was to select the best type of sensor for further tests.

Secondly the reference electrodes were fitted in ten three-axial spherical sensors, which were tested and calibrated in order to select the best seven. It was expected that the art of quality production would not be mastered directly. In this last test the calibration source is moved over a 10 sphere sensor array, and in combination with simulation experiments of that configuration the calibration(see fig. 6.9) quantities for the sensors are obtained as well.

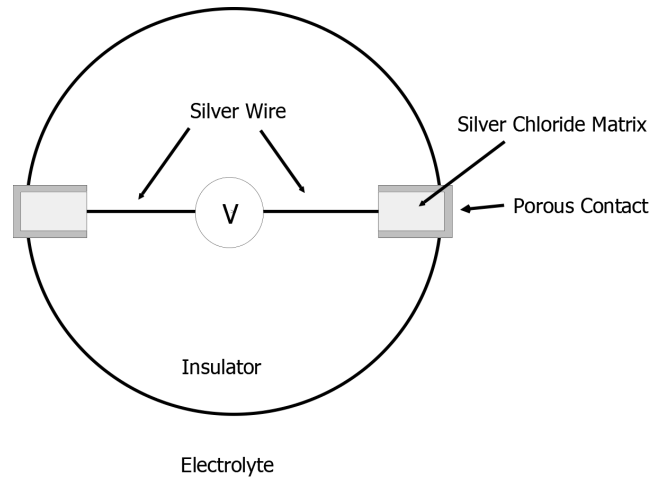


Figure 6.8: Field measurement schematic.

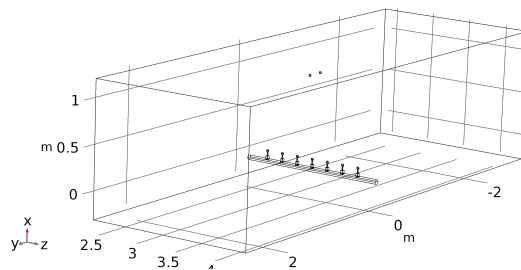


Figure 6.9: Simulation set-up for calibration.

6.3.2. Results

One sensor with glass tube electrodes (containing solved silver chloride) and one with pellet electrodes (with a silver chloride matrix) were made and tested. Both types of sensor were placed in water with a conductivity of 0.143 S/m. After the sensors were first placed in water measurements were done. No source was yet present so the measured values represent an offset with noise. Initially the offset and noise values were very high, but after one hour they had become stable. Values for offsets and noise of both sensors of a stable measurement are given in table 6.1. These represent a typical measurement under equal circumstances. Note that the sensor axes are labeled A, B and C, as they do not align with the x , y and z axes. This had to be done because the sensors had to be mounted in z direction. It can be

| Sensoraxis | A | B | C | Sensoraxis | A | B | C |
|------------------|--------|-------|--------|------------------|------|--------|--------|
| Offset (mV) | -0.616 | 3.089 | -0.727 | Offset (mV) | 0.55 | -2.826 | -2.852 |
| Noise (μ V) | 25.6 | 107.2 | 52.9 | Noise (μ V) | 767 | 1305 | 715 |

(a) Pellet electrodes

(b) Glass electrodes

Table 6.1: Comparison of pellet and glass reference electrodes.

seen that the offsets of both sensors are comparable, but the noise of the glass electrodes is much higher. This was the case for every single measurement. After this the sensors were tested with the calibration source. The amplitude of the signal produced by the calibration source is about 1 mV. The noise of the glass electrodes made it very difficult to discern the signal. The signal of the pellet electrodes was very linear with the calibration source current. Because of the superior performance of the pellet electrodes these were chosen for use in the scale model set-up. This choice was also practical because the pellet electrodes are only 5 mm in thickness, but the glass electrodes 40 mm. Therefore the sensors could be made as small as 32 mm in diameter. Ten sensors were produced, and the seven with the

smallest noise values were installed in the set-up.

All ten sensors were tested with the calibration source. The calibration source was moved over the sensors, to stop for 3 minutes exactly over every sensor. This scenario was simulated in comsol as well. The measured and simulated values of the electric field were compared. The result of this comparison for one sensor are shown in fig. 6.10. It can

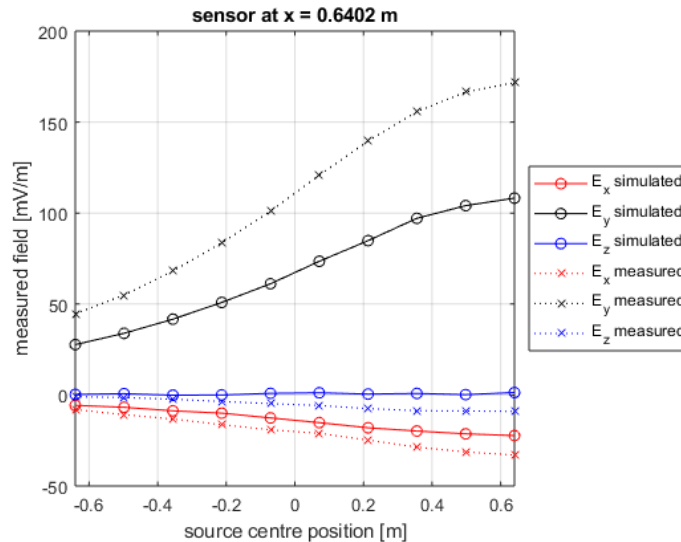


Figure 6.10: Comparison of simulated to measured sensor calibration measurements.

be seen that the measured and simulated values for the x and y direction differ a factor of 1.6. No explanation has yet been found. The measured and simulated values for the z direction differ up to 10 mV m^{-1} when the source is closest to the sensor, but this difference becomes smaller as the source goes further away.

With the measurement array of the seven best sensors installed the shift of the offset was tested over two periods of 14 hours. This is a long period, as a typical measurement using the scale model will take about half an hour. The results of this experiment can be seen in fig. 6.11. It is to be noted that the y -axes of the graphs are scaled differently. It can be seen that the offsets for the different sensors drifted by amounts varying from 0.01 to 1.73 mV; Also as the absolute value of the offset becomes large, the ADC changes its scaling as to accommodate this voltage, but this results in a lower resolution. The resolution of the ADC is 6.5 digits. Depending on the offset the last digit can represent 0.001 (sensor 1.3), 0.01 (sensor 1.2) or 0.1 (sensor 1.1) mV; The rate of change of the offset is for only 2 sensor axes higher than 0.05 mV h^{-1} . The signal level on the sensors when using the scale model is typically no larger than 1 mV, and the duration about half an hour. It is concluded that the shift in offset is small enough not to influence a single measurement significantly, but that offsets should be measured before every measurement. Increasing the signal level might improve the results. The easiest way of increasing signal level is positioning the sensors closer to the scale model. When the signature is measured at a lower depth it will show more details and local effects, and it increases the signal level.

6.4. Sacrificial Anode Cathodic Protection

6.4.1. Method

In order to validate the polarisation curves, the first measurement with the ship was with a sacrificial anode cathodic protection system. The set up for this can be seen in fig. 6.3. On the front of the ship six $10 \times 10 \text{ cm}$ steel patches are mounted. On the rear of the ship six zinc anodes are mounted. Inside the ship all of the anodes are connected and all of the steel patches as well. A connection between anodes and steel is made via a shunt measurement resistor of 1Ω . The ship is then placed in the water and multiple runs are measured. These

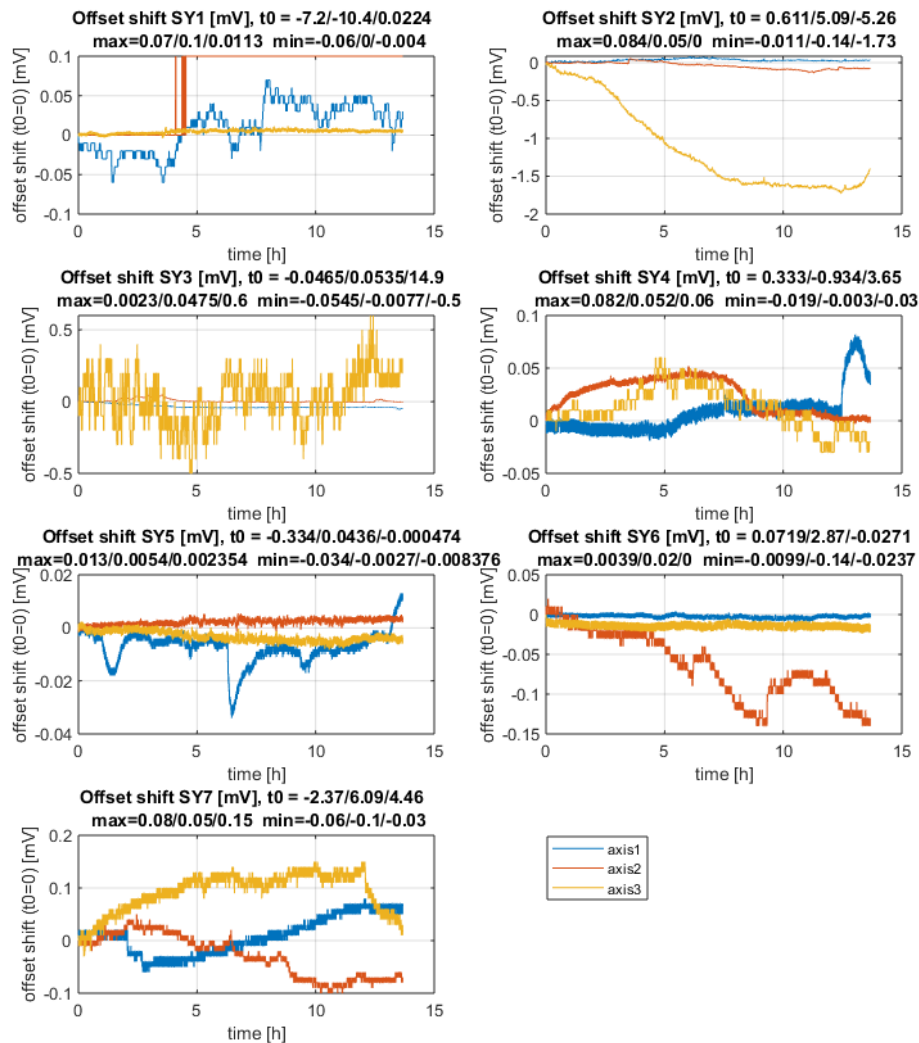


Figure 6.11: Offset shift over a period of 14 hours.

are then compared to the reference simulations.

6.4.2. Results

The scale model with sacrificial anode protection was sailed over the measurement array. The measurements of each sensor form the signature on a line at the depth they are placed. The measurements of the sensor directly underneath the keel of the ship can be seen in fig. 6.12. It can be seen that the y component is small as the ship is symmetric in $y = 0$. The x component is negative, representing a current from stern to bow. The z component changes sign near the middle of the ship at $x = 0$, as is to be expected.

When the data of all seven sensors is plotted in a two-dimensional plot the entire signature of the ship at the sensor depth is obtained. Such a signature plot can be seen in fig. 6.13. This plot looks capricious. Partly this is due to the small signal-to-noise ratio of the underlying data. But it is also due to the fact that resolution in y direction (2.4 cm) is 10 times smaller than the resolution in x direction (20 cm), and in order to print the image the data is interpolated to pixel size. Simulation software like comsol uses smoothing image

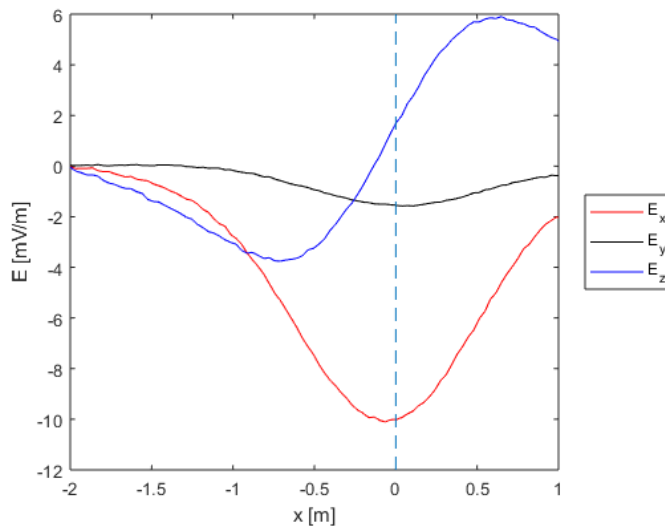


Figure 6.12: Electric field components at $y = 0$

filters when plotting coarse data, but this is not done here because it would not show the actual measurements.

The measurement with the scale model and sacrificial anode cathodic protection was repeated four days later. The results of this second measurement can be seen in fig. 6.14. When comparing figs. 6.13 and 6.14, it can be seen they differ quite a lot. This also can be seen from the comparison of the data of one sensor in fig. 6.15. The z and x components are 14% larger after 4 days, and the y component looks differently altogether, much larger and the location of the maximum value has shifted 0.3 m. For the increase in current there is no obvious or explanation. The set-up was not changed in any way. On both days the conductivity of the water was the same as well. The change in y component might be attributed to a slight rotation of the scale model of these days. Also corrosion on the mounted side of the port-side steel was detected, which might create an asymmetry.

The next day a third experiment was done. The results can be seen in fig. 6.16. They are not quite what would be expected. Instead of further increasing or staying the same, the measurements for x and z decreased to 75% of the values the day before. It might be that the polarisation curve changes the first week the materials are in the water, but it would not be expected to change both ways rapidly. Only one change to the test set up was made on the 30th of January; in order to reduce the forces on the ship it was sailed slower than before. On the 25th and 29th the sailing speed had been 2.5 mm s^{-1} , on the 30th 1.0 mm s^{-1} . Further tests showed that indeed the currents increase with increasing sailing speed, but not enough data points are as of yet obtained to show the exact relation. Although little research has been conducted into corrosion under flow conditions, literature does indeed suggest that increasing speed increases the current, see for instance [35] and their second figure. But it also suggest this effect should only occur at much higher speeds.

Comparison of the scale model experiments with sacrificial anode protection with a simulation is somewhat difficult as polarisation curves under flow conditions are not yet available.

6.5. Impressed current cathodic protection

After the test with the sacrificial anodes has been conducted, an ICCP system is implemented on the scale model. The initial current setting is the current measured at the sacrificial anodes. The main goal of this test is the implementation of a functioning ICCP system. Because of the complex results of the previous tests, tests with the ICCP system are not possible in the scope of this research.

6.6. Verification of the inverse method

In order to verify the inverse method, the ICCP system has to be functional and reference electrodes have to be fitted at the hull. A damage distribution is added to the scale model by placing uncovered steel patches on the hull. The measurements of the reference electrodes are the input for the inverse method. The outcome of this method is a reconstructed damage distribution and signature. The reconstructed damage distribution is compared to the actual one. The actual signature of the scale model is measured and compared to the reconstructed (simulated) signature.

6.7. Interpretation of the scale model experiments

As the test set-up for scale model experiments had to be devised and built from scratch without much relevant literature it was difficult to do so. It can be concluded that a lot of relevant physics and chemistry is still unexplored, major questions remain unanswered:

- Why do the sensors show offsets?
- Why do these offsets shift?
- In what way are polarisation curves influenced by flow rates, and why?

Nonetheless the results are a good first step in attaining the goal, verification of the inverse method. Underwater electric field measurements are possible, but not yet perfect. It can be concluded that a scale model set-up is possible, although more research is needed to fully understand all the measurements.

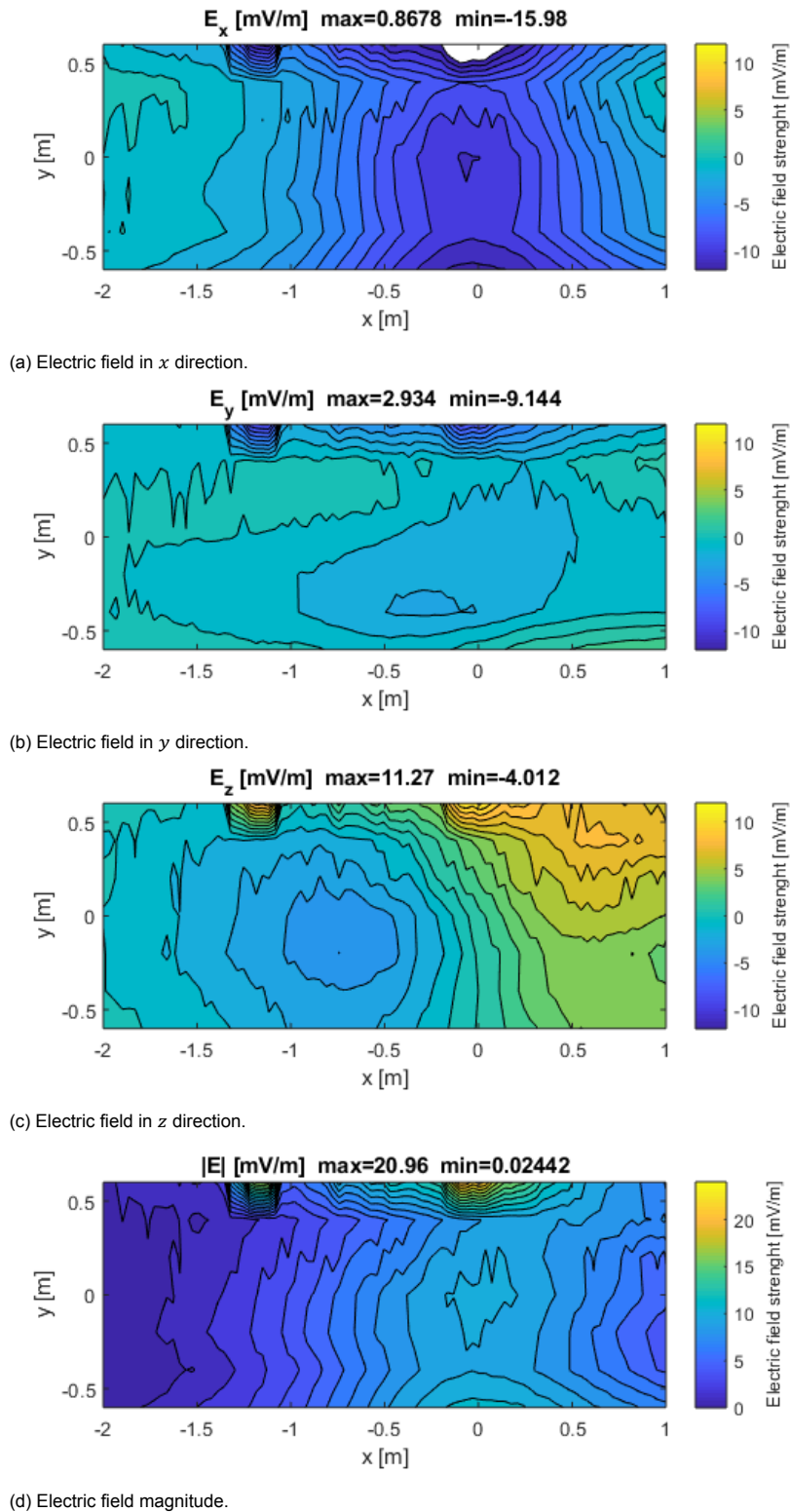


Figure 6.13: Signature of the scale model with sacrificial anode protection, measured at $z = 1.10\text{m}$ below the waterline on the 25th of January.

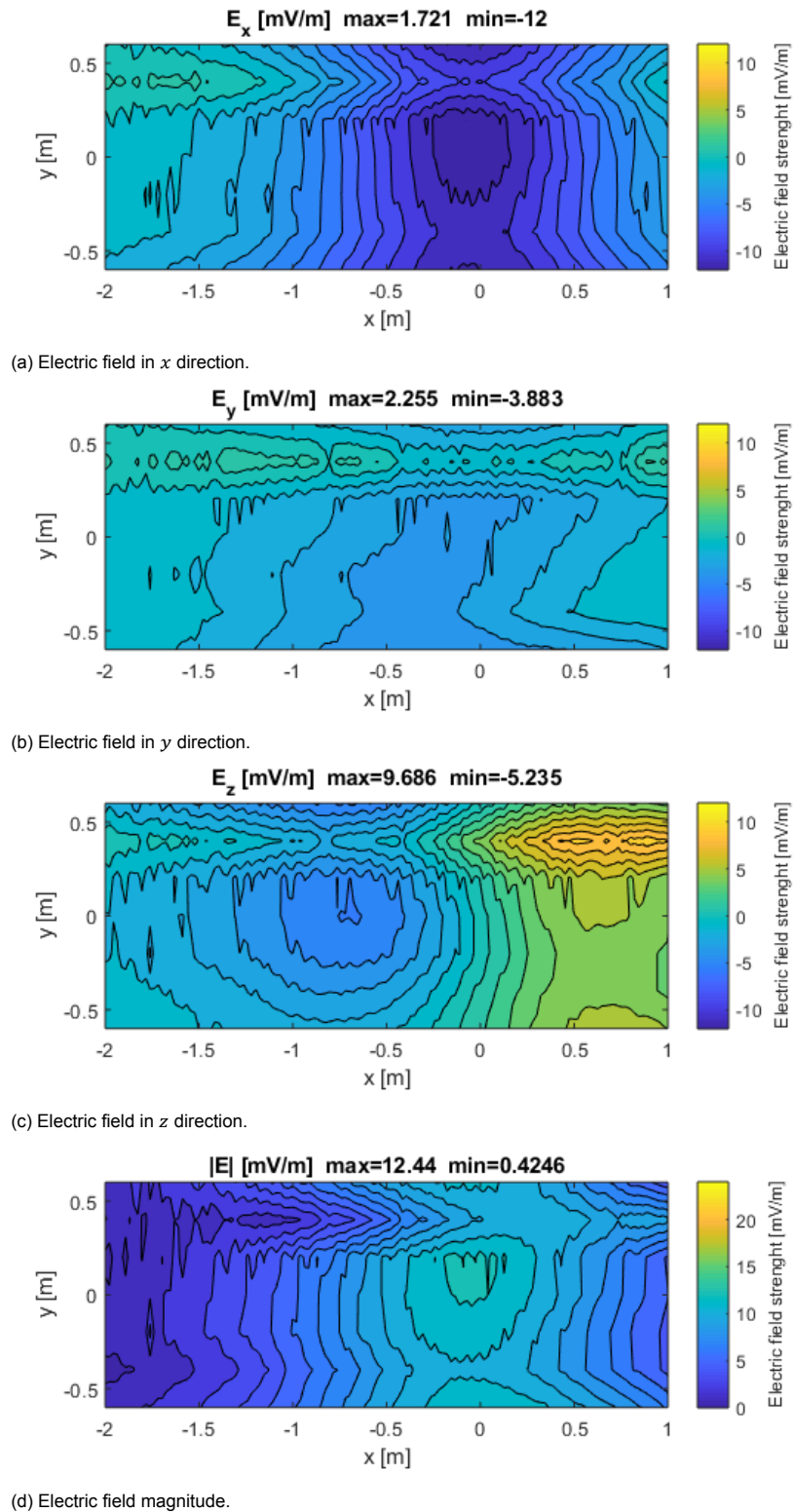


Figure 6.14: Signature of the scale model with sacrificial anode, measured at $z = 1.10\text{m}$ below the waterline protection on the 29th of January.

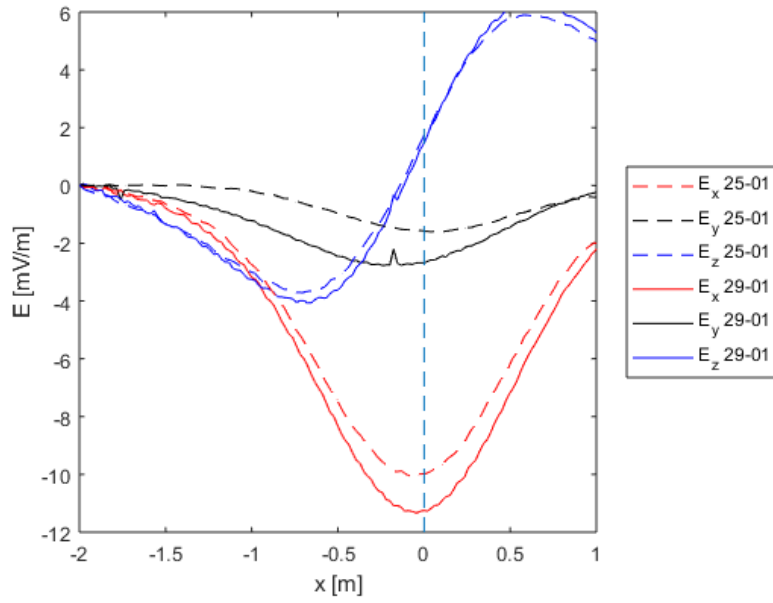


Figure 6.15: Electric field components at $y = 0$, 4 days apart

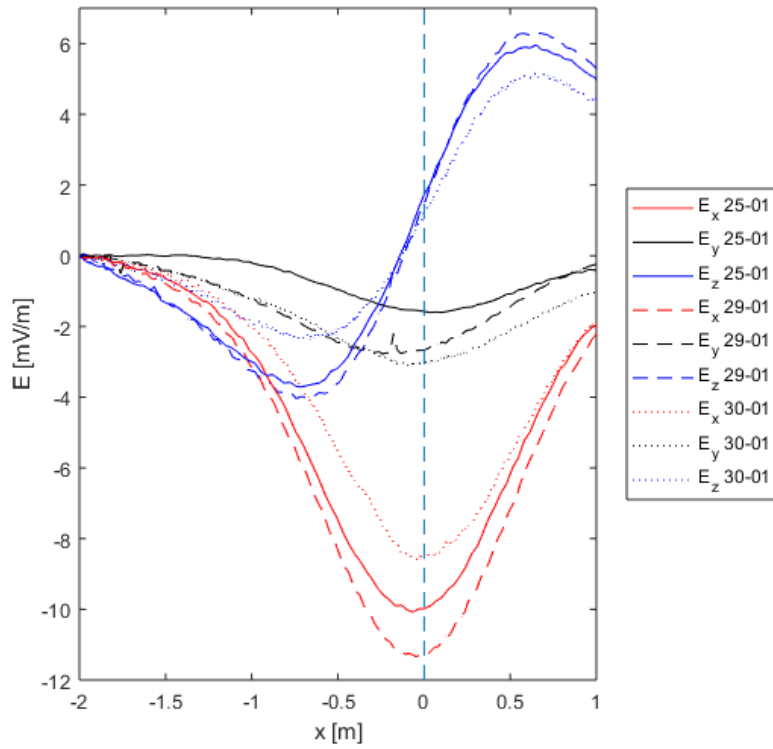


Figure 6.16: Electric field components at $y = 0$, 3 different days

7

Conclusions

Three methods for inversion are developed: the analytical method, the numeric (FEM) method and the brute force method. The analytical method is used in simulations for exploring the limits of inversion. The numeric method runs into mathematical difficulties, simulation shows how well it performs. The brute force method is an attempt to obtain damage distributions of real ship geometries by just using the forward model and a lot of computing power.

The experiments focus mainly on proving that the simulations of the physics correspond to reality, which is difficult because everything has to be developed from scratch. If all works well the inverse method could be applied to scale model tests as well, but that phase of testing was not reached in the scope of this thesis.

7.1. Conclusions and discussion on inverse methods

The development of a method for reconstruction of the damage distribution using ICCP system measurements led to the following conclusions:

- The best results for damage reconstruction that can be achieved in theory can be explored by a simple analytic model[section 4.7.1];
- The inverse problem can be described using FEM, and after regularisation solved using gradient-based methods, but all results for numerical methods suffer from poor condition numbers and are therefore unstable when implemented[section 4.7.2];
- Brute force inversion, inversion by repeatedly calculating the forward problem, can be employed in reconstruction the damage distribution of ships. It requires large computation times, and is somewhat sensitive to noise, but in general it works well[chapter 5];
- No very detailed description of the geometry is needed as regularisation will smooth away details and the inverse solver performs better with fewer degrees of freedom [section 4.4 and section 4.5];
- Rules for the placement of reference electrodes were derived. With 8 points of measurement a damage reconstruction can be realised [section 4.7.1]. But resolution is limited by the number of reference electrodes. For future ships a number of reference electrodes of at least one hundred is advised[section 5.3].

Admittedly the results of the methods are not as perfect as hoped for. The application of a method for damage reconstruction using ICCP system measurements is still very far off as it would require ships with many reference electrodes, and there are only a few ships that have more than six.

7.2. Conclusions and discussion on scale model analysis

The development of a scale model testing facility led to the following conclusions.

- Electric field sensors based on $Ag/AgCl$ reference electrodes were developed. They showed good linearity with the field, but also large and shifting offsets that were not explained[section 6.3];
- Simulations and measurements of a set-up with a calibration source show good similarity, but a factor of 1.6 difference that has not yet been explained[section 6.3.2];
- Tests with a scale model ship with a sacrificial anode protection system show large variations over the time of four days[section 6.4];
- The same tests show that polarisation curves are strongly dependent on the speed of the ship. As polarisation curves for moving electrolytes are not yet available this poses a challenge to modelling[section 6.4].

As the scale model testing facility developed at TNO is unique, everything had to be developed from scratch. This resulted in major challenges outside the original scope of the project. Important questions remain unanswered. The drifting offsets of the sensors are not explained and also the relation between the speed and the polarisation curve remains unknown. The results indicate that the physical simulation model was too simple. Probably the Poisson equation should be expanded to the Poisson-Nernst-Planck equation.

7.3. Answers to the research questions

The research questions of this thesis were:

To what accuracy and with what measurements can the damage distribution on a ship's hull be reconstructed?

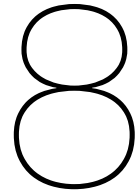
With subquestions:

- What type of mathematical model is best suited for inversion?
- Can a damage reconstruction method be implemented on a scale model?
- How could a damage reconstruction method be implemented on a ship?

To the main research question the answer is: the accuracy is limited by the number of reference electrodes. A resolution of half the distance between reference electrodes is possible in theory, using brute force methods.

The most suitable mathematical approach is not to construct an inverse model but to repeatedly calculate the forward model with different parameters until the right ones are found. Currently the scale model testing facility is not yet developed far enough to test the inverse method, but it is likely testing will be possible in the near future once the major open questions are answered.

It is unlikely that damage reconstruction using ICCP system measurements will be implemented on ships any time soon as current ships have few (1-6) reference electrodes, which would give a very poor resolution. If future ships will have many more reference electrodes (a hundred or more), implementation is possible. It would however still require a lot of computation power.



Recommendations

This research led to a large number of new questions that will require attention. The main topics are:

- research into quantification metrics for signature reconstruction. What does a mine see? How should we then rate our models?
- research into methods for dealing with badly conditioned models to get the best possible results;
- further research in to the parameter fitting part of the brute force method. How can be made to converge faster and always to the correct solution?
- research into electric field sensor for use in water. Why do $Ag/AgCl$ sensors show shifting offsets? How can these sensors be improved?
- research into how polarisation curves change as the electrolyte flows. Can this effect be described by a simple mathematical model?
- further research into scale model with different configurations of passive and active protection of steel and copper;
- verification of the method for damage estimation with scale model experiments.

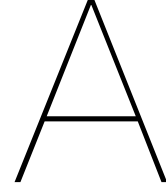
Research into these topics will continue at TNO.

Bibliography

- [1] O Abootalebi, A Kermanpur, M R Shishesaz, and M A Golozar. Optimizing the electrode position in sacrificial anode cathodic protection systems using boundary element method. *Corrosion Science*, 52:678–687, 2010.
- [2] Kenji Amaya, Naoki Yeneya, and Yuki Onishi. Obtaining corrosion rates by bayesian estimation: Numerical simulation coupled with data. *The Electrochemical Society Interface*, pages 53–57, Winter 2014.
- [3] Shigeru Aoki and Yoshihiro Urai. Inverse analysis for estimation galvanic corrosion rate. In *Inverse Problems in Engineering Mechanics*. Springer Verlag, Berlin, Germany, 1993.
- [4] Shigeru Aoki, Kikuo Kishimoto, and Matsuho Miyasaka. Prediction of potential and current distribution in galvanic corrosion and cathodic protection systems (partially japanese). *Materials*, 37(418):757–762, 1987.
- [5] Daniela Calvetti and Erkki Somersalo. *Introduction to Bayesian Scientific Computing*. Springer New York, New York, NY, 2007.
- [6] Cathodic Marine Engineering PTE LTD. Impressed current cathodic protection (iccp) systems, 2018. URL <https://cathodicme.com/cathodic-protection/impressed-current-cathodic-protection-iccp-systems/>. [Online; accessed 17-October-2018].
- [7] S Chaabane, C Elhechmi, and M Jaoua. A stable recovery method for the robin inverse problem. *Mathematics and Computers in Simulation*, 66:367–383, May 2004.
- [8] Nak-Sun Choi et al. Comparison of three modeling methods for identifying unknown magnetization of ferromagnetic thin plate. *J. Elec. Eng. Tech.*, 6(6):799–805, June 2011.
- [9] Hyun-Ju Chung, Chang-Seob Yang, Gi-Woo Jeung, Jae-Jin Jeon, and Dong-Hun Kim. Accurate prediction of unknown corrosion currents distributed on the hull of a naval ship utilizing material sensitivity analysis. *IEEE Tr. Mag.*, 47(5):1282–1287, May 2011.
- [10] Thomas Engel and Philip Reid. *Physical Chemistry*. Pearson Education Ltd., Harlow, UK, 3 edition, 2014.
- [11] Arnaud Guibert. *Diagnostic de corrosion et prédiction de signature électromagnétique de structures sous-marines sous protection cathodique (Diagnosis of Corrosion and Prediction of Electromagnetic signature of Cathodically Protected Underwater Structures)*. PhD thesis, Institut National Polytechnique de Grenoble, December 2009. (French).
- [12] Arnaud Guibert, Jean-Louis Coulomb, Olivier Chadebec, and Corinne Ranou. Ships hull corrosion diagnosis from close measurements of electric potential in the water. *IEEE Tr. Mag.*, 45(3):1828–1831, May 2009.
- [13] Arnaud Guibert, Jean-Louis Coulomb, Olivier Chadebec, and Corinne Ranou. Corrosion diagnosis of a ship mock-up from near electric-field measurements. *IEEE Tr. Mag.*, 46(8):3205–3208, August 2010.

- [14] Giwoo Jeung, Chang-Seob Yang, Hyun-Ju Chung, Se-Hee Lee, and Dong-Hun Kim. Magnetic dipole modeling combined with material sensitivity analysis for solving an inverse problem of thin ferromagnetic sheet. *IEEE Tr. Mag.*, 45(10):4169–4172, October 2009.
- [15] Denny A. Jones. *Principles and Prevention of Corrosion*. Prentice Hall, 2 edition, 1996.
- [16] Kikuo Kishimoto, Hiroyuki Miyasaka, and Shigeru Aoki. Boundary element analysis of an inverse problem in galvanic corrosion[sic]. *JSME Int. J.*, 32(2):256–262, 1989.
- [17] F H Kreuger. *Industrial High Voltage*, volume 1. Delft University Press, 1995.
- [18] L A Lacerda, de and J M Silva, da. A dual bem genetic algorithm scheme for the identification of polarization curves of buried slender structures. *CMES*, 14(3):153–160, August 2006.
- [19] P Miltiadou and L C Wrobel. Optimization of cathodic protection systems using boundary elements and genetic algorithms. *Corrosion*, 58(11):912–921, november 2002.
- [20] Panayiotis Miltiadou and Luiz C Wrobel. A bem-based genetic algorithm for identification of polarization curves in cathodic protection systems. *Int. J. Numer. Meth. Eng.*, 54:159–174, 2002.
- [21] Panayiotis Miltiadou and Luiz C Wrobel. Identification of coating defects in cathodically protected underground pipelines. *Int. J. Numer. Meth. Eng.*, 58:913–932, 2003.
- [22] Matsuho Miyasaka, Kazuhiro Hashimoto, Kikuo Kishimoto, and Shigeru Aoki. Boundary element analysis of galvanic corrosion problems - computational accuracy on the galvanic field with screen plate (partially japanese). *Materials*, 38(418):1079–1084, 1988.
- [23] E Santana Diaz and R Adey. Optimisation of the performance of an iccp system by changing current supplied and position of the anode. *Boundary Elements*, 24:475–485, 2002.
- [24] E Santana Diaz and R Adey. Predicting the coating condition of ships using iccp system data. <https://www.beasy.com/cathodic-protection/cathodic-protection-publications.html>, 2003. [Accessed: 2018-09-12].
- [25] E Santana Diaz and R Adey. Optimising the location of anodes in cathodic protection systems to smooth potential distribution. *Advances in Engineering Software*, 36:591–598, May 2005.
- [26] E Santana Diaz, R Adey, and J Baynham. Prediction of the condition of a structure subject to corrosion based on inverse analysis. *Tr. on Modelling and Simulation*, 34: 203–212, 2003.
- [27] E Santana Diaz, R Adey, J Baynham, and Y H Pei. Optimisation of iccp systems to minimise electric signatures, 2004. URL <https://www.beasy.com/signature-management/signature-management-publications.html>. [Accessed: 2018-09-12].
- [28] J A F Santiago and J C F Telles. A solution technique for cathodic protection with dynamic boundary conditions by the boundary element method. *Advances in Engineering Software*, 30:663–671, 1999.
- [29] J A F Santiago, W J Mansur, and J C F Telles. Time dependent effects in cathodic protection systems using boundary elements. In *Proceedings of the First International Offshore and Polar Engineering Conference*, pages 280–287. The Interational Society of Offshore and Polar Engineers, August 1991.

- [30] W J Santos, J A F Santiago, and J C F Telles. An application of genetic algorithms and the method of fundamental solutions to simulated cathodic protection systems. *CMES*, 87(1):23–40, 2012.
- [31] W J Santos, J A F Santiago, and J C F Telles. Optimal positioning of anodes and virtual sources in the design of cathodic protection systems using the method of fundamental solutions. *Engineering Analysis with Boundary Elements*, 46:67–74, June 2014.
- [32] W J Santos, J A F Santiago, and J C F Telles. Using the gaussian function to simulate constant potential anodes in multiobjective optimization of cathodic protection systems. *Engineering Analysis with Boundary Elements*, 73:35–41, September 2016.
- [33] David Schäfer. *Vorhersage und Umrechnung korrosionsbedingter UEP-Signaturen von Wasserfahrzeugen (Prediction and Conversion of Corrosion Dependent UEP Signatures of Vessels)*. PhD thesis, Universität Duisburg-Essen, April 2015. (German).
- [34] A. Segal. *Finite element methods for the incompressible Navier-Stokes equations*. TU Delft, 2017. URL http://ta.twi.tudelft.nl/users/vuik/burgers/fem_notes.pdf. [Online; accessed 10-Januari-2019].
- [35] Nakarin Srisuwan, Nathalie Ochoa, Nadine Pébère, and Bernard Tribollet. Variation of carbon steel corrosion rate with flow conditions in the presence of an inhibitive formulation. *Corrosion Science*, 50:1245–1250, Februari 2008.
- [36] The MathWorks Inc. Optimisation decision table, 2018. URL <https://nl.mathworks.com/help/optim/ug/optimization-decision-table.html>. [Online; accessed 6-December-2018].
- [37] C Thiel et al. Localization of coating defects by using the impressed current cathodic protection system. MARELEC Conference Presentation slides, 2017.
- [38] Andrey Nikolaevitch Tikhonov and Vasiliy Yakovlevitch Arsenin. *Solutions of Ill-Posed Problems*. V.H. Winston & Sons, 1977. trans. F. John.
- [39] Christiaan Johannes Maria Verhoeven, Antoine Staveren, van, G L E Monna, M H L Kouwenhoven, and E Yildiz. *Structured Electronic Design*. Kluwer Academic Publishers, 2003.
- [40] X Wang, B Hou, and Z Lan. Boundary element modelling of the impressed current cathodic protection of an offshore platform. *WIT Tr. State of the Art in Sc. and Eng.*, 99:221–230, May 2017.
- [41] Wikipedia contributors. Numerical partial differential equations — Wikipedia, the free encyclopedia, 2018. URL https://en.wikipedia.org/w/index.php?title=Numerical_partial_differential_equations&oldid=858263616. [Online; accessed 15-October-2018].
- [42] William Wordsworth. Mutability, 1822. URL <https://www.poetryfoundation.org/poems/45531/mutability>. [Online; accessed 1-February-2019].
- [43] L C Wrobel and P Miliadou. Genetic algorithms for inverse cathodic protection problems. *Eng. Analysis with Boundary Elements*, 28:267–277, 2004.
- [44] Jianhua Wu, Shaohua Xing, Chenghao Liang, Lu Lu, and Yonggui Yan. The influence of electrode position and output current on the corrosion related electro-magnetic field of ship. *Advances in Eng. Software*, 42:902–909, July 2011.
- [45] Chang-Seob Yang et al. Efficient methodology for solving an inverse magnetostatic problem by utilizing material sensitivity. *J. App. Physics*, 103:103–105, January 2008.



Finite element method

The domain Ω is the entire volume on which the FEM is applied, and it consists solely of seawater with material parameters σ and ε . Equation (4.5) can be rewritten to:

$$-\nabla \cdot \varepsilon(\vec{x}) \nabla V(\vec{x}) = q(\vec{x}). \quad (\text{A.1})$$

Which is the strong formulation of the FEM problem.

The interior of the domain, being seawater, holds no static charge and therefore is source free.

A.1. Discrete formulation

The strong FEM formulation of eq. (A.1) can be written in variational form

$$\iiint_{\Omega} \nabla \cdot (-\varepsilon \nabla V(\vec{x})) v(\vec{x}) d\Omega = \iiint_{\Omega} q(\vec{x}) v(\vec{x}) d\Omega. \quad (\text{A.2})$$

Where v is called a 'test function'. v is to be specified later.

Integration by parts yields

$$\iiint_{\Omega} \varepsilon \nabla(V(\vec{x})) \cdot \nabla(v(\vec{x})) d\Omega = \iiint_{\Omega} q(\vec{x}) v(\vec{x}) d\Omega + \iint_{\Gamma} -\varepsilon \nabla V(\vec{x}) v(\vec{x}) \cdot \hat{n} d\Gamma. \quad (\text{A.3})$$

The D0, D1 and N0 type boundary conditions give $\nabla V = 0$ on Γ so they drop out. $q = 0$ on the interior domain, so it drops out as well. But it is important to notice here that indeed volumetric charges and boundary current densities are modelled as the same sources as per eq. (4.9).

The domain of computation is now discretized in N elements, using n nodes. The solution $V(\vec{x})$ will be approximated by the finite element solution $V^h(\vec{x})$ which is represented as:

$$V^h(\vec{x}) = \sum_{k=1}^n u_k \varphi_k(\vec{x}). \quad (\text{A.4})$$

Where u_k is the k -th coefficient of u the vector of node voltages. φ_k is the k -th basis function, corresponding to this node. If eq. (A.3) is discretised using eq. (A.4) this yields:

$$\iiint_{\Omega} \varepsilon \left(\sum_{k=1}^n u_k \nabla(\varphi_k(\vec{x})) \right) \cdot \nabla(v(\vec{x})) d\Omega = \iiint_{\Omega} q(\vec{x}) v(\vec{x}) d\Omega + \iint_{\Gamma} -\varepsilon \nabla V(\vec{x}) v(\vec{x}) \cdot \hat{n} d\Gamma. \quad (\text{A.5})$$

As the summation can be taken out of the integral

$$\sum_{k=1}^n u_k \left(\iiint_{\Omega} \varepsilon \nabla(\varphi_k(\vec{x})) \cdot \nabla(v(\vec{x})) d\Omega \right) = \iiint_{\Omega} q(\vec{x}) v(\vec{x}) d\Omega + \iint_{\Gamma} -\varepsilon \nabla V(\vec{x}) v(\vec{x}) \cdot \hat{n} d\Gamma. \quad (\text{A.6})$$

If now the test function $v(\vec{x}) = \varphi_r(\vec{x})$ (the r -th basis function) for $1 \leq r \leq n$, it can be rewritten to

$$\sum_{k=1}^n u_k \left(\iint_{\Omega} \varepsilon \nabla(\varphi_k(\vec{x})) \cdot \nabla(\varphi_r(\vec{x})) d\Omega \right) = \iint_{\Omega} q(\vec{x}) \varphi_r(\vec{x}) d\Omega + \iint_{\Gamma} -\varepsilon \nabla V(\vec{x}) \varphi_k(\vec{x}) \cdot \hat{n} d\Gamma \text{ for } 1 \leq k \leq n. \quad (\text{A.7})$$

This can be programmed as

$$A \cdot u = f. \quad (\text{A.8})$$

With A an n by n matrix, u the vector of n coefficients of V^h and f the input vector of the same size.

Choosing test functions the same as the basis functions is a method known as the method of *Galerkin*, after the Soviet mathematician. The main advantage of this method is that the matrix A will be symmetrical and positive definite, making it computationally easy to use. This is why this is a widely used method. The main alternative for the choice of basis functions is the spectral method, which allows computationally easy solutions in k -space or spatial frequency domain, which is not necessary in this research. Although the nice properties of A will be partially lost when altering the system of equations later on, Galerkins method still remains the easiest and fastest method [34].

A.2. Meshing of the domain

The mesh of the domain is built using *comsol*. The most common type of mesh element is the tetrahedral one. This mesh element is very popular because the associated basis functions are the most simple ones, and therefore the construction of the matrix A is straightforward as well. More complex elements may give better results for the same computational effort. There is an entire field of mathematical science that centres around the question if it is in given circumstances better to increase the number of elements or if it is better to choose elements of higher order. For the simplicity of the solution however first the most simple and straightforward elements are used.

A.3. Basis functions

Many methods for choosing basis functions exist, but the most simple are the first order lagrangian elements. Given an element that is the convex region between the four nodes $\vec{x}_1 = (x_1, y_1, z_1)$, $\vec{x}_2 = (x_2, y_2, z_2)$, $\vec{x}_3 = (x_3, y_3, z_3)$, $\vec{x}_4 = (x_4, y_4, z_4)$. For this element there are four basis functions φ that are 1 in one node and zero in the other three.

$$\begin{aligned} \varphi_1(x, y, z) &= a_1x + b_1y + c_1z + d_1 \\ \varphi_2(x, y, z) &= a_2x + b_2y + c_2z + d_2 \\ \varphi_3(x, y, z) &= a_3x + b_3y + c_3z + d_3 \\ \varphi_4(x, y, z) &= a_4x + b_4y + c_4z + d_4 \end{aligned} \quad (\text{A.9})$$

And it is given:

$$\begin{pmatrix} a_1 & b_1 & c_1 & d_1 \\ a_2 & b_2 & c_2 & d_2 \\ a_3 & b_3 & c_3 & d_3 \\ a_4 & b_4 & c_4 & d_4 \end{pmatrix} \begin{pmatrix} x_1 & x_2 & x_3 & x_4 \\ y_1 & y_2 & y_3 & y_4 \\ z_1 & z_2 & z_3 & z_4 \\ 1 & 1 & 1 & 1 \end{pmatrix} = \begin{pmatrix} 1 & 0 & 0 & 0 \\ 0 & 1 & 0 & 0 \\ 0 & 0 & 1 & 0 \\ 0 & 0 & 0 & 1 \end{pmatrix}. \quad (\text{A.10})$$

So it is quite easy to derive the basis functions from the locations of the nodes. For φ_r it is given that it has value 1 on node r , 0 on all other nodes, and that it is linear in between. For nodes part of more than one element this will result in continuous basis functions consisting of more parts, but still defined on every element.

The volume v of an element can be calculated using

$$v = \frac{1}{6} \left\| \det \begin{pmatrix} x_1 - x_4 & x_2 - x_4 & x_3 - x_4 \\ y_1 - y_4 & y_2 - y_4 & y_3 - y_4 \\ z_1 - z_4 & z_2 - z_4 & z_3 - z_4 \end{pmatrix} \right\| \quad (\text{A.11})$$

where the $\| \dots \|$ operator denotes the euclidean norm.

A.4. Assembling system matrices and source vectors

A.4.1. Assembling A from the system

When considering a single entry of matrix A

$$A_{r,k} = \iiint_{\Omega} \varepsilon \nabla(\varphi_r(\vec{x})) \cdot \nabla(\varphi_k(\vec{x})) d\Omega. \quad (\text{A.12})$$

But φ_r and φ_k only overlap if these basis functions exist on the same element. In that case on the element η

$$A_{r,k} = \iiint_{\eta} \varepsilon \begin{pmatrix} a_r \\ b_r \\ c_r \end{pmatrix} \cdot \begin{pmatrix} a_k \\ b_k \\ c_k \end{pmatrix} d\eta = \varepsilon \cdot v \cdot (a_r \cdot a_k + b_r \cdot b_k + c_r \cdot c_k). \quad (\text{A.13})$$

Functions around vertices directly connected by an edge overlap on more than one element but still the matrix can be constructed in an element-by-element fashion. The contribution of an element η that is the space between vertices that have the global labels κ , λ , μ and ν , to the matrix A :

$$A_{\eta} = \begin{pmatrix} A_{\kappa,\kappa} & A_{\kappa,\lambda} & A_{\kappa,\mu} & A_{\kappa,\nu} \\ A_{\lambda,\kappa} & A_{\lambda,\lambda} & A_{\lambda,\mu} & A_{\lambda,\nu} \\ A_{\mu,\kappa} & A_{\mu,\lambda} & A_{\mu,\mu} & A_{\mu,\nu} \\ A_{\nu,\kappa} & A_{\nu,\lambda} & A_{\nu,\mu} & A_{\nu,\nu} \end{pmatrix}. \quad (\text{A.14})$$

By calculating all these element contributions, the matrix A can be built by adding these entries to the right positions in matrix A . As these calculations can be done in an element-by-element fashion they are easy to process in parallel.

A.4.2. Assembling f from the sources and implementing the boundary conditions

For the vector f the process is analogous.

$$f_r = \iiint_{\Omega} q(\vec{x}) \varphi_r(\vec{x}) d\Omega + \iint_{\Gamma} -\varepsilon \nabla V(\vec{x}) \varphi_r(\vec{x}) d\Gamma. \quad (\text{A.15})$$

Dirichlet boundary conditions are of the type $V = V_1$. If they are implemented on node r , $f_r = V_1$ and row r of A is set to all zeroes except $A_{r,r} = 1$. This forces the solution $V^h_r = u_r \cdot \varphi_r = V_1$.

Neumann boundary conditions are of the type $\frac{\partial V}{\partial \hat{n}} = \frac{1}{\sigma} \vec{J}_1 \cdot \hat{n}$. They are described on a node r by the integral

$$\iint_{\Gamma} -\varepsilon \nabla V(\vec{x}) \varphi_r(\vec{x}) d\Gamma = \iint_{\Gamma} -\frac{\varepsilon}{\sigma} \vec{J}_r \varphi_r(\vec{x}) d\Gamma. \quad (\text{A.16})$$

Where the positive normal direction is to the outside of Ω . On a tetrahedral element with boundary nodes κ, λ, μ the contribution of the boundary to f is

$$\begin{pmatrix} f_{\kappa} \\ f_{\lambda} \\ f_{\mu} \end{pmatrix} = -\frac{1}{3} \cdot \frac{\varepsilon}{\sigma} \cdot \alpha \begin{pmatrix} J^n(x_{\kappa}, y_{\kappa}, z_{\kappa}) \\ J^n(x_{\lambda}, y_{\lambda}, z_{\lambda}) \\ J^n(x_{\mu}, y_{\mu}, z_{\mu}) \end{pmatrix}. \quad (\text{A.17})$$

With α the area of the triangle κ, λ, μ

$$\alpha = \frac{1}{2} \|(\vec{x}_{\kappa} - \vec{x}_{\lambda}) \times (\vec{x}_{\kappa} - \vec{x}_{\mu})\|. \quad (\text{A.18})$$

If an element has only one or two vertices on the boundary the area term is zero and therefore the boundary current density has no contribution.

Robin boundary conditions are of the type $V - p^{-1}(-\frac{\sigma}{\delta} \frac{\partial V}{\partial n}) = 0$. They are implemented like Neumann boundary conditions. The Robin boundary condition can be written as $\frac{\partial V}{\partial n} = -\frac{\delta}{\sigma} \cdot p(V)$. If $p(V)$ is linearised in a point (V_1) , using the result of eq. (A.17), it can be written as

$$\begin{pmatrix} f_{\kappa} \\ f_{\lambda} \\ f_{\mu} \end{pmatrix} = -\frac{1}{3} \cdot \frac{\varepsilon}{\sigma} \cdot \alpha \cdot \delta \begin{pmatrix} p^1_{\kappa} V_{\kappa} + p^0_{\kappa} \\ p^1_{\lambda} V_{\lambda} + p^0_{\lambda} \\ p^1_{\mu} V_{\mu} + p^0_{\mu} \end{pmatrix}. \quad (\text{A.19})$$

The V_r terms can now be moved to the left side of eq. (A.7). The value $-\frac{1}{3} \cdot \frac{\varepsilon}{\sigma} \cdot \alpha \delta p^1_r$ will be from element $A_{r,r}$. This can then be solved iteratively by using Newton's method.

There is some freedom in assigning boundary conditions to the boundaries of the inverse model. For the forward model there is only one possibility as described above. When for the inverse problem the Robin conditions are removed, because the damage is unknown, only Neumann conditions remain. For the analytic model the damage is modelled as a Neumann boundary solving for the potential at the reference electrodes, but the potential at infinity is assumed to be known, *which does not represent a real scenario*. A Poisson equation with only Neumann boundary condition is known to have an infinite number of solutions [34] because the potential at infinity is not known, which means it cannot be solved straightforwardly. Also, whatever the numeric method chosen, this will result in a representation of the system that has a null space, being a constant potential offset, which means *it cannot be inverted*.

Therefore, somehow, Dirichlet or Robin boundary condition must be introduced. This can be done by modelling the reference electrodes as Dirichlet boundaries, as suggested by [7], and then solving for the current at those points instead of solving for the voltages. This final system can now be solved. This is done in matlab using the `mldivide` routine. The currents that come out of this system are then used as a new point for the linearisation of the polarisation curves, and the system can be built and solved again. This is repeated until the change in currents falls below some minimal threshold.

B

Results of the test with the slate

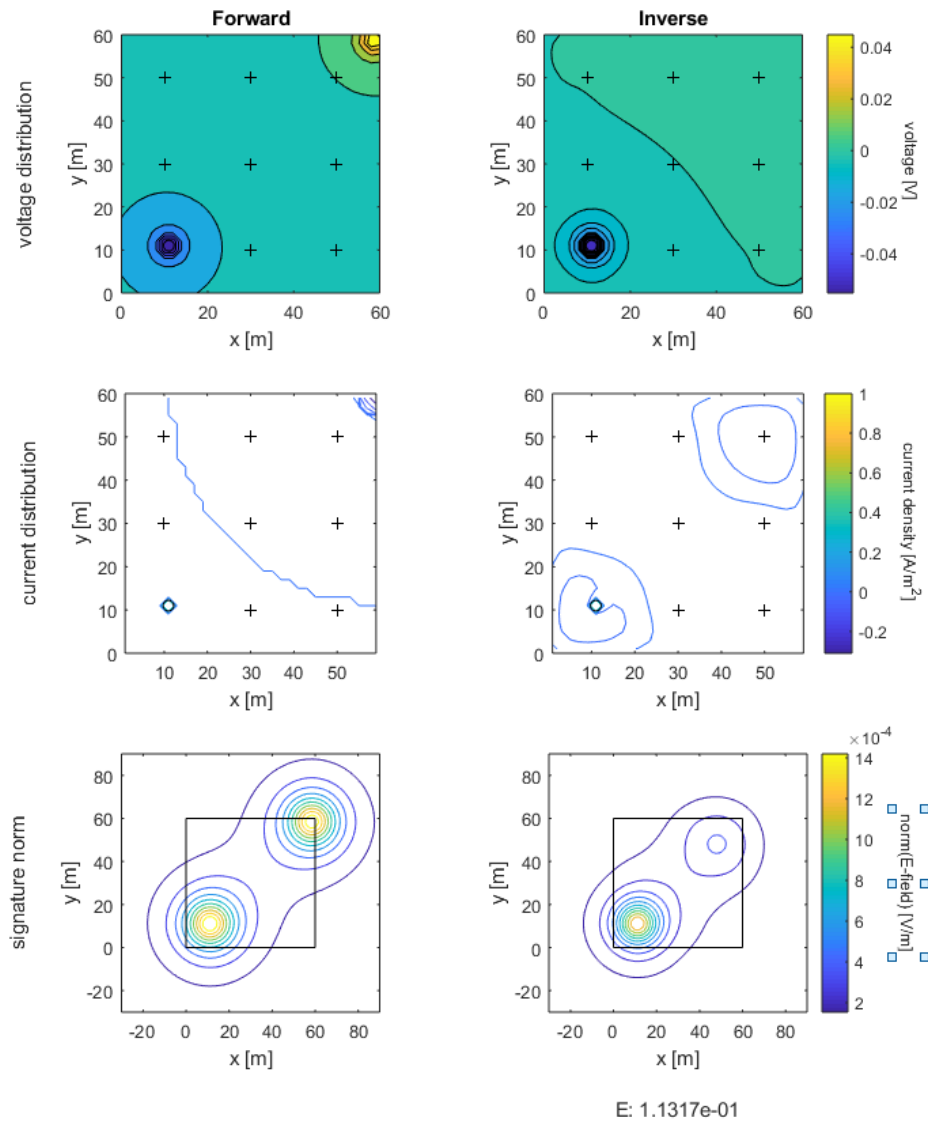


Figure B.1: Not resolved: Damage is located beyond the measurement points. E=11.3%

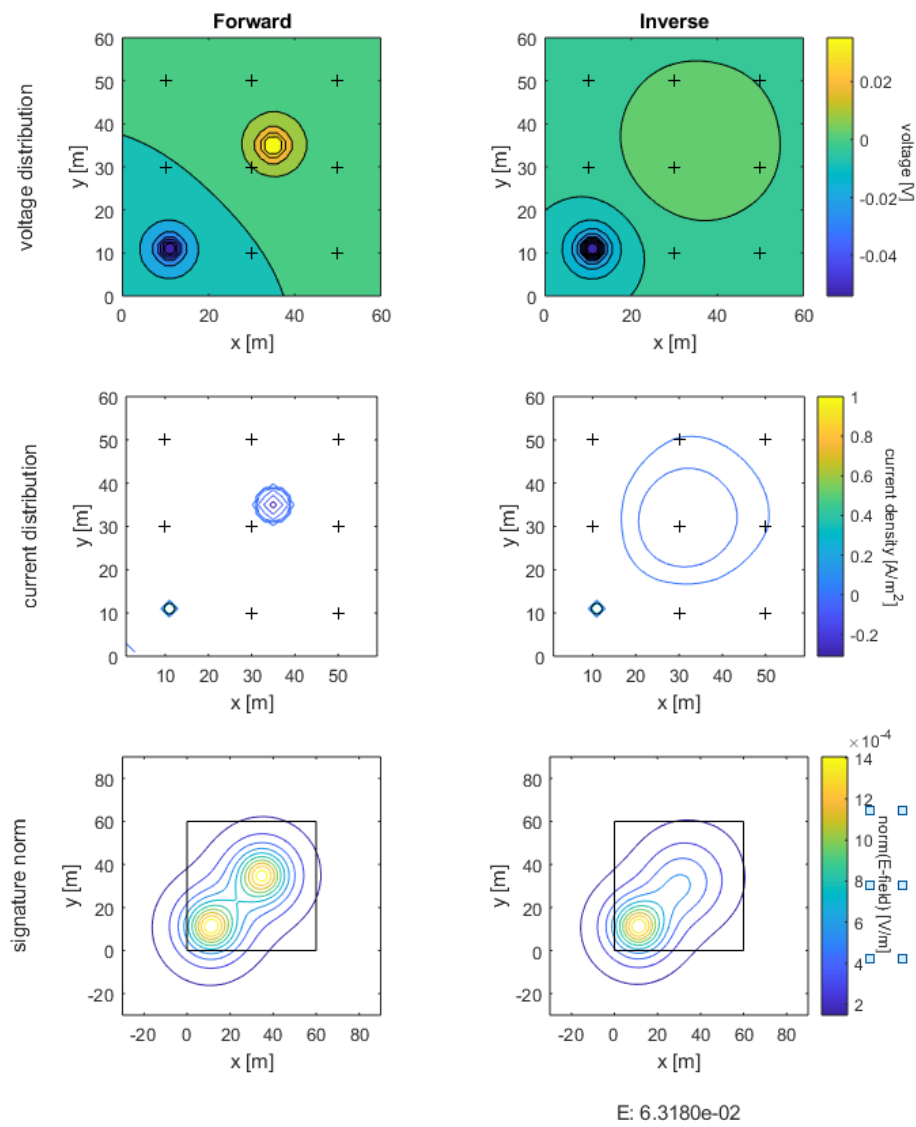


Figure B.2: Poorly resolved: Damage is located before the measurement points. E=6.3%

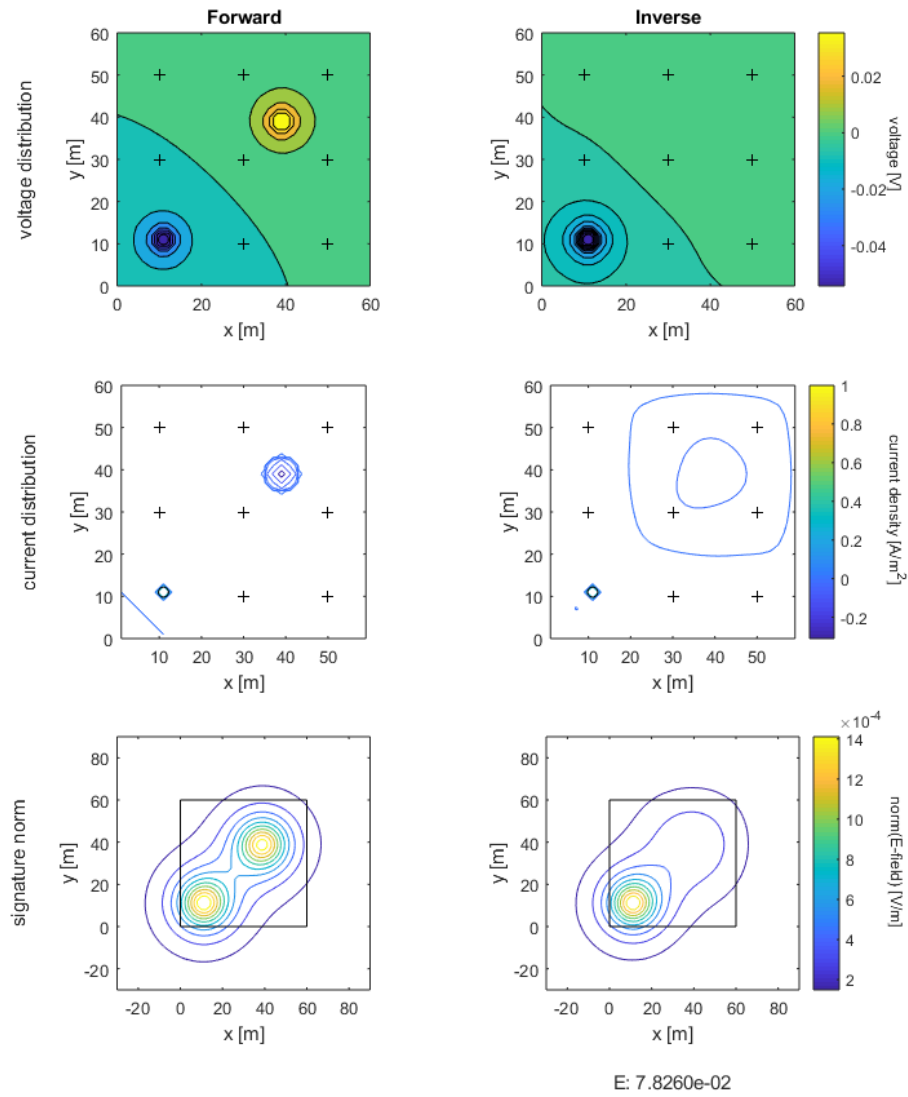


Figure B.3: Poorly resolved: Damage is located far(12.7m) from a measurement point. E=7.8%

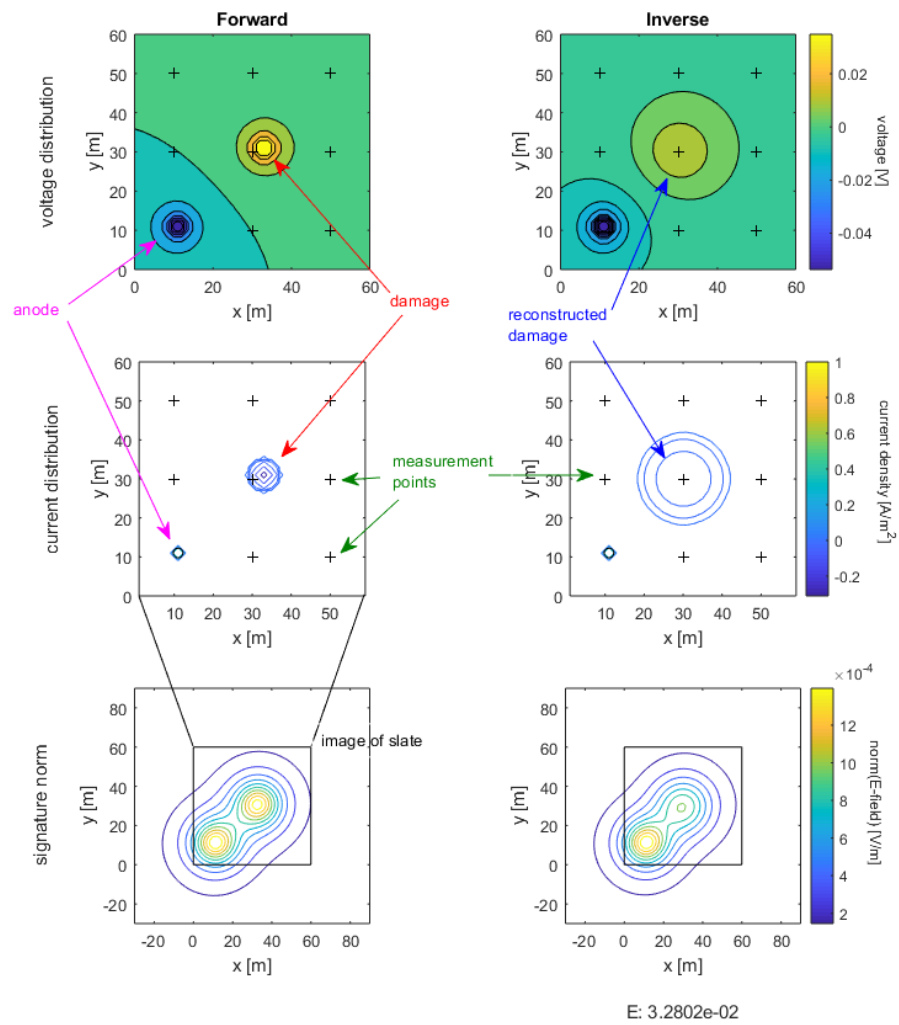


Figure B.4: Somewhat resolved: Damage is located near(3.2m) a measurement point. $E=3.3\%$

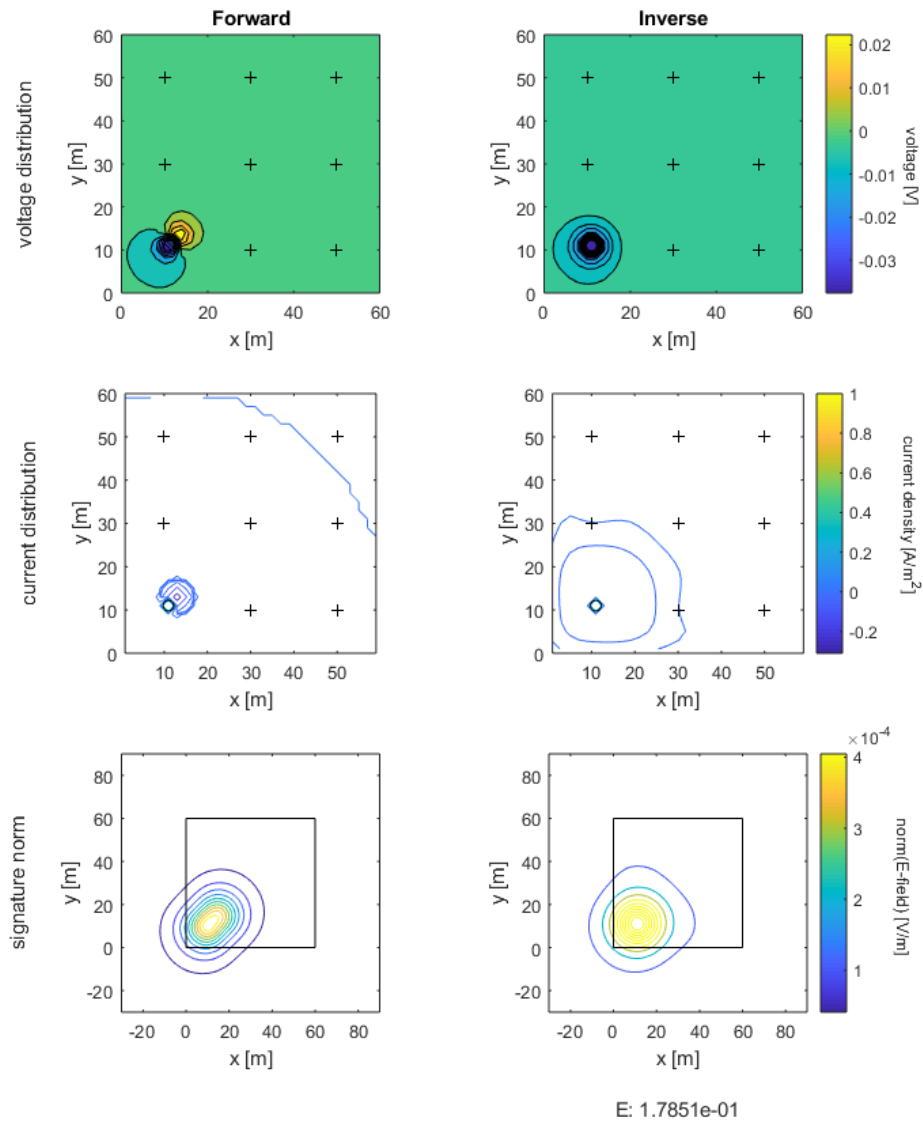


Figure B.5: Not resolved: Damage is located near(2.8m) the anode. E = 17.9%

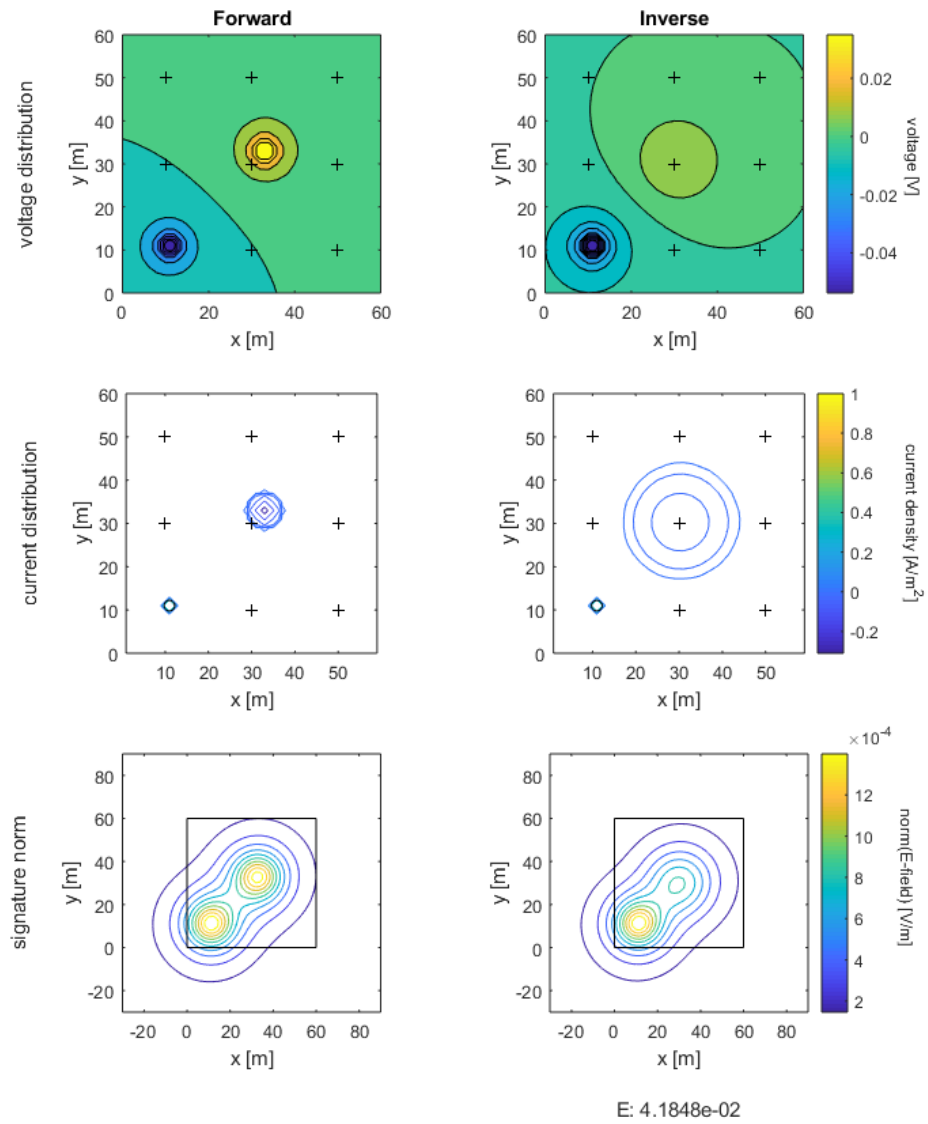


Figure B.6: Somewhat resolved: Damage is located far(18.4m) from the anode. E=4.2%

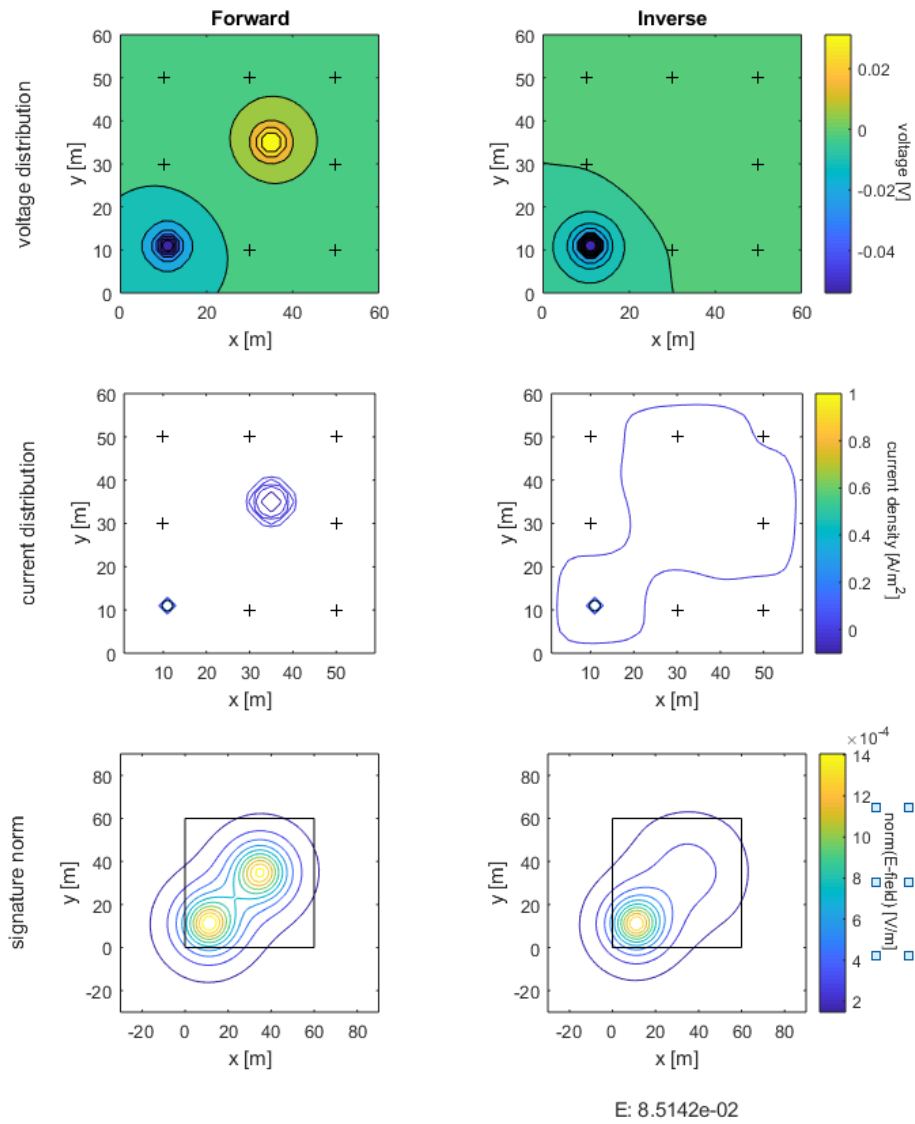


Figure B.7: Poorly resolved: Measurement points only around the edge $E=8.5\%$

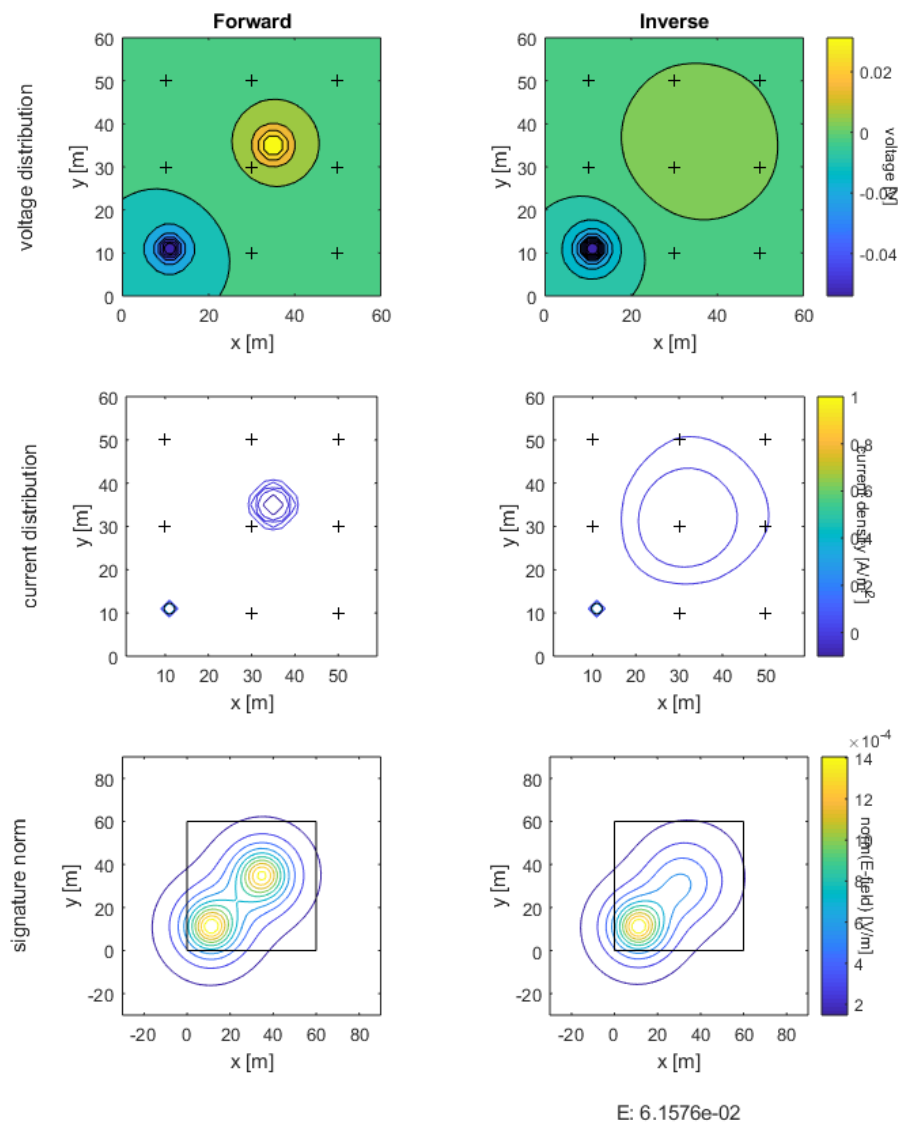
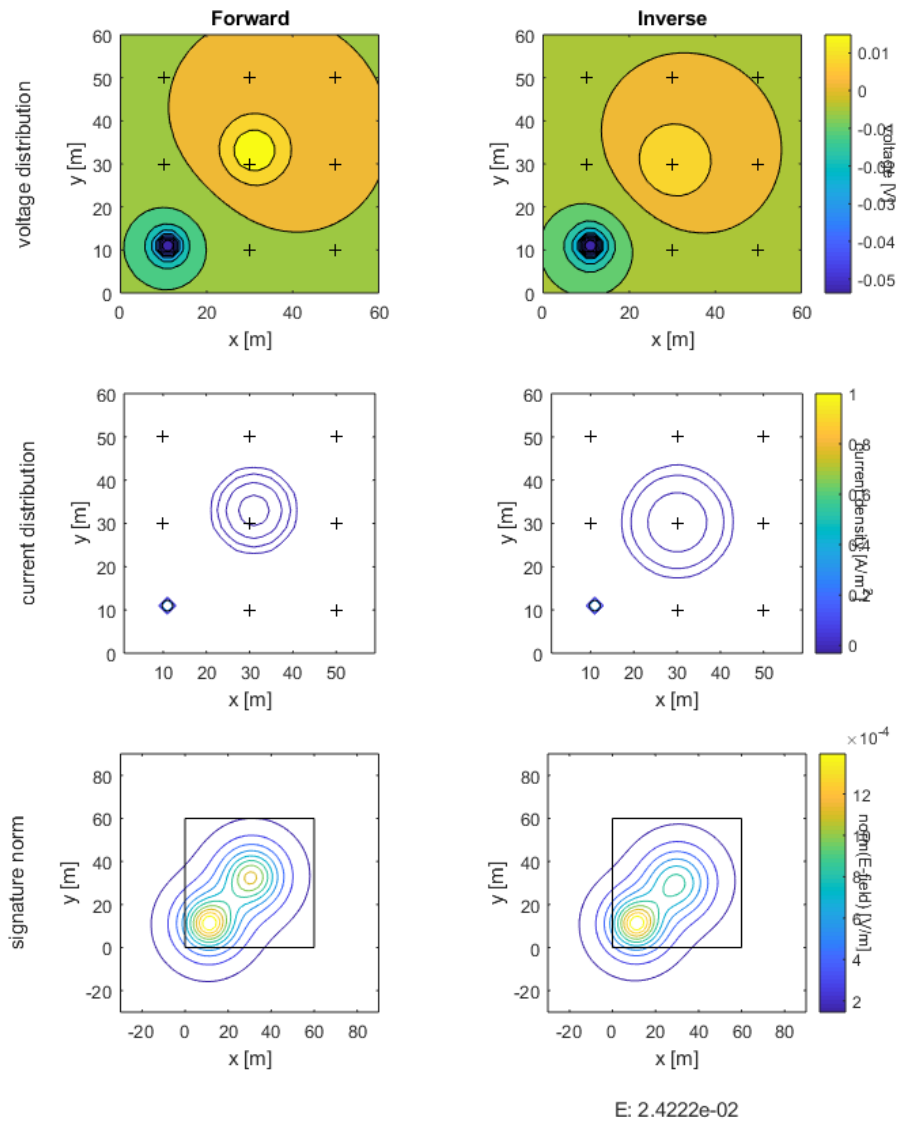


Figure B.8: Poorly resolved: Measurement points uniformly distributed E=6.2%

Figure B.9: Smoothing of a smooth gaussian-shaped damaged area. $E = 2.4\%$

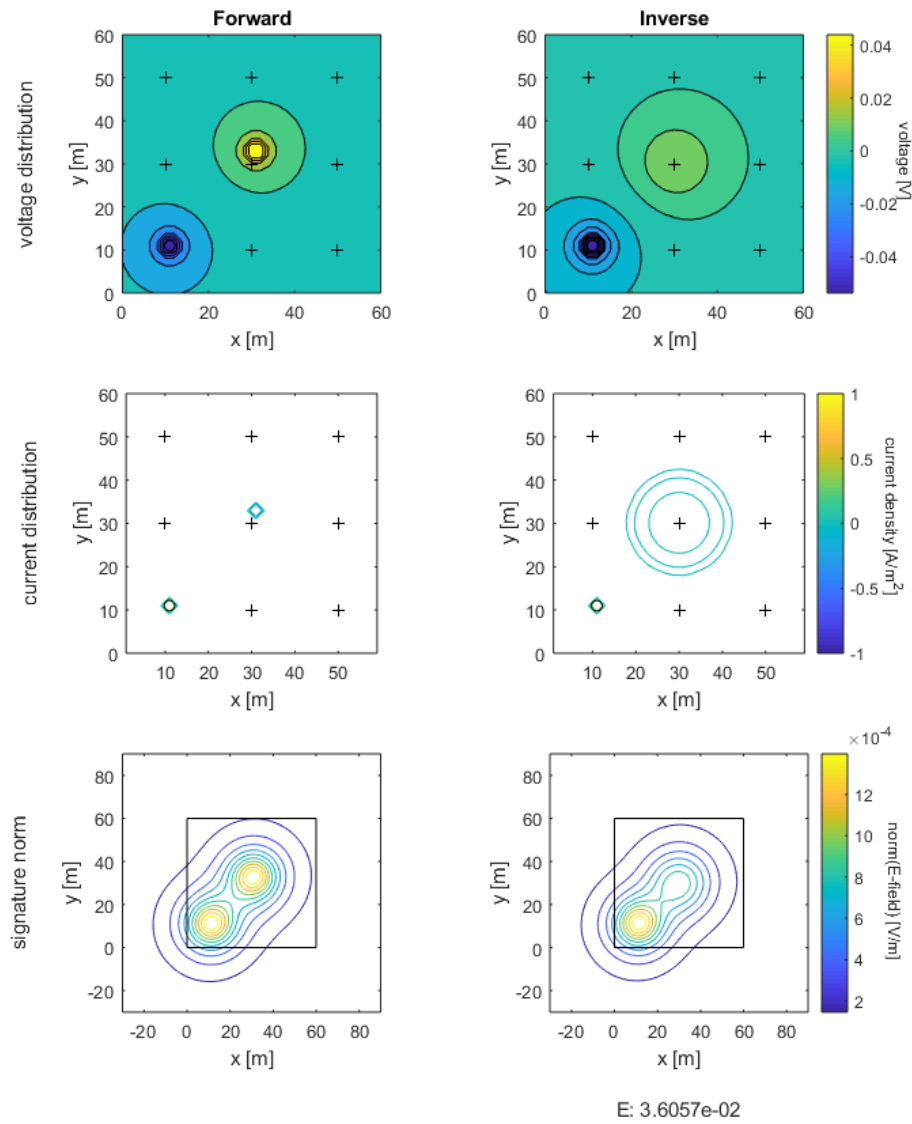
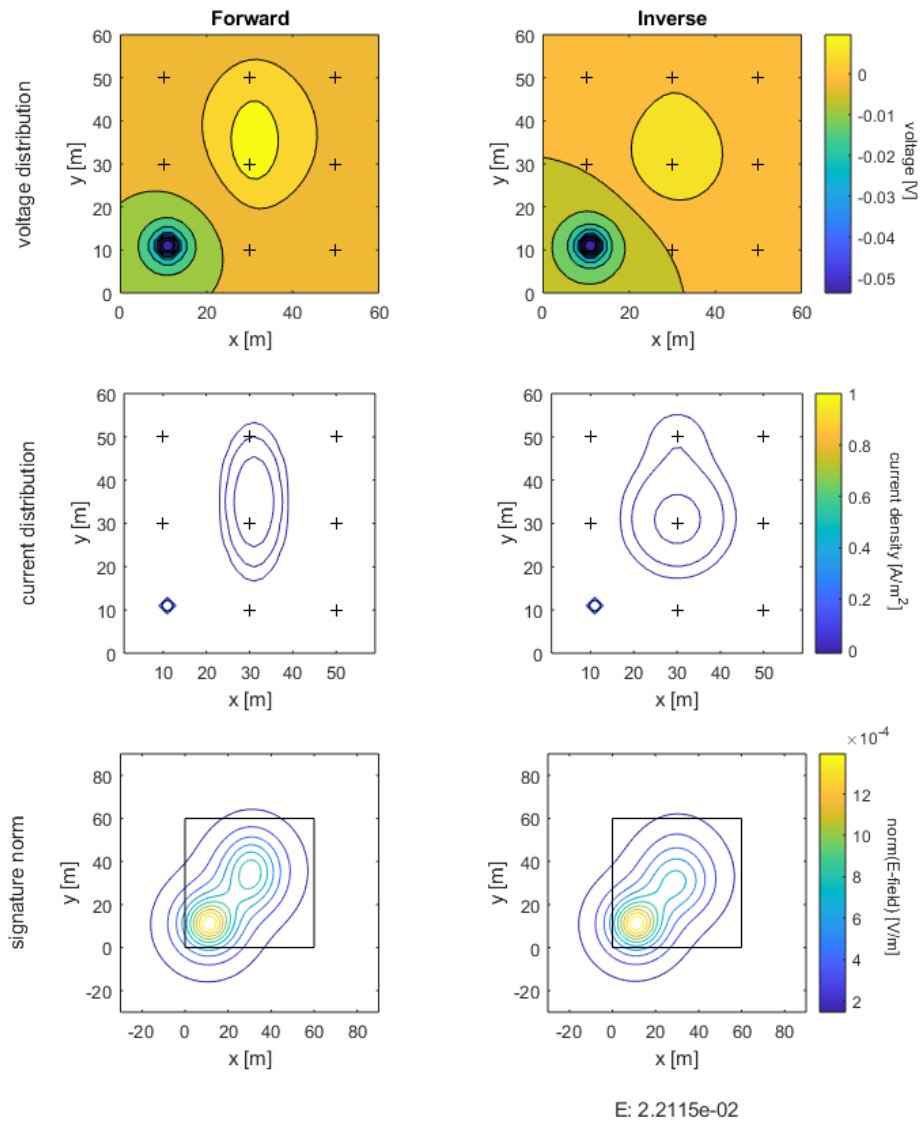


Figure B.10: Smoothing of an abrupt diamond shaped damaged patch. E = 3.6%

Figure B.11: Somewhat resolved: extensive damage, $E = 2.4\%$

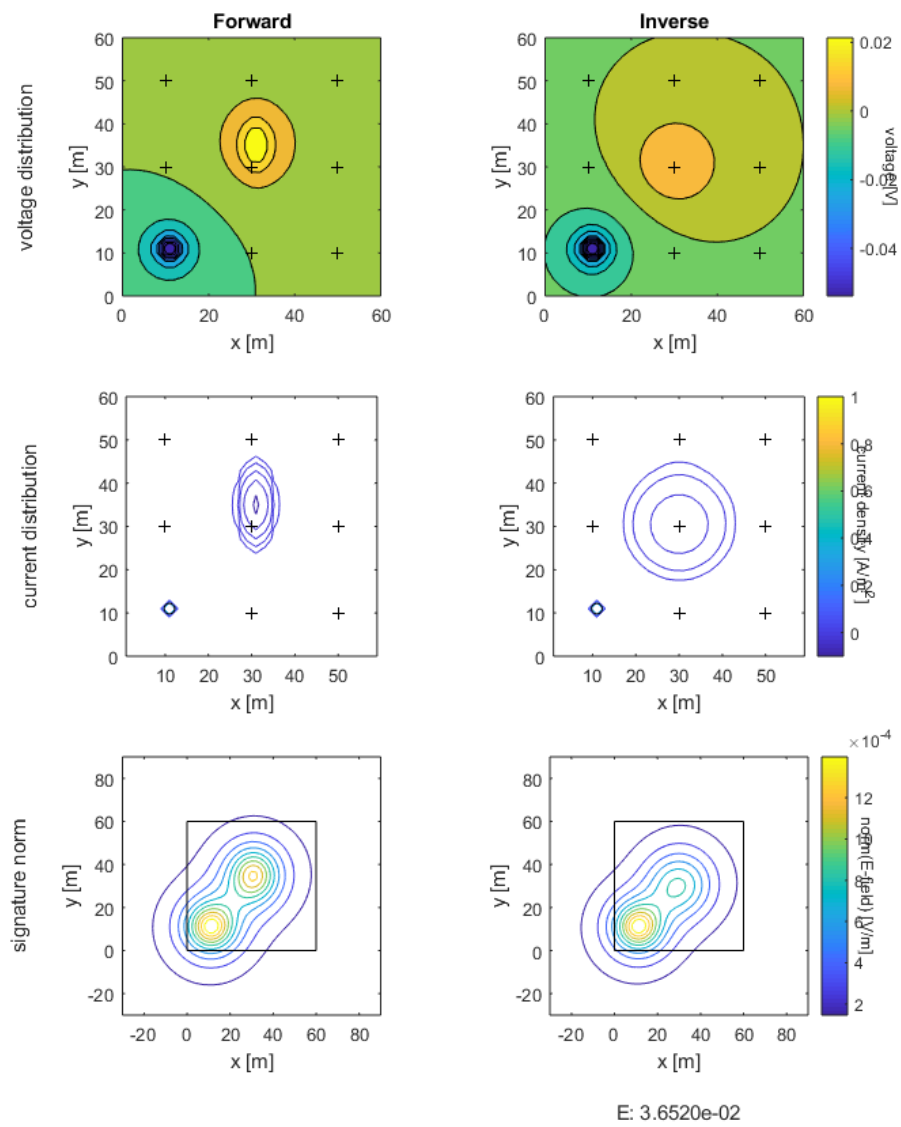
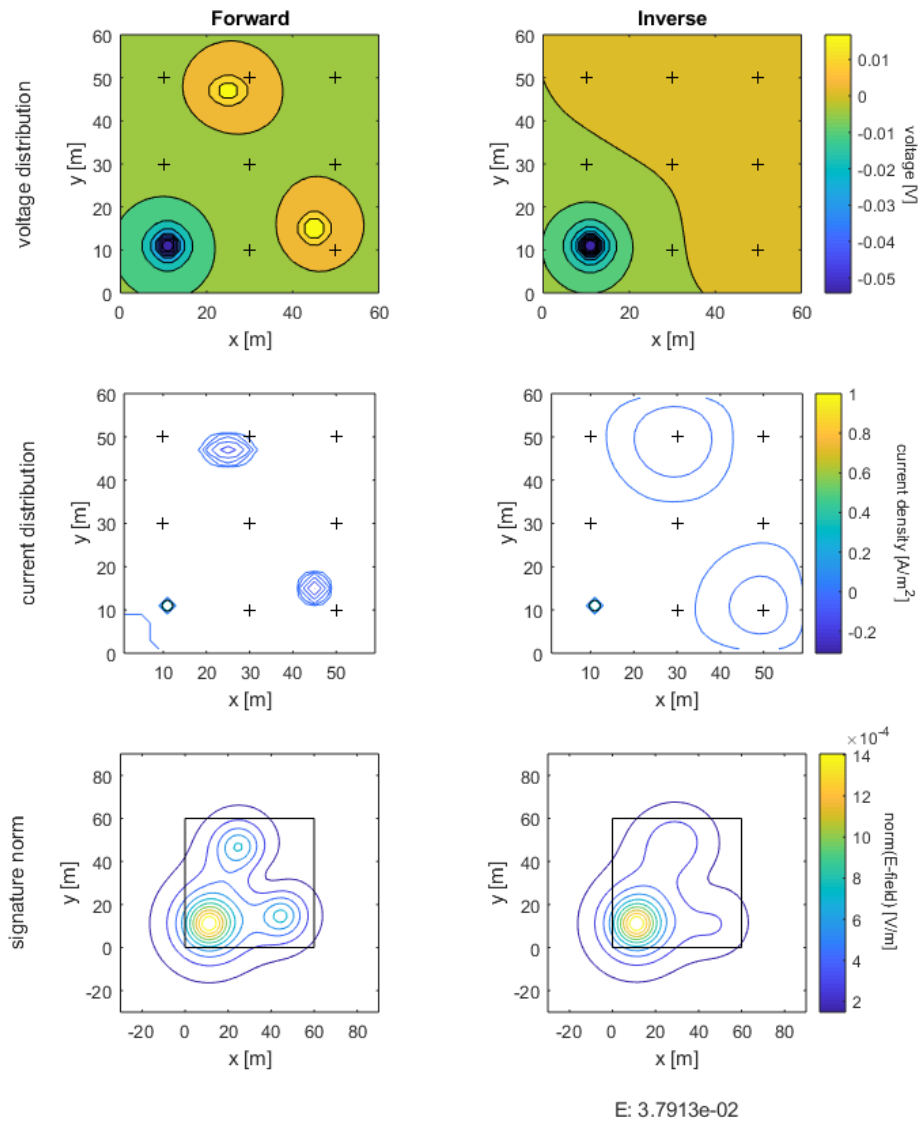


Figure B.12: Less well resolved: localised damage, $E = 3.6\%$

Figure B.13: Somewhat resolved: Two far away damages $E=3.8\%$

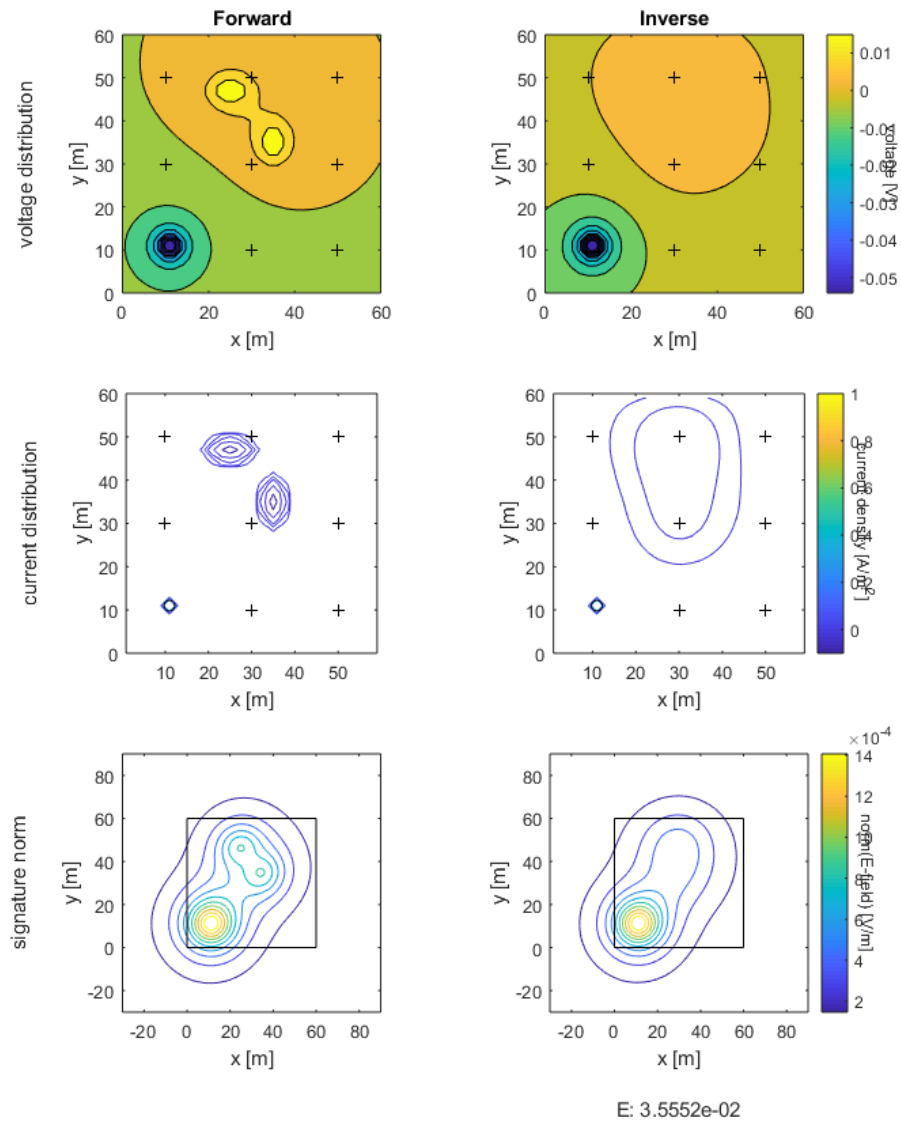
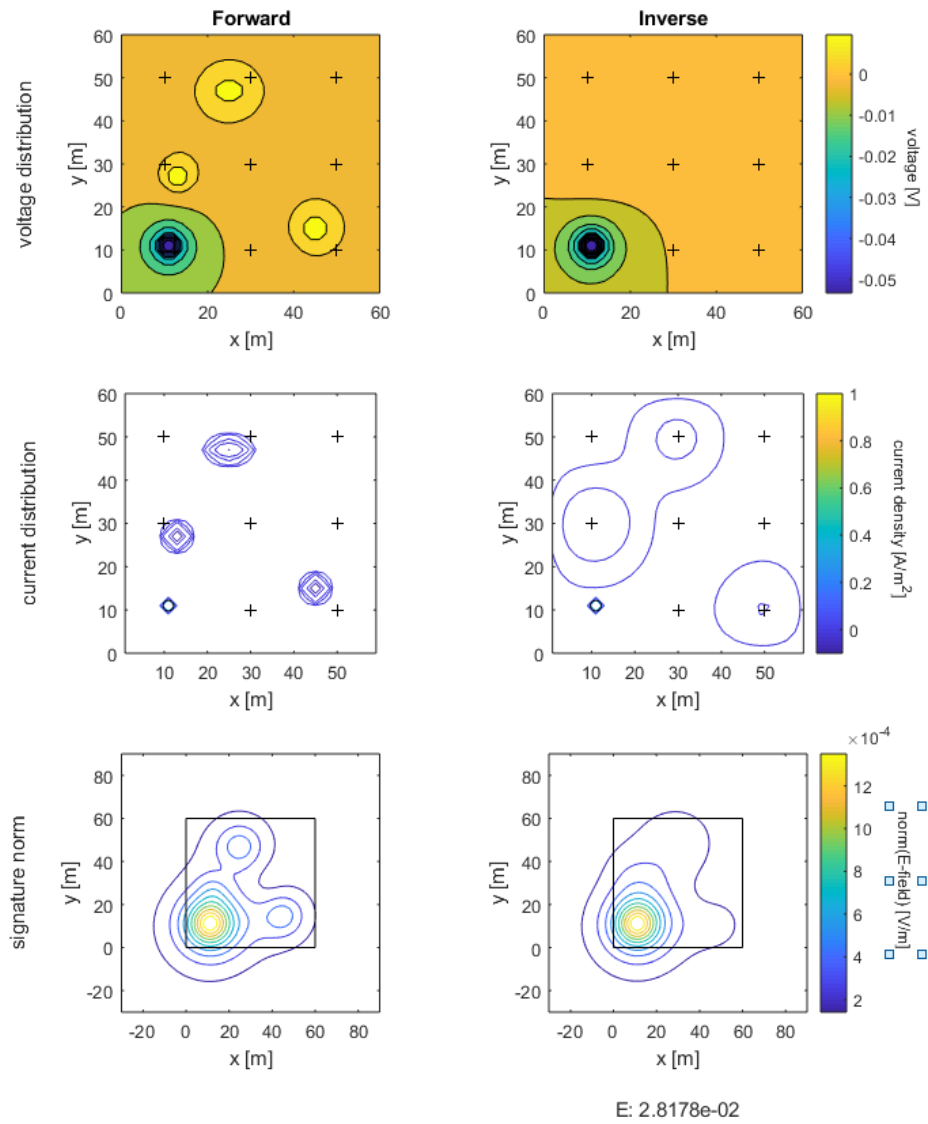
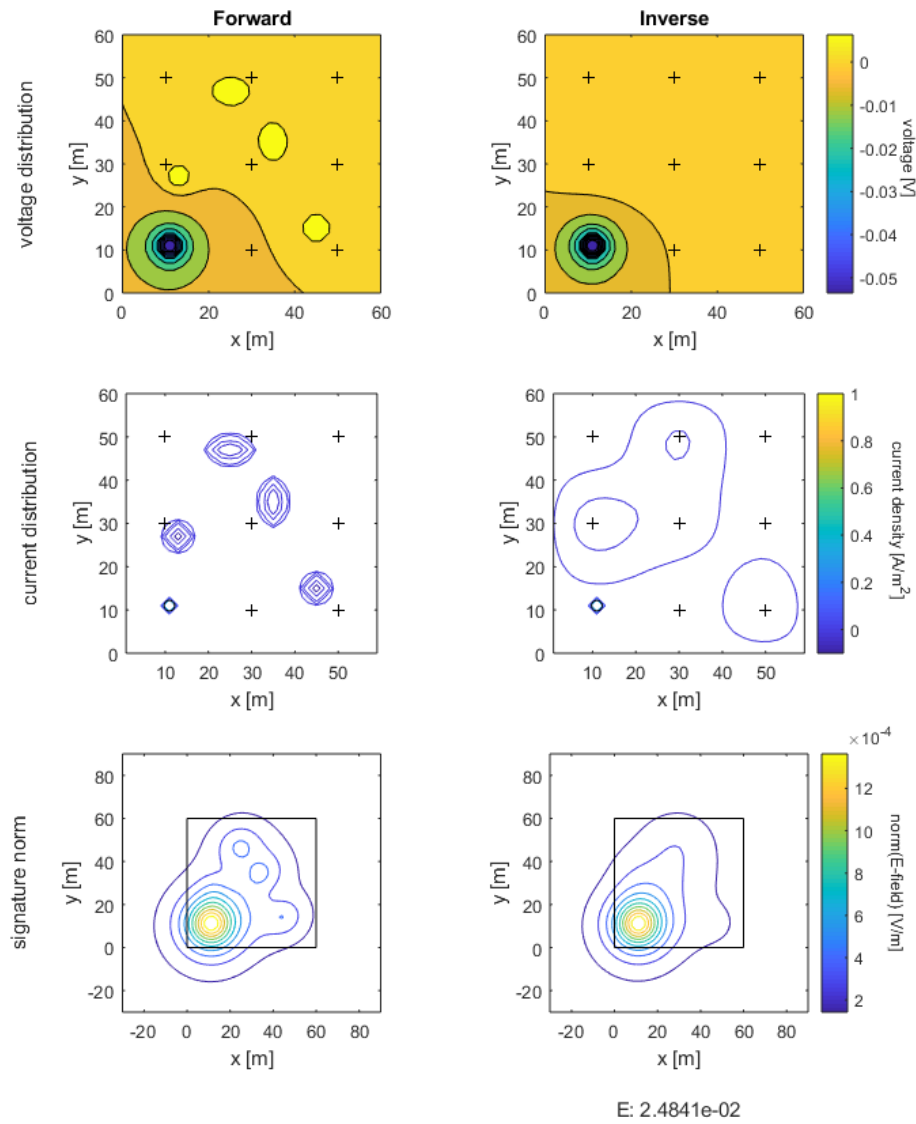
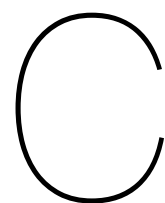


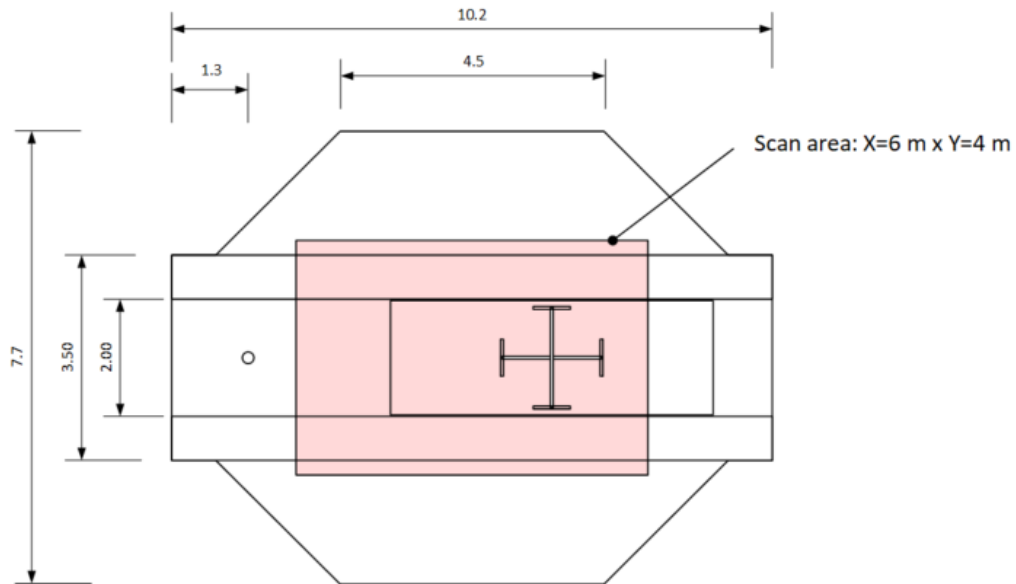
Figure B.14: Somewhat resolved: Two close damages $E=3.6\%$

Figure B.15: Somewhat resolved: Three damages $E=2.8\%$

Figure B.16: Somewhat resolved: Four damages $E=2.5\%$



Additional scale model blueprints



Tank: 5.50 x 1.95 x 2.0 (H) m

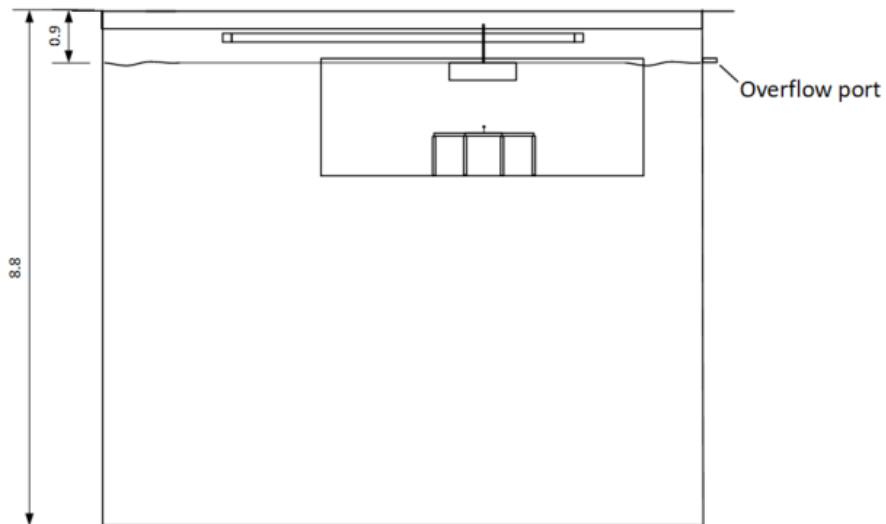


Figure C.1: Top view of the set-up in the TNO basin and cut through along the long side of the tank. Property of TNO, reproduced with permission.

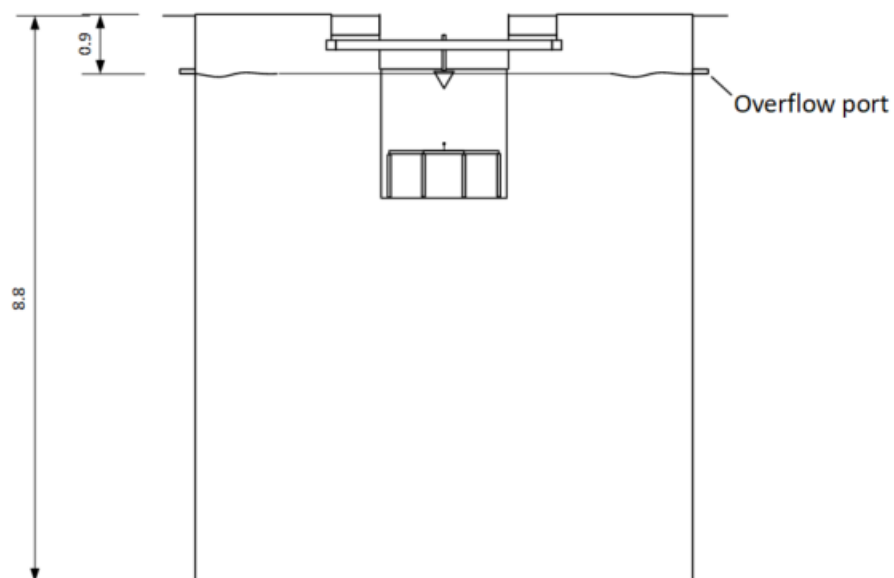
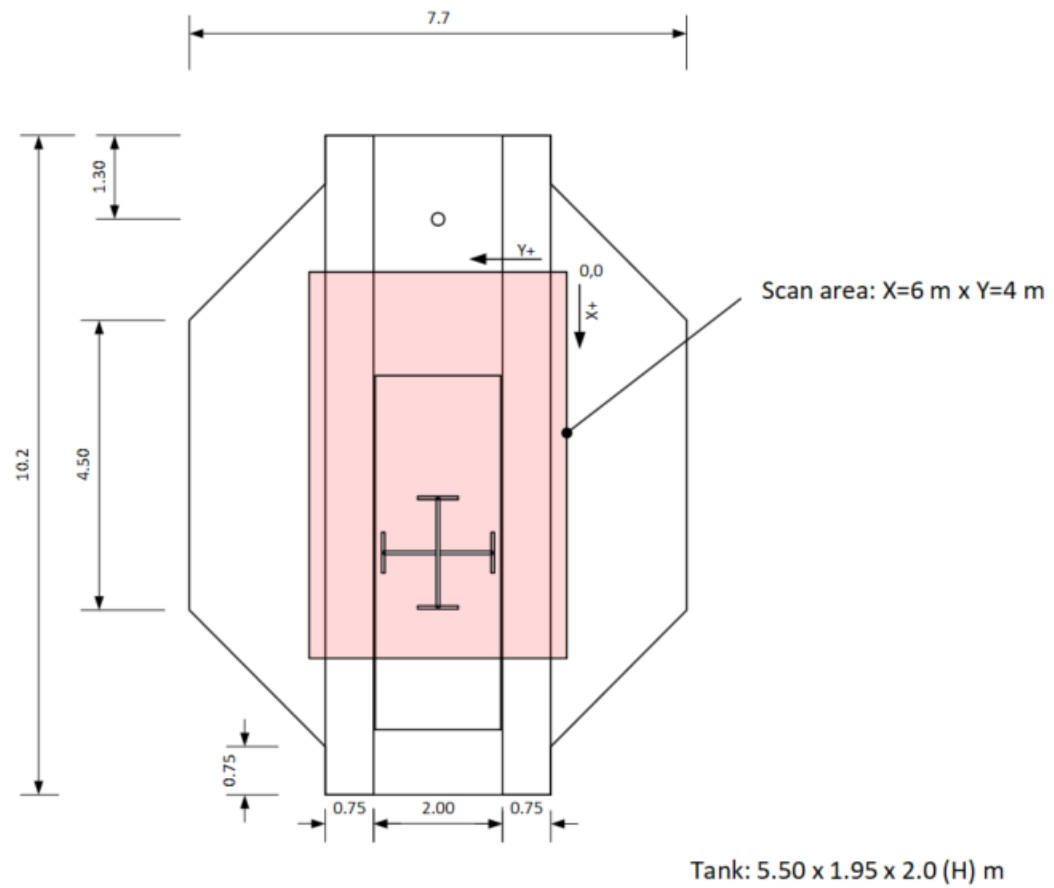


Figure C.2: Top view of the set-up in the TNO basin and cut through along the short side of the tank. Property of TNO, reproduced with permission.

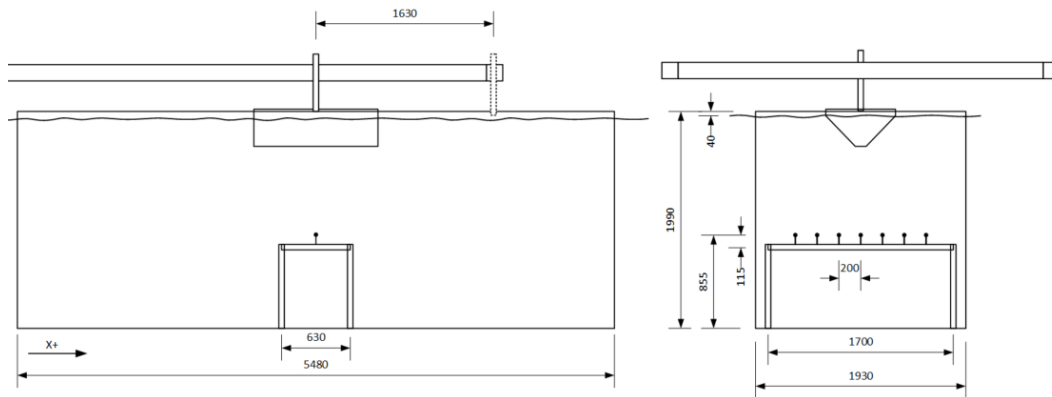


Figure C.3: Dimensions that determine the vertical distance between the ship model and the sensors. Property of TNO, reproduced with permission.

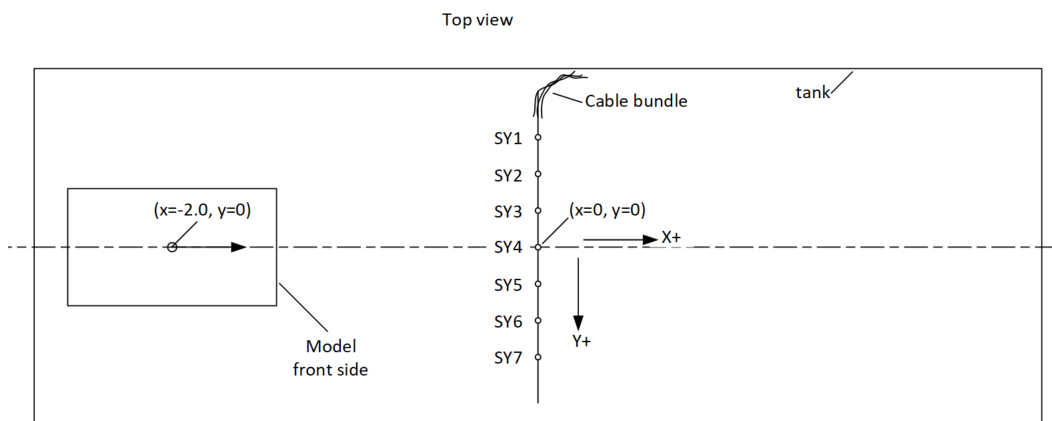


Figure C.4: Top view of the tank with the sensor frame defining the x,y coordinate system and the location of the sensors. The ship model is draw at location $x = -2.0$ m, $y = 0$ m. Property of TNO, reproduced with permission.